UNIVERSITY OF HAWAII
LIBRARY

JOURNAL OF THE LESS-COMMON METALS

VOL. 3 (1961)

JOURNAL

of the

LESS-COMMON METALS

INTERNATIONAL JOURNAL ON THEIR CHEMISTRY AND METALLURGY

EDITORS

J. W. CUTHBERTSON *(Nottingham)*
F. FAIRBROTHER *(Manchester)*

EDITORIAL ADVISORY BOARD

J. BÉNARD *(Paris)*
MAURICE COOK *(Birmingham)*
C. DECROLY *(Brussels)*
L. E. DJINGHEUZIAN *(Ottawa)*
J. M. FLETCHER *(Harwell)*
B. W. GONSER *(Columbus, Ohio)*
M. HANSEN *(Frankfurt a.M.)*
A. IANDELLI *(Genoa)*
W. KLEMM *(Münster)*
W. J. KROLL *(Corvallis, Ore.)*
P. MURRAY *(Harwell)*
H. NOWOTNY *(Vienna)*
L. M. PIDGEON *(Toronto)*
A. R. POWELL *(Wembley)*
O. C. RALSTON *(Hyattsville, Md.)*
A. E. VAN ARKEL *(Leyden)*
H. W. WORNER *(Melbourne)*
L. F. YNTEMA *(Menlo Park, Calif.)*

VOL. 3 1961

ELSEVIER PUBLISHING COMPANY
AMSTERDAM

Printed in The Netherlands by
NEDERLANDSE BOEKDRUK INRICHTING N.V., 'S-HERTOGENBOSCH

VOL. 3 No. 1
FEBRUARY 1961

UNIVERSITY OF HAWAII
LIBRARY
JUL 7 '61

NAL OF THE

LESS-COMMON METALS

AN INTERNATIONAL JOURNAL ON
THEIR CHEMISTRY AND METALLURGY

HBERTSON (Nottingham)
ROTHER (Manchester)

AL ADVISORY BOARD:
D (Paris)
E COOK (Birmingham)
LY (Brussels)
GHEUZIAN (Ottawa)
TCHER (Harwell)
NSER (Columbus, Ohio)
EN (Frankfurt a.M.)
LLI (Genoa)
M (Münster)
LL (Corvallis, Ore.)
AY (Harwell)
TNY (Vienna)
GEON (Toronto)
ELL (Wembley)
STON (Hyattsville, Md.)
ARKEL (Leyden)
RNER (Melbourne)
EMA (Menlo Park, Calif.)

ELSEVIER

GENERAL INFORMATION

Types of contributions

(a) Original research work not previously published in other periodicals.
(b) Reviews on recent developments in various fields.
(c) Short communications.
(d) Bibliographical notes and book reviews.

Languages

Papers will be published in English, French or German.

Submission of papers

Papers should be sent to one of the following Editors:

Professor J. W. CUTHBERTSON (*Metallurgy*), Department of Metallurgy, The University, University Park, Nottingham, England.
Professor F. FAIRBROTHER (*Chemistry*), The University of Manchester, Department of Chemistry, Manchester 13, England.

Authors should preferably submit two copies in double-spaced typing on pages of uniform size. Legends for figures should be typed on a separate page. The figures should be in a form suitable for reproduction, drawn in Indian ink on drawing paper or tracing paper, with lettering etc. in thin pencil. The sheets of drawing or tracing paper should preferably be of the same dimensions as those on which the article is typed. Photographs should be submitted as clear black and white prints on glossy paper.
All references should be given at the end of the paper. They should be numbered and the numbers should appear in the text at the appropriate places.
A summary of 50 to 200 words should be included. Authors of papers in French or German are encouraged to supply also a translation of the summary in English.

Reprints

Twenty-five reprints will be supplied free of charge. Additional reprints can be ordered at quoted prices. They must be ordered on order forms which are sent together with the proofs.

Publication

The *Journal of the Less-Common Metals* will have six issues to the volume, approx. 500 pages per volume.
Subscription price: £ 5.7.6 or Dfl. 57.— per volume (post free).
For advertising rates apply to the publishers.

Subscriptions

Subscriptions should be sent to:

ELSEVIER PUBLISHING COMPANY, Spuistraat 110-112, Amsterdam-C., The Netherlands.

FFECT OF ALLOYING ON THE MECHANICAL PROPERTIES OF NIOBIUM*

R. T. BEGLEY AND J. H. BECHTOLD

Metallurgy Dept., Westinghouse Research Laboratories, Beulah Road, Pittsburgh 35, Pa. (U.S.A.)

(Received October 5th, 1960)

SUMMARY

The effects of additions of those elements which are near neighbors in the periodic table on the mechanical properties of niobium have been studied. These effects vary widely and follow no simple general rule. Some of the most important observations are as follows:

(1) At low temperatures alloy additions increase strength due to normal solid-solution strengthening and by raising the range over which strength becomes strongly temperature-dependent. The fracture transition temperature range is raised, in part due to the strength increase and in part due to changes in fracture characteristics. When compared at equal atom percentages, the group tungsten–molybdenum exert the greatest increase in fracture transition temperature; titanium and hafnium have relatively little effect; and zirconium and vanadium are intermediate.

(2) When compared at room temperature, equal atom percentages of vanadium and chromium appear to give the largest increase in strength; titanium and hafnium the smallest; and the remaining elements are intermediate. With the purity, grain size and test procedures used here, additions of over 10 w/o molybdenum or tungsten resulted in very low room-temperature ductility.

(3) At 1095°C when compared at equal atom percentages, zirconium and vanadium show the largest increase in strength; titanium has very little effect; molybdenum, tungsten and hafnium are intermediate strengtheners. Limited data on chromium indicate it to be a potent strengthener.

(4) No single alloy addition confers the best combination of mechanical properties. Elements like molybdenum and tungsten, which confer reasonably good increases in low- and high-temperature strength, result in a significant increase in the low-temperature fracture transition. Titanium strengthens at low temperature with very little effect on fracture transition but has very little effect on high temperature strength. Zirconium and hafnium appear to be somewhat intermediate in their effects on low- and high-temperature strength and ductility. On the basis of workability, low-temperature ductility, and elevated temperature strength, vanadium additions appear to be very attractive. The only apparent disadvantage is the hot shortness condition observed in the 20 w/o V alloy.

(5) Interstitial elements appear to exert a very pronounced effect on the elevated temperature properties of certain niobium-base alloys.

INTRODUCTION

iobium possesses a number of properties which make it attractive for nuclear pplications and for structural components in aircraft and space vehicles. These

* Prepared for the Conference on Niobium, Tantalum, Molybdenum and Tungsten, held in The epartment of Metallurgy, The University of Sheffield, September 1960.

properties include a high melting point (2468°C), moderate density (8.56 g/cm³), excellent fabricability, low ductile-to-brittle transition temperature range, and a low thermal neutron absorption cross-section (1.1 barns). In common with all the refractory metals, niobium has poor oxidation resistance, even at moderately elevated temperatures. Although the oxides of niobium are porous and essentially non-protective, Nb_2O_5 remains solid to about 1500°C. Thus the oxidation problem associated with niobium is considerably less formidable than that encountered with molybdenum or tungsten, which form relatively low melting and volatile oxides.

Recently, progress has been made in improving both the mechanical properties and the oxidation resistance of niobium by alloying[1,2]. Several promising niobium-base alloys are now, or soon will be, commercially available. Despite the high level of interest in niobium and its alloys, relatively little systematic data have been reported concerning the effect of binary alloy additions on mechanical properties.

The work described in this paper was undertaken to evaluate the effects of alloying niobium with most of its near neighbors in the Periodic Table and thereby assess the engineering potentialities of a number of niobium alloy systems. Emphasis was therefore directed toward determining trends of behavior and outlining areas for more intensive study, rather then extensively evaluating several alloy compositions.

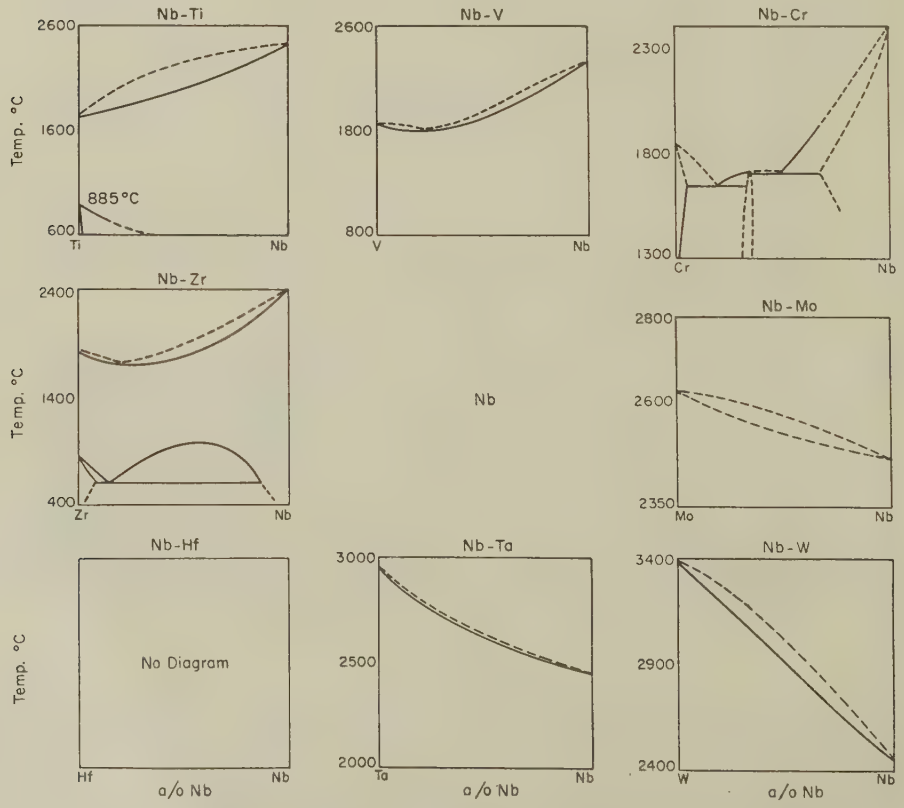


Fig. 1. Phase diagrams of niobium with its near neighbors in the Periodic Table.

ALLOY SELECTION

The alloy additions selected for evaluation were titanium, zirconium, hafnium, vanadium, chromium, molybdenum and tungsten. These elements include all of niobium's near neighbors in the Periodic Table, with the exception of tantalum. The phase diagrams of the binary systems formed by niobium and its near neighbors are shown in Fig. 1. Niobium forms a continuous series of solid solutions with tungsten, molybdenum, tantalum, vanadium, and β-titanium. Niobium and β-zirconium form a continuous series of solid solutions only above 1000°C. The solubility of zirconium in niobium is approximately 13 a/o* at 610°C, and the solubility decreases with decreasing temperature[3]. Although a complete phase diagram is not available for the Nb–Hf system, DUWEZ[4] has reported that niobium and hafnium form a b.c.c. solid solution up to about 70 a/o hafnium, at 1000°C. The only alloy element studied which has relatively low solubility in niobium at elevated temperatures is chromium.

The alloying elements selected are characterized by high melting points. With the exception of titanium, the melting temperatures of all of the alloy additions are in excess of 1800°C. The alloy compositions evaluated are listed in Table I.

TABLE I

COMPOSITION OF NIOBIUM BINARY ALLOYS

Element	*Nominal composition*		*Analyzed composition*	
	w/o	*a/o*	*w/o*	*a/o*
Ti	5.0	9.3	4.33	8.0
Ti	7.5	13.5	6.7	12.0
Ti	20.0	32.6	18.0	30
Zr	0.6	0.6	0.64	0.64
Zr	5.0	5.1	—	—
Zr	10	10.2	—	—
Zr	20	20.3	20.24	20.5
Hf	5	2.75	—	—
Hf	10	5.5	9.47	5.4
Hf	20	11.6	20.9	11.8
V	1	1.9	—	—
V	5	8.8	4.86	8.0
V	10	16.9	10.5	17.5
V	20	31.3	19.03	30.0
Cr	1.25	2	—	—
Cr	2.5	4	1.57	2.5
Cr	6.0	10	—	—
Mo	1	0.9	0.72	0.6
Mo	5	4.9	5.03	4.9
Mo	10	9.7	—	—
Mo	20	19.5	—	—
W	1	0.5	0.87	0.4
W	5	2.6	2.47	1.2
W	10	5.3	9.72	5.1
W	20	11.2	19.9	11.1

* In this paper the term "a/o" is used to denote "atom percent", and "w/o" to denote "weight percent".

The criteria used to evaluate the alloys included relative workability, and room and elevated temperature (1095°C) tensile properties. Additional tensile tests were conducted on selected alloys to provide preliminary data concerning the effect of solute additions on the ductile-to-brittle transition behavior of niobium alloys. No attempt was made to study the oxidation characteristics of the binary alloys, since this subject has been explored by a number of investigators[5,6].

MATERIALS AND EXPERIMENTAL PROCEDURE

The niobium was obtained from the Union Carbide Metals Company in the form of roundels (pellets approximately 1/8 in. diameter, 1/2 in. long) and small beads (approximately 1/8 in. diameter). A typical analysis of the niobium used is listed in Table II. The starting material was selected as representative of good commercial

TABLE II

TYPICAL ANALYSIS OF NIOBIUM

Analysis (w/o)						
O	*N*	*C*	*Ta*	*Ti*	*Zr*	*H*
0.036	0.011	0.025	<0.5	0.01	<0.03	0.0003

The following alloy additions, of good commercial purity, were used: titanium, sponge; zirconium, crystal bar; hafnium, crystal bar; vanadium, chips; chromium, hydrogen reduced electrolytic flake; molybdenum, sheet trimmings; tungsten, powder and high purity crushed rod.

purity at the time this program was initiated. The as-melted hardness of the base-material was about 115 V.P.N.

Alloys weighing 100 to 150 g were prepared by conventional d.c. non-consumable arc melting, using a tungsten electrode. The cold-pressed alloy charges were placed in water-cooled copper crucibles in an arc furnace and melted under high purity argon. Each sample was melted four to six times to attain homogeneity, the sample being inverted after each melt. Most of the alloys were prepared in the form of buttons approximately $2\frac{1}{2}$ in. in diameter and 3/8 in. thick. Several of the Nb-V and Nb-W alloys were melted in rectangular crucibles to form rods approximately 5/8 in. diameter, $3\frac{1}{2}$ in. long.

The button samples were ground to remove any surface irregularities, and then inserted in stainless steel jackets. The jackets were evacuated and sealed off. The jacketed assembly was then rolled at 1200-1300°C to provide sheet material approximately 0.08 in. thick. The rod samples were forged in swaging dies at 1200°C to approximately 7/16 in. diameter bar. These samples were heated in an atmosphere of flowing argon and forged in air. The hot-worked material was ground to remove the contaminated surface layer and then etched in a 60% HNO_3–40% HF solution.

Button-head tensile specimens were machined from the rod stock and flat sheet specimens from the material which was prepared by rolling jacketed buttons. The round specimens had a 1 in. gage length and a 0.200 in. gage diameter. The sheet tensile samples were 0.050 in. thick, 0.250 in. wide, and also had a 1 in. gage length.

All the alloys were tested in the fully recrystallized condition. The machined

specimens were wrapped in niobium foil and annealed in vacuum for 1 h at 1600°C. Low temperature tests were conducted in a constant strain rate tensile machine of the type described by MANJOINE, WESSEL AND PRYLE[8]. Temperatures below ambient were obtained in apparatus described by WESSEL AND OLLEMAN[9]. Elevated temperature testing was carried out in vacuum at pressures below $1 \cdot 10^{-4}$ mm of Hg. The equipment and testing techniques used were similar to those described by MANJOINE AND LAWTHERS[10]. All specimens were tested at a strain rate of $1 \cdot 10^{-3}$ sec^{-1}. Most of the alloys were analyzed after testing for the metallic alloy addition and the interstitial impurities O, N and C. With the exception of Cr, recovery of alloy additions was generally satisfactory, as shown in Table I. Analyses showed that no significant contamination occurred during melting, working, or testing.

RESULTS

Workability

Excellent cold-rolling characteristics were exhibited by Nb–Ti alloys containing up to 20 w/o Ti. Alloys containing Hf, V and Mo could be rolled or forged readily at 1200–1300°C, except at the highest alloy additions, 20 w/o. All of the Nb–W alloys could be hot worked without difficulty. The poorest results were obtained with the Nb–6.0 w/o Cr and Nb–20 w/o Zr alloys, which cracked severely on hot working. The generally good workability of the binary alloys studied illustrates the relative freedom possible in alloying niobium as compared with other refractory metals such as molybdenum and tungsten. The hot-working temperatures used in this study (1200–1300°C) are, in general, below the recrystallization ranges of the alloys. More detailed observations on the effect of binary solute additions on the workability and hardness of niobium have been reported by BEGLEY AND PLATTE[11].

Low temperature properties

An evaluation of the room temperature properties of niobium alloys is complicated by the ductile-to-brittle transition phenomenon. The strength of unalloyed niobium starts to increase rapidly with decreasing temperature about 0°C[12]. In unalloyed samples of niobium of the grade used in this investigation, the yield strength increases from about 25,000 p.s.i. at room temperature to over 100,000 p.s.i. at —196°C (*cf.* Fig. 2). This rapid increase in strength with decreasing temperature is part of the ductile-to-brittle transition phenomenon. At room temperature alloy additions can increase strength due to a relatively temperature-independent increment added to the strength of the pure metal, or to an increase in the transition temperature range. Data for two titanium- and two tungsten-containing alloys indicate that solid solution additions increase room temperature strength due to both mechanisms (Fig. 2). This can be seen by comparing the strength of the 11 a/o tungsten (20 w/o) at room temperature and 400°C. At room temperature the alloy addition resulted in a strength increase of about 50,000 p.s.i., while at 400°C, where the strength has apparently become quite temperature-independent, the increase is only about 25,000 p.s.i. The 25,000 p.s.i. increment at 400°C is probably close to the more or less temperature-independent solid-solution strengthening. The additional 25,000 p.s.i. at room temperature is due to a shift to a higher temperature of the range over which the yield strength becomes sharply temperature-dependent.

Insufficient data exist to determine whether this behavior exhibited by the tita-

nium- and tungsten-containing alloys is characteristic of all additions to niobium or to determine the relative effects of the individual alloying elements on the two strengthening factors. It is important, however, to recognize that both factors can enter into the room-temperature strength of niobium-base alloys. In attempts to correlate the strengthening effect of alloying elements with various proposed theories of solid-

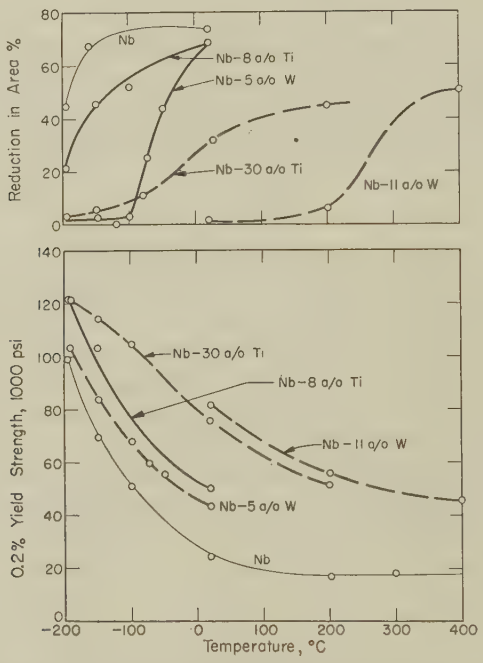


Fig. 2. Effect of temperature on the yield strength and ductility of several niobium binary alloys.

solution strengthening, only the relatively temperature-independent increment should be used. This usually cannot be estimated from room-temperature test data on niobium alloys and consequently room-temperature data are not sufficient to make basic studies on strengthening mechanisms. It is also important from a practical alloy-design standpoint to know whether strengthening is due to regular solid-solution strengthening or to an increase in the transition temperature range.

Alloy additions which raise the temperature range over which the strength increases rapidly usually raise the temperature range over which the change from ductile rupture to brittle fracture occurs. Data in Fig. 2 show this to be true for titanium- and tungsten-containing alloys. However, it is also clearly evident that tungsten causes a much greater increase in the fracture-transition temperature than titanium, when compared at alloy contents which give equivalent strength increases.

The observed brittle fractures were completely transgranular with the exception of the 30 a/o Ti alloy (18 w/o), which failed by complete intergranular separation. The reason for the intergranular failure of the Nb–30 a/o Ti alloy is not understood.

Although results are not yet complete on the transition temperature behavior of all of the alloys, sufficient data exist to make some general comparisons. Fig. 3 shows

the temperatures, as a function of atom percent alloy addition, above which the alloys exhibit over 10% reduction in area. The alloys fall into two general classes: those with tungsten and molybdenum, which greatly increase the fracture-transition temperature; and those with titanium and hafnium, which have very little

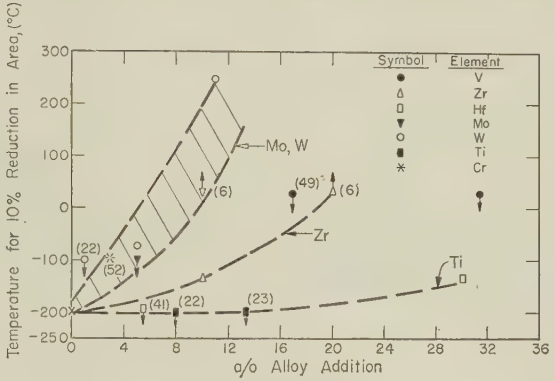


Fig. 3. Effect of binary additions on the ductile–brittle transition of niobium (approximate).

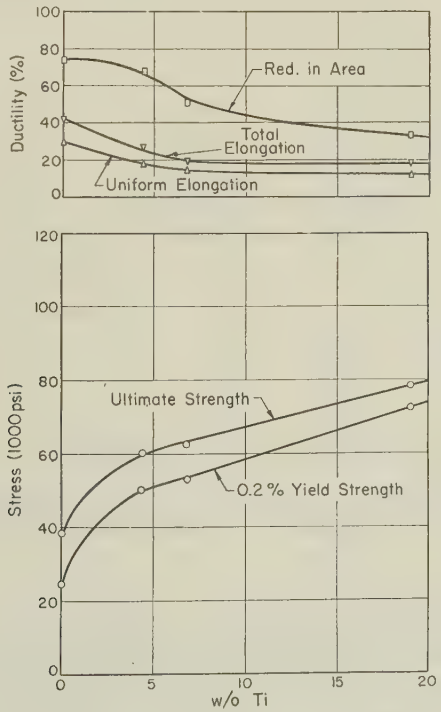


Fig. 4. Effect of titanium additions on the room temperature tensile properties of niobium.

effect. Zirconium alloys are intermediate between these two groups. However, the higher-zirconium-content alloys are two-phase and probably should not be compared with the other alloys. Low temperature data are not complete for vanadium alloys.

However, room temperature data indicate that vanadium behaves more like titanium, zirconium, and hafnium than molybdenum and tungsten.

It should be emphasized that the transition-temperature phenomena are greatly influenced by purity, grain size, and prior metallurgical history. Care was exercised in maintaining these factors as constant as possible in the materials studied; however,

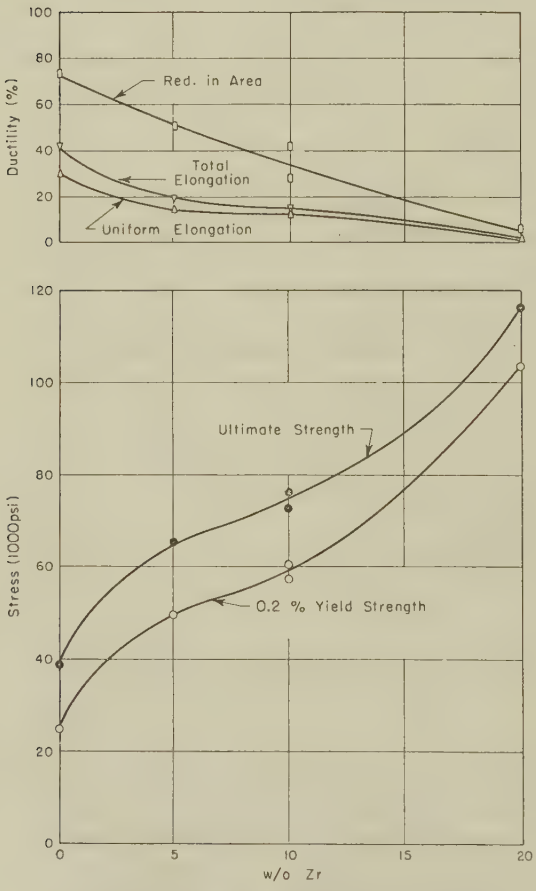


Fig. 5. Effect of zirconium additions on the room temperature tensile properties of niobium.

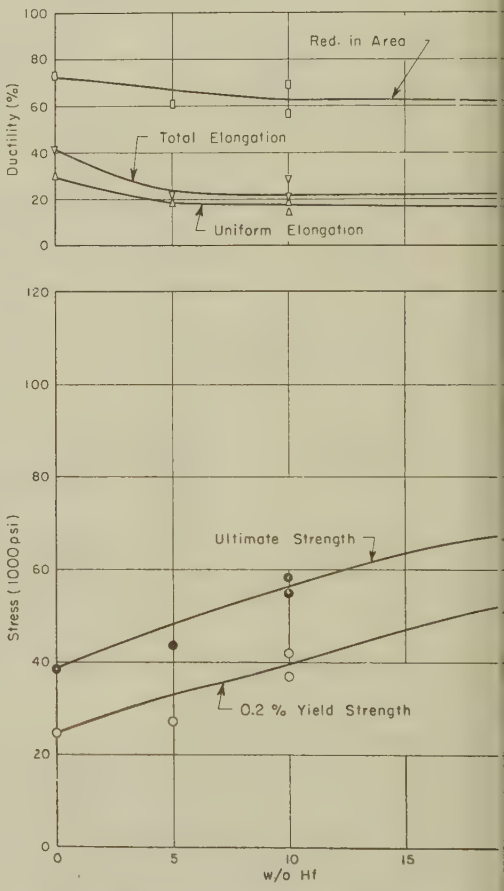


Fig. 6. Effect of hafnium additions on the room temperature tensile properties of niobium.

caution should be exercised in comparing these data with data from samples of widely differing purity and metallurgical history. At the present time no adequate explanation of the effect of substitutional solute additions on the ductile–brittle transition of niobium is available. However, this phenomenon is of significant practical and theoretical importance, and appears to be an area for fruitful study.

The effect of composition on room-temperature tensile properties for the individual alloying elements is shown in Figs. 4 through 9. The strength data are summarized in Fig. 10 where the alloys are compared on an atom percent basis. At equivalent

atom percentages beyond 5 a/o, vanadium appears to be the best room-temperature solid-solution strengthener. This strengthening is achieved without appreciable loss in ductility. In the more dilute range, 5 a/o or less, limited data indicate chromium to be better than vanadium. Titanium and hafnium are the least effective strengtheners. However, they also have the smallest effect in decreasing ductility. Molybdenum and

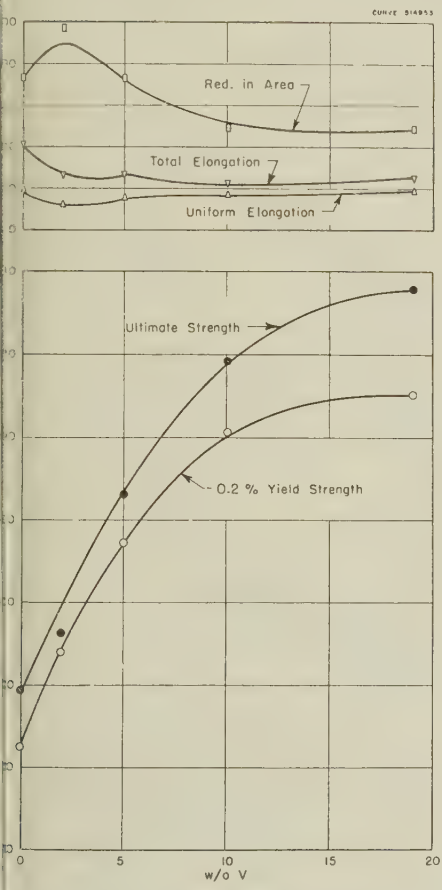


Fig. 7. Effect of vanadium additions on the room temperature tensile properties of niobium.

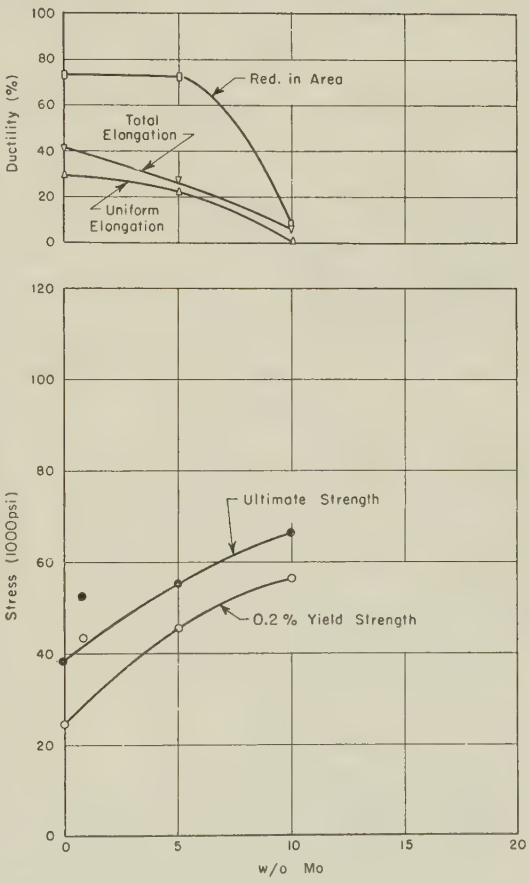


Fig. 8. Effect of molybdenum additions on the room temperature tensile properties of niobium.

tungsten are intermediate in strengthening, but the strengthening occurs at the expense of ductility. At less than 10 a/o additions the fracture transition is raised above room temperature. Zirconium is an intermediate strengthener and the effect on ductility is also intermediate. It should be pointed, however, that appreciable amounts of second phase are observed at room temperature in compositions beyond 10 a/o zirconium. Consequently, the 20 a/o zirconium alloy reflects some second-phase hardening.

As pointed out previously, we would not expect the strengthening effect to correlate

with a simple physical parameter, such as atomic size of the alloy addition, etc., and no correlation with such parameters was found.

Elevated temperature properties

The effects of binary solute additions on the elevated temperature strength of niobium were evaluated by means of vacuum tensile tests at 1095°C (2000°F). All testing was done in vacuum at pressures below $1 \cdot 10^{-4}$ mm of Hg. The test speci-

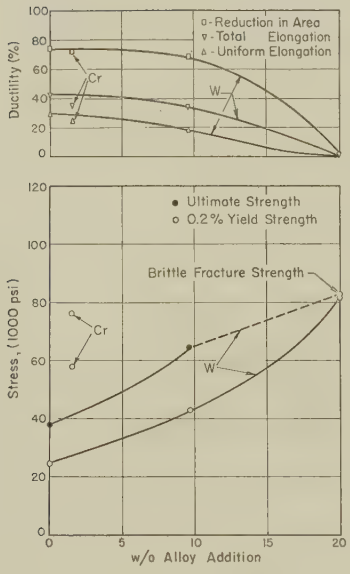


Fig. 9. Effect of chromium and tungsten additions on the room temperature tensile properties of niobium.

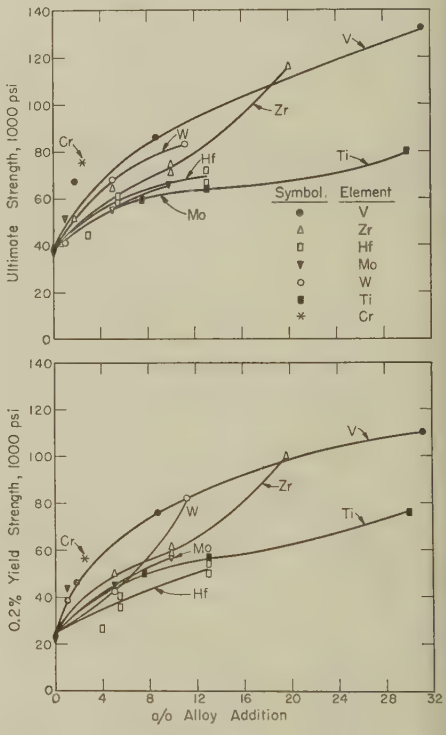


Fig. 10. Effect of binary alloy additions on the room temperature tensile properties of niobium.

mens were loosely wrapped in niobium foil to minimize contamination. Hardness values determined on the specimens before and after testing indicated that no contamination by gaseous impurities occurred.

The effect of alloy additions on the yield strength, ultimate strength, and elongation at fracture are summarized in Fig. 11. The data are replotted on the basis of atom percent alloy addition in Fig. 12. Also included are the data of GEMMEL[7] for niobium–titanium alloys. The test temperature (1095°C) was slightly in excess of one-half the absolute melting temperature of pure niobium. It is therefore to be expected that appreciable solid solution strengthening would be observed in a short time tensile test. The data of Fig. 12 show that, with the exception of titanium, all of the alloy additions evaluated significantly increased the strength of niobium. Limited data indicate that small additions of chromium are very effective in raising the yield and

ultimate strength. Very significant strengthening was also obtained with zirconium and vanadium additions. Hafnium, molybdenum, and tungsten were somewhat less effective strengtheners. GEMMEL's data for Nb–Ti alloys show that very little increase in tensile strength is obtained with titanium additions up to 15 a/o.

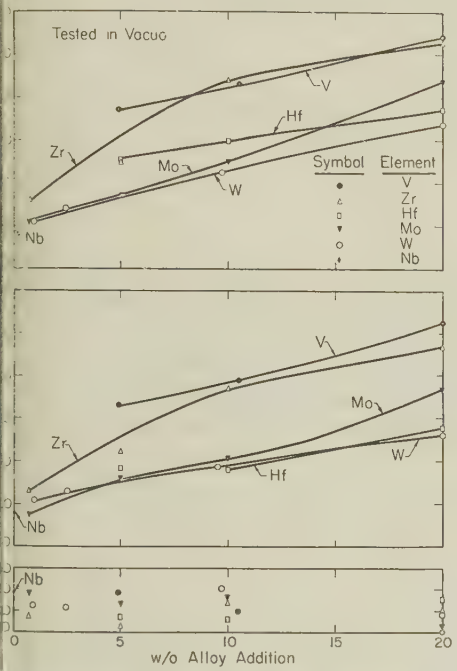


Fig. 11. Effect of binary alloy additions on the tensile properties of niobium at 1095°C (2000°F).]

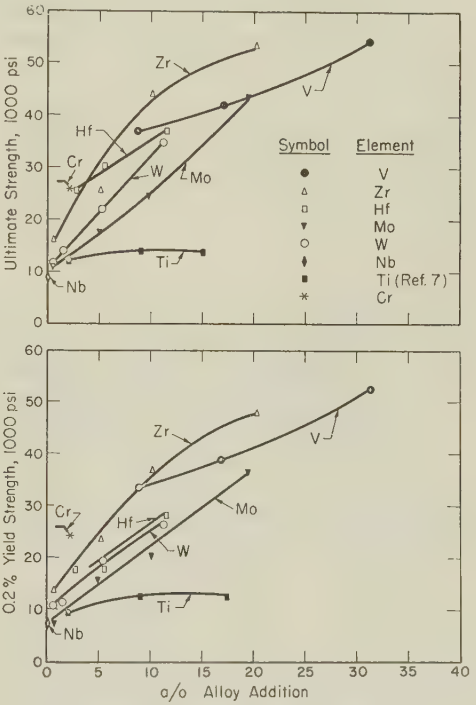


Fig. 12. Effect of binary alloy additions on the tensile properties of niobium at 1095°C (2000°F).

With one exception, the ductility of all the alloys tested was generally satisfactory (Fig. 11). While some of the alloys had elongation values ranging from 5 to 20%, the reduction in area at fracture was quite high, generally well in excess of 40%. The exception was the Nb–20 w/o V alloy, which had almost no ductility at 1095°C. The fracture was completely intergranular. Metallographic examination indicated that a grain boundary phase was present, possibly a vanadium oxide. Additional work is in progress to determine the composition of the grain boundary phase and means for its elimination.

Interstitial impurities appear to exert a very significant influence on the properties of certain niobium base alloys. This is illustrated by the results obtained on Nb–Hf alloys which are listed in Table III. Alloy NC-184, containing 5 w/o Hf, was prepared from the base material used for other alloys in this study. Alloy NC-250 also contained 5 w/o Hf but was prepared using niobium powder of higher oxygen content. As shown in Table III, the elevated temperature yield strength of the high oxygen alloy was more than double that of the low oxygen heat. These results suggest that the interaction of hafnium and one or more of the interstitial elements present results in a

TABLE III

PROPERTIES OF NIOBIUM–HAFNIUM ALLOYS

Specimen	Nominal Composition (w/o)	Analysis (w/o)	Test temp. (°C)	0.2% Yield strength (p.s.i.)	Ultimate strength (p.s.i.)	Elongation (%)		Red. in area (%)
						Uniform	Total	
NC-184-1	Nb–5Hf	<0.04 O_2	25	33,100	50,500	17.1	25.2	58.4
NC-184-2	Nb–5Hf	<0.04 C	1095	18,400	25,500	4.9	14.4	57.8
NC-250-2	Nb–5Hf + O_2		—196	110,600	142,700*	0	12.4	17.0
NC-250-1	Nb–5Hf + O_2	0.067 O_2	25	48,200	63,550	18.5	24.3	46.0
NC-250-3	Nb–5Hf + O_2	0.028 C	1095	47,300	49,200	1.4	18.6	42.5
NC-250-4	Nb–5Hf + O_2		1205	35,500	36,000	0.3	9.2	64.2

* True stress at fracture.

dispersed phase which contributes to elevated temperature strength. X-ray diffraction patterns of residues extracted from the high oxygen alloys showed the presence of HfO_2. The properties of alloy NC-250 are rather remarkable. Yield strength decreases very slightly between room temperature and 1095°C. At 1200°C the yield strength is still 35,500 p.s.i. Furthermore, considerable ductility is retained at temperatures as low as —196°C. The results described suggest that the dispersion of HfO_2 significantly increases the elevated temperature strength of Nb–Hf alloys. However, the role of interstitial impurities in niobium-base alloys is still not completely defined. Additional work is in progress in this area.

ACKNOWLEDGEMENTS

The authors wish to acknowledge the help of R. W. PALMQUIST in preparing the alloys, and that of W. H. PRYLE, R. HOVAN and E. VANDERGRIFT in carrying out the mechanical property testing. This work was sponsored by the United States Air Force under Contracts AF 33(616)-5754 and AF 33(616)-6258, monitored by the Materials Central, Wright Air Development Division, Wright Patterson Air Force Base, Ohio. Lts. J. P. PAGE and C. S. HARTLEY served as project engineers.

REFERENCES

1 *Recent Advances in Columbium Base Alloys*, Flight Propulsion Laboratory Dept., General Electric Co., July, 1959.
2 E. S. BARTLETT AND J. A. HOUCK, Physical and mechanical properties of columbium and columbium-base alloys, *Defense Metals Information Center (Battelle Mem. Inst.) Rept. No. 125* (Feb. 1960).
3 B. A. ROGERS AND D. F. ATKINS, *Trans. A.I.M.E.*, 203 (1955) 1034.
4 P. DUWEZ, *J. Appl. Phys.*, 22 (1951) 1174.
5 C. T. SIMS, W. D. KLOPP AND R. I. JAFFEE, *Trans. Am. Soc. Metals*, 51 (1959) 256.
6 A. B. MICHAEL, in *Reactive Metals*, Vol 2, Interscience Publishers, New York, 1959, p. 487.
7 G. D. GEMMEL, *Trans. A.I.M.E.*, 215 (1959) 898.
8 M. J. MANJOINE, E. T. WESSEL AND W. H. PRYLE, *A.S.T.M. Bull.*, 226 (1957) 31.
9 E. T. WESSEL AND R. D. OLLEMAN, *A.S.T.M. Bull.*, 187 (1953) 56.
10 D. D. LAWTHERS AND M. J. MANJOINE, in *High Temperature Materials*, John Wiley and Sons, New York, 1959, p. 486.
11 R. T. BEGLEY AND W. N. PLATTE, Development of niobium base alloys, *W.A.D.C. Tech. Rept. 57-344, Pt. IV* (April 1960).
12 E. T. WESSEL, L. L. FRANCE AND R. T. BEGLEY, Flow and fracture characteristics of electron-beam melted columbium. Paper presented at *A.I.M.E. Columbium Metallurgy Symposium, Hotel Sagamore, Lake George, New York, June 9–10, 1960.*

PRELIMINARY MEASUREMENTS ON THE THERMAL AND ELECTRICAL CONDUCTIVITIES OF MOLYBDENUM, NIOBIUM, TANTALUM AND TUNGSTEN*

R. P. TYE

Basic Physics Division, National Physical Laboratory, Teddington, Middx. (Great Britain)

(Received October 5th, 1960)

SUMMARY

The thermal conductivity and electrical resistivity of the four metals have been measured to the order of 300°C and the electrical resistivity measurements have been extended to above 1300°C.

The results are presented together with a discussion on the behaviour of the Lorenz function for the materials and some comparison is made with other data at temperatures above 0°C.

As part of the general research programme of the Thermal Properties section of the Basic Physics Division, measurements of the thermal and electrical conductivities of pure metals are being carried out over a wide temperature range. In this instance some measurements of thermal conductivity and electrical resistivity have recently been made from room temperature to approximately 300°C on the four metals which constitute the subject of the conference. The electrical resistivity measurements have been extended to above 1200°C for molybdenum tantalum and tungsten and another sample of niobium for which some results have already been published by POWELL[1].

The materials for the investigation of the properties of pure metals were, in the main, chosen from the Johnson Matthey spectrographically standardized materials. The molybdenum, tantalum and tungsten were such materials, but the niobium was a sample obtained from Murex Ltd., and was of slightly higher purity than the rods of niobium previously measured at N.P.L. The details of the sizes and identification numbers of the materials are given in Table I.

TABLE I

DETAILS OF MATERIALS USED IN THE INVESTIGATION

Material	*Catalogue No.*	*Approximate diam. (mm)*	*Approximate length (cm)*
Mo	JM720	5	15
Nb	—	6	10
Ta	JM615	4·5	10
W	JM740	4	10

* Prepared for the Conference on Niobium, Tantalum, Molybdenum and Tungsten, held in The Department of Metallurgy, The University of Sheffield, September, 1960.

The niobium contained less than 0.1% Ta, 0.01% C, 0.01% Si, 0.01% N_2, 0.01% Fe, 0.015% Ti and 0.01% O_2 and was sintered above 2000°C and cold swaged.

The Johnson Matthey materials were chosen since they could be readily obtained and were reproducible in composition and would thus form a comprehensive series on which physical properties could be measured.

In the first instance experimental determinations of electrical resistivity were made at 20°C and values of 5.65, 14.5 and 5.45 microhm cm^2/cm were obtained for the Mo, Ta and W respectively. These were in fairly good agreement with those values which were stated for these materials in the available literature and showed that what little differences there were could be attributable to small variations in composition or in condition. A value of 15.0 microhm cm^2/cm was obtained for the Nb sample. This is lower than the values of 16.9 and 16.2 microhm cm^2/cm obtained for the other samples of Nb measured at N.P.L. but was still considerably higher than the value of 13.1 at 20°C published in the Metals Handbook for a sample stated to be 'Fansteel' material. It is however only 1.5% lower than the sample measured by TOTTLE[2] for a material of approximately the same purity. On heat treatment to 1450°C the electrical resistivity at 20°C of one of the Nb samples previously reported by POWELL had changed from 16.9 to 17.6 microhm cm^2/cm and the analysis of the material indicated that there had been a small increase in the oxygen content. This is in line with the behaviour found by TOTTLE for increase of electrical resistivity with oxygen content. Thermal conductivity determinations were made by the normal steady state longitudinal flow method used at N.P.L.[3] and indicated in Fig. 1. The sizes of the materials were much smaller than usually required for these measurements and the

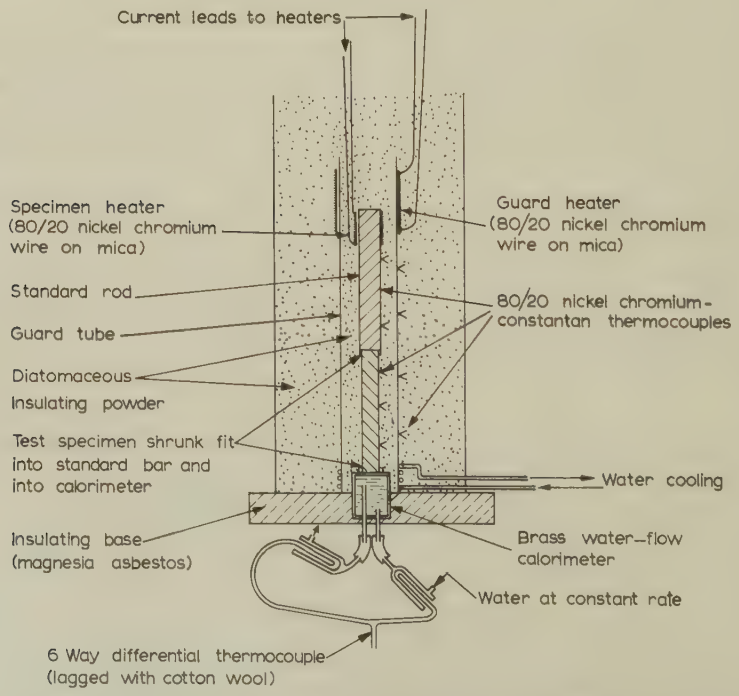

Current leads to heaters
Specimen heater (80/20 nickel chromium wire on mica)
Guard heater (80/20 nickel chromium wire on mica)
Standard rod
80/20 nickel chromium-constantan thermocouples
Guard tube
Diatomaceous insulating powder
Test specimen shrunk fit into standard bar and into calorimeter
Water cooling
Insulating base (magnesia asbestos)
Brass water-flow calorimeter
Water at constant rate
6 Way differential thermocouple (lagged with cotton wool)

Fig. 1. Thermal conductivity apparatus for good conducting materials in rod form.

apparatus had to be adapted for these small rods by joining them to a 1/4 in. diameter rod of Armco iron standard material and decreasing the diameter of the guard tube to 1.5 in. Great care was taken with matching of the gradients in the composite bar and guard tube, and to reduce the radial losses for any small out of match conditions the interspace between the two was packed with an insulation powder of thermal conductivity of 0.000335 J cm/cm² sec deg. C. This is approximately half the value of the diatomaceous earth powder insulant normally used. After correction to the centre of the test material, agreement of better than 2% was obtained between the energy measured in terms of the standard material and that derived from the water flowing at the base of the test sample. Parallel electrical resistivity measurements were made at the same time as the above determinations.

The values of thermal conductivity and electrical resistivity obtained from smooth curves drawn through the experimental points, together with the Lorenz function, their product divided by the absolute temperature, are given in Table II.

TABLE II

VALUES OF THERMAL CONDUCTIVITY, ELECTRICAL RESISTIVITY AND LORENZ FUNCTION FOR Mo, Nb, Ta AND W

Material	*Mean temp. (°C)*	*Thermal conductivity (J cm/cm² sec deg. C)*	*Electrical resistivity (Microhm cm²/cm)*	*Lorenz function × 10⁸ (J ohm/sec deg. C °Abs)*
Mo	50	1.37	6.25	2.66
	100	1.35	7.4	2.68
	200	1.31	9.9	2.74
	300	1.23	12.45	2.68
	350	1.19	13.75	2.63
Nb	50	0.50_5	16.5	2.58
	100	0.51	18.7	2.56
	200	0.52	23.2	2.55
	300	0.53_5*	27.7*	2.58*
Ta	50	0.58_2	15.45	2.78
	100	0.58_5	17.72	2.78
	200	0.58_5	22.25	2.76
	250	0.58_2	24.4	2.71
W	50	1.78	6.1	3.36
	100	1.68	7.3	3.29
	200	1.52	9.8	3.15
	300	1.38	12.45	3.0
	350	1.32	13.7	2.91

* Figures are extrapolated

To extend the electrical resistivity measurements to temperatures above 1200°C and to study the effect of these moderate heat treatments on the properties of the materials, the samples of Mo, Ta and W were in turn assembled with platinum current leads and platinum–platinum/10% rhodium thermocouples insulated in pure sintered alumina tubes to serve for temperature measurement and potential leads. They were then mounted in a horizontal platinum-wound tubular evacuated furnace of sintered alumina and heated uniformly.

Electrical resistivity measurements were taken on heating up to and cooling down from about 1400°C for each material. One of the rods of Nb reported by POWELL at lower temperatures had also been measured to 1450°C previously, resulting in a

change of resistivity. The values for the Mo, Ta and W together with those for the above Nb sample are given in Table III.

TABLE III

VALUES OF ELECTRICAL RESISTIVITY TO HIGH TEMPERATURES FOR Mo, Nb, W AND Ta

Mean temp. (°C)	*Electrical resistivity (microhm cm²/cm)*			
	Mo	*Nb*	*W*	*Ta*
20	5.65	16.9	5.45	14.5
100	7.45	20.5	7.3	17.7
200	9.9	24.8	9.8	22.25
300	12.45	28.6	12.45	27.1
400	15.1	32.5	15.2	31.4
500	17.85	36.0	18.1	35.6
600	20.6	39.4	21.4	39.8
700	23.3	42.9	24.6	44.1
800	26	46.3	27.8	48.1
900	28.7	49.5	30.9	51.7
1000	31.5	52.6	34.3	55.4
1100	34.4	55.8	37.7	59.2
1200	37.2	58.9	41.4	62.9
1300	40.1	62.0	45.1	66.5
1400	43	64.8	49.7	—
1450	44.7	66.5	51.8	—
20(on cooling)	5.65	17.6	5.45	14.5

DISCUSSION OF RESULTS

The results obtained indicate that the molybdenum, tantalum and tungsten rods are stable metals and that the heat treatment given has not affected their thermal properties. The Mo and W are interesting materials in that they have closely similar electrical resistivities up to 400°C but their thermal conductivities differ by 30% at 50°C and 12% at 350°C. From the Lorenz function it would appear that the tungsten has a much higher lattice component of thermal conductivity at normal temperatures, thus giving rise to the higher total conductivity. However, the sharp decrease in this relationship indicates that the component is becoming smaller at the higher temperatures and flattening out towards some constant value, which according to MOTT AND JONES[4] should be higher than the classical theoretical value of 2.45 for a transition metal. This is confirmed to some extent by the results of OSBORN[5] at temperatures higher than those of the above investigation.

There is some data for tungsten at high temperatures but they are based on measurements on fine wires of the material where there are three main difficulties in the measurement. In the first case there is the measurement of the temperature gradient and in the second place the heat lost by radiation is of a comparable order to that actually conducted. Finally, the method requires accurate knowledge of the emissivity and other constants of the material at these high temperatures. Thus the work of WORTHING[6] has been adjusted by FORSYTHE AND WORTHING[7] and LANGMIUR[8] when first a new absolute temperature scale for tungsten was used and secondly a new value for its emissivity was used. The total variation in this work and that of OSBORN

is only of the order of 15% at 1300°C and 30% at 2300°C. The results so far obtained for tungsten are in good agreement with those of KANNULUICK[9] over the limited temperature range he studied and could well link on with those of OSBORN, who also measured electrical resistivity and whose values gave a reasonably constant Lorenz function.

The results for molybdenum would seem to agree with a value by KANNULUICK at normal temperatures, allowing for slight differences in purity. On extrapolation they could link in with the work of LUCKS AND DEEM[10], RASOR AND MCCLELLAND[11] and FIELDHOUSE *et al.*[12] at the temperatures above 500°C, though the results of these workers do diverge at the higher temperatures. The high temperature work does not contain resistivity data and no real guide to the Lorenz function can be obtained. However, using a value from the present work for the resistivity of $43 \cdot 10^{-6}$ microhm m^2/cm together with a value of RASOR AND MCCLELLAND of 0.23 J cm/cm^2 sec deg. C both at 1400°C would give a reasonable figure of $2.5 \cdot 10^{-8}$ Joule ohm/sec deg. C Abs for the Lorenz function. On the other hand, the results of OSBORN at the higher temperature would appear to be decreasing too rapidly to give this order of the Lorenz function.

There is very little data available above 0°C for the properties of tantalum other than a value by BARRATT AND WINTER[13] which has a small negative coefficient over the very small temperature range, and some widely diverging values by WORTHING, RASOR AND MCCLELLAND and FIELDHOUSE *et al.*[14] at high temperatures. The results so far obtained indicated that the Lorenz relationship is reasonably constant and that the metal has a lattice component of the order of 12% over the temperature range studied. Because of the lack of data and the diverging values this is obviously a material for further study at high temperatures.

There is little data on the properties of niobium other than the two quoted elsewhere. It would appear that the properties of this metal are readily affected by small changes in composition, particularly by increase in oxygen content. The samples measured at N.P.L., including the present one, are consistent in that there is a rise in the thermal conductivity accompanied by a corresponding fall in electrical resistivity for increasing purity of the metal. The Lorenz function for the three are of the same order and differ by only 4% from room temperature to 300°C. For the present sample the Lorenz function differs by 13% from TOTTLE's value and the thermal conductivity is lower for a sample of lower electrical resistivity.

Finally, from the behaviour so far of the results for the metals, the Lorenz relationship would seem to serve as a useful basis to use for calculating the thermal conductivity of these metals from values obtained from the relatively simple measurements of electrical resistivity. The work on these and other pure metals is being continued at N.P.L. in order that present discrepancies may be resolved and that accurate data for these physical properties of the elements may be available when required.

ACKNOWLEDGEMENTS

The author is indebted to Messrs. MUREX LTD. for supplying the sample of niobium and to Miss M. J. WOODMAN who assisted with the experimental work. The work has been carried out as part of the research programme of the National Physical Laboratory and this paper is published by permission of the Director of the Laboratory.

REFERENCES

1 R. W. Powell, *J. Inst. Metals*, 85 (1956) 553.
2 C. R. Tottle, *J, Inst. Metals*, 85 (1956) 375.
3 R. W. Powell and R. P. Tye, *Engineer*, 209 (1960) 729.
4 N. F. Mott and H. Jones, *Theory of the Properties of Metals and Alloys*, Oxford University Press, 1936.
5 R. H. Osborn, *J. Opt. Soc. Am.*, 31 (1941) 428.
6 A. G. Worthing, *Phys. Rev.*, 4 (1914) 535.
7 W. E. Forsythe and A. G. Worthing, *J. Astrophys.*, 61 (1925) 146.
8 I. Langmiur, *Phys. Rev.*, 7 (1916) 302.
9 W. G. Kannuluick, *Proc. Roy. Soc. (London)*, 141 (1933) 159.
10 C. F. Lucks and H. W. Deem, *W.A.D.C. Tech. Rept., 55–496* (1956).
11 N. S. Rasor and J. D. McClelland, *W.A.D.C. Tech. Rept. 56–400* (1956).
12 I. B. Fieldhouse, J. C. Hedge, J. I. Lang and J. E. Waterman, *W.A.D.C. Tech. Rept. 55–495 Pt. I* (1955).
13 T. Barratt and R. M. Winter, *Proc. Phys. Soc. (London)*, 26 (1914) 347.
14 I. B. Fieldhouse, J. C. Hedge and T. E. Waterman, *W.A.D.C. Tech. Rept. 55–495 Pt. III* (1955).

THE EFFECT OF OXYGEN ON THE MECHANICAL PROPERTIES OF ZONE-REFINED NIOBIUM*

M. J. LEADBETTER** AND B. B. ARGENT

Department of Metallurgy, University of Sheffield, Yorks. (Great Britain)

(Received October 5th, 1960)

SUMMARY

The yield point behaviour of niobium containing varying quantities of oxygen has been investigated. Oxygen raises the yield stress at 293°K and 77°K. Twinning is observed in zone-melted niobium at 77°K but this is inhibited by oxygen additions.

INTRODUCTION

In recent years much work has been carried out on the plastic deformation and brittle fracture of mild steel[1,2,3]. Little work has however been done on the other body-centred cubic metals. The increasing interest in the refractory metals vanadium, tantalum, molybdenum and niobium, as possible construction materials for gas turbines and certain components in nuclear power plants indicates the need for further investigation of their mechanical properties.

Some work has been done on the mechanical properties of comparatively pure and commercial niobium[5-8], and this has been critically reviewed by JOHNSON[9]. In the present investigation the effect of controlled additions of oxygen (up to 0.1 wt.%) on the mechanical properties of high purity zone-refined niobium has been studied.

EXPERIMENTAL METHODS

Floating-zone melting and refining of niobium by electron bombardment

A sample of high purity niobium was prepared by electron bombardment floating-zone refining. The apparatus used is based on the design of CALVERLY, DAVIS AND LEVER[10], and is contained in a glass chamber evacuated with a 9 in. oil diffusion pump to an ultimate pressure of $1.6 \cdot 10^{-6}$ mm of mercury. The apparent leak rate was 0.3 lusec.

An 8 in. long rod, 0.281 in. in diameter was machined from a sintered bar supplied by Murex Limited. The analysis of this material was (wt.%): Ta, <0.3; O_2, 0.006; Fe, <0.07; W, trace; C, 0.01; Sn, Mo absent.

* Prepared for the Conference on Niobium, Tantalum, Molybdenum und Tungsten, held in The Department of Metallurgy, The University of Sheffield, September, 1960.

** Now at The Steel Company of Wales Limited, Port Talbot, Glamorgan.

The rod was mounted in the apparatus between two pieces of niobium and given one fast pass at 5 in. per hour followed by four refining passes at $1\frac{1}{2}$ in. per hour. The refined niobium was reduced from 0.281 to 0.100 in. diameter using a rotary swage. It was then etched, wrapped in tantalum foil and annealed for 4 h at 1150°C in a mullite tube vacuum furnace at a pressure less than 10^{-5} mm mercury and a leak rate less than $3 \cdot 10^{-3}$ lusec. Small surface defects from the initial swaging were removed with a fine jewellers file, and the 0.100 in. diameter material was swaged to 0.075 in. diameter. It was then etched, re-examined for surface defects and swaged to 0.050 in. diameter. The final material thus had a reduction in area of 75% and gave fairly small grain sizes on recrystallization. To obtain smaller grain sizes a further niobium sample was prepared with 96% reduction in area by omitting the intermediate anneal.

Recrystallization of high purity niobium

ADAMS, ROBERTS AND SMALLMAN[4] found a minimum recrystallization temperature of 1075°C. In attempting to duplicate these results excessive grain growth occurred, probably due to the purity of the present material. The minimum recrystallization temperature for the material which had been deformed 75% was subsequently found to be 930°C. A range of grain sizes was obtained by a combination of different times and temperatures of heat treatment in the range 950°C to 1300°C. Ten grain size counts were made for each set of specimens and it was noted that the grain size varied considerably in the larger grain size specimens; this could not be overcome. Five inch long recrystallized alumina tubes of 1.5 mm internal diameter were used to support the wire test pieces during all heat-treatments. These tubes were outgassed before use by heating to 1300°C for 4 h *in vacuo*. When in use the ends of the tubes were sealed with tantalum foil to getter any oxygen entering the system. Samples which were to have no oxygen additions before mechanical testing were heat-treated inside a niobium tube. Forty test pieces, 3 in. long, were heat treated giving 8 samples of five different grain sizes. The grain sizes are given in Table I.

TABLE I

GRAIN SIZES

Batch number	*Grain size (2d)(cm)*
I	0.027
II	0.019
III	0.013
IV	0.0115
V	0.0055

Anodising niobium

Niobium-oxygen alloys can be obtained by several processes. One of these is the gas absorption and diffusion technique[11]. Another method is the use of master alloys[12]. However, it would be difficult to obtain a range of oxygen contents from 0.01 wt. % to 0.1 wt. % by these methods.

A controlled method of adding very small quantities of oxygen to niobium is to

heat-treat samples coated with an anodic oxide film. Previous workers[13,14] have used air-saturated ammonium borate solution or 70 wt. % nitric acid for anodising niobium.

Adherent second-order films were obtained in the present work using 70 wt. % nitric acid with a platinum gauze cathode and an applied potential of 100 V. Assuming the second order film to be non-porous Nb_2O_5, 5000 Å thick, and that oxygen could be completely diffused into the niobium wire, it was calculated that oxygen pick-up would be in the order of 0.01 wt. % per treatment. Specimens were anodised and then annealed for 4 h at 800°C in a mullite tube vacuum furnace, to allow the oxygen to diffuse into the test pieces. The temperature of 800°C was chosen to be below the recrystallization temperature of niobium.

After the first anodising and diffusion treatment one sample was analysed. This process was repeated five times. Oxygen analyses were carried out using a semi-micro vacuum fusion gas analysis apparatus (see next section). A graph of wt. % oxygen against the number of anodising treatments is shown in Fig. 1. From this it is seen

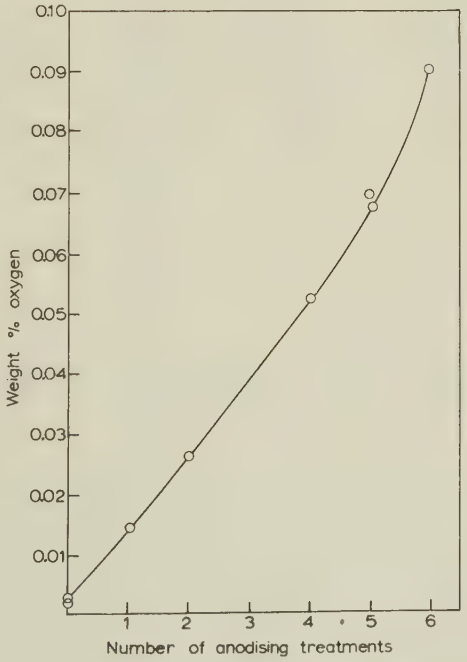


Fig. 1. Oxygen content as a function of the number of anodising treatments for 0.050 in. diameter niobium wire.

that each anodising treatment provides approximately 0.013 wt. % oxygen. Specimens for mechanical testing were given one, three and six anodising/diffusion treatments. In all, 10 zone-refined specimens and 30 specimens containing oxygen were produced. Oxygen analyses for the test pieces are shown in Table II.

Gas analysis

Previous workers have developed apparatus for the analysis of oxygen, hydrogen

TABLE II

Sample	*Lower yield stress (p.s.i. × 10³) (at 293°K)*	*Grain size (cm)*	*Wt. % oxygen*	*Wt. % hydrogen*	*Wt. % nitrogen*
I Ao	14.6	0.027	0.015		
II Ao	9.8	0.019	0.010		
III Ao	10.7	0.013	0.008		
IV Ao	10.2	0.0115	0.009		
V Ao	10.1	0.0055	0.008	0.0003	0.002
I A1	(12.2)	0.027	0.032		
II A1	12.25	0.019	0.020		
III A1	12.0	0.013	0.021		
IV A1	12.6	0.0115	0.021		
V A1	14.9	0.0055	0.030		
I A3	21.9	0.027	0.050	0.0002	0.003
II A3	19.2	0.019	0.041	0.0002	0.003
III A3	19.6	0.013	0.048	0.0004	
IV A3	20.6	0.0115	0.046		
V A3	18.1	0.0055	0.047		
I A6	33.3	0.027	0.088		
II A6	29.3	0.019	0.088		
III A6	33.0	0.013	0.090	0.00035	0.006
IV A6	31.1	0.0115	0.089	0.0004	0.005
V A6	33.0	0.0055	0.097		
Zone-refined material			0.0025		
			0.003		
			0.003		
			0.003		
			0.0035		
			0.004		

and nitrogen in small metal samples[16–20], and the apparatus constructed for this investigation includes many features used by them.

The samples are dissolved in a molten platinum bath contained in a graphite crucible. The blank rate of the apparatus at 1880°C is $< 4\,\mu$/h. Oxygen reacts with carbon to form carbon monoxide and this together with nitrogen and hydrogen is vacuum extracted to the analysis section of the apparatus. The gases are analysed by observing changes in pressure in the analysis system when carbon dioxide and hydrogen are successively removed. These pressures are measured with a double-range McLeod gauge. Oxygen from the samples is extracted as carbon monoxide and is oxidised by Hopcalite (activated manganese dioxide) to carbon dioxide. This can then be removed from the system by the use of a liquid nitrogen trap. Hydrogen is removed from the analysis system by the use of a palladium osmosis tube. This tube is heated to 550°C and hydrogen then diffuses out into the atmosphere. Residual gases are assumed to be nitrogen.

Mechanical testing

A Polanyi type machine was used in the present work. It consists of two rigid rods mounted on a base plate with cross-members at the top holding a beam and a mirror system. A carriage slides on the rigid rods and is driven by a screw thread, which in turn can be driven by a motor through a gear train. 0.050 in. diameter wire specimens

were soldered into grips located in seats on the carriage, and on a stirrup attached to the beam.

The machine is operated at a constant strain rate of $4.5 \cdot 10^{-5}$ sec^{-1} for specimens of $1\frac{1}{2}$ in. gauge length. Two beams were used, one for loads up to 250 lb. and the other for loads up to 750 lb. The deflection of the light beam is nominally proportional to the applied stress. Corrections for the deflection of the beam and grip assembly were applied by substituting a silver steel "rigid" test piece for the sample, and straining this over the required range.

The niobium test pieces were soldered into grips for the Polanyi machine. However, much difficulty was encountered when attempting to "wet" niobium with soft solder. CHURCHMAN[6] dipped the ends of niobium samples into molten copper for 30 sec under vacuum and then into a solder bath. The method used in the present work is the same as that of ADAMS, ROBERTS AND SMALLMAN[4], who shot-blasted the ends of their test-pieces and then electro-plated a 0.025 mm copper layer onto them to allow tinning.

Test-samples of $2\frac{1}{2}$ in. in length were mounted in a special aluminium jig, which allowed a 180° arc of the ends of the sample to be shot blasted whilst being supported from underneath. Following this the samples were degreased with alcohol and petroleum ether to present a clean surface for electro-plating in an acid copper sulphate bath. A jig was used to hold the test-pieces whilst they were being soldered into the grips and during mounting in the Polanyi machine.

Twenty samples were tested at 293°K, and a further twenty at 77°K. Tests were normally stopped at the onset of necking.

SUMMARY OF RESULTS

Typical stress–strain curves at 293° and 77°K for one grain size (0.013 cm diameter) are shown in Figs. 2 and 3. The samples tested at 293°K showed clearly defined yield points and a progressive increase in yield stress with increasing oxygen content.

Room temperature tests

The magnitude of the yield point drop increased with increasing oxygen content (Fig. 2). Table II summarizes the data on lower yield stress, grain size, oxygen, hydrogen and nitrogen content. A duplicate carbon analysis was carried out by the Swinden Laboratories (United Steel Companies) and gave a mean value of 0.006 wt. %. The zone refined niobium had an oxygen content of 0.003 wt. %. During heat treatment this increased to ~0.009 wt. % and this represents an oxygen pick-up of 0.006 wt. % from the dynamic vacuum system and the oxide film formed at room temperature.

The lower yield stress values of the purest samples (0.009 wt. % oxygen) are compared with those of other workers[4,6,9,21] in Table III. The faster strain rates used by them tend to give a higher lower yield stress but the increase would only be of the order 20%[4,22], and thus the lower yield stresses obtained in the present work probably reflect the purity of the material used.

Plots of the lower yield stress values (p.s.i.) *versus* $d^{-\frac{1}{2}}$ (cm$^{-\frac{1}{2}}$) (where d is half the grain diameter) showed much scatter in the case of the higher oxygen contents; the plot for the purest sample (~0.009 wt. % oxygen) is shown in Fig. 4. This shows a very slight positive slope. Only four points were plotted, a value for sample IAo

being omitted as this had an oxygen content of 0.015 wt. % due to pick-up during heat treatment at 1300°C. The value for K_y in PETCH's expression

$$\sigma_y = \sigma_i + K_y d^{-\frac{1}{2}}$$

(where σ_y is the shear stress for yield propagation, σ_i is the shear stress resisting the movement of dislocations across the slip plane after they have been unpinned, K_y is

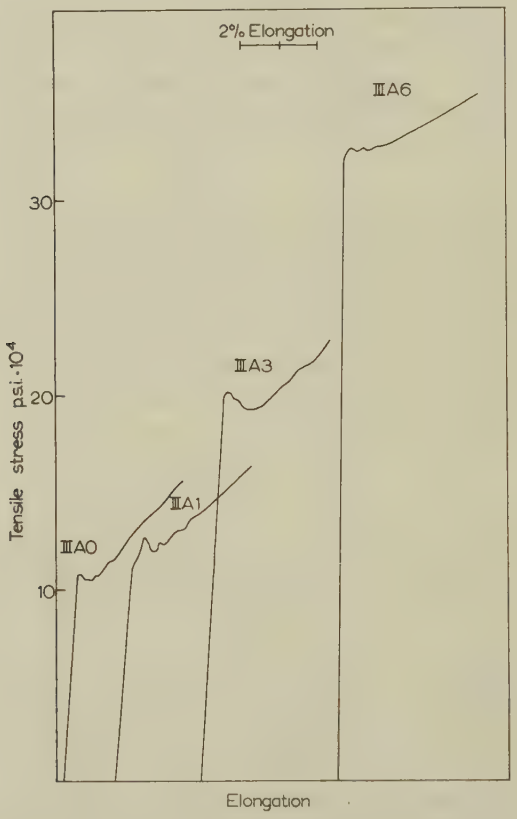


Fig. 2. Stress–strain curves for niobium with varying oxygen content (mean grain diameter 0.013 cm) tested at 293°K.

a measure of the dislocation locking strength, and d is half the grain diameter) was found, by the method of least squares, to be $2.75 \cdot 10^2$ c.g.s. units. The standard error was $4.74 \cdot 10^3$ c.g.s. units. K_y is thus less than that obtained by CHURCHMAN[6] ($3–5 \cdot 10^6$ c.g.s. units), ADAMS, ROBERTS AND SMALLMAN[4] ($2.76 \cdot 10^6$ c.g.s. units), and WILCOX AND HUGGINS[21] ($1.72 \cdot 10^6$ c.g.s. units), and cannot be distinguished from JOHNSON[9] (K_y = zero).

Lower yield stress values are plotted against oxygen for all the test pieces (Fig. 5). The points tend to fall in a band with no obvious dependence on grain size.

TABLE III

Worker	σ_i(*p.s.i.*) *Tensile stress*	*Temperature* (°*K*)	*Strain rate* ($sec^{-1} \times 10^{-4}$)
JOHNSON[9]	25,600	293	0.88
CHURCHMAN[6]	25,000	293	4.2
WILCOX AND HUGGINS[21]	21,700	297	0.8
ADAMS, SMALLMAN AND ROBERTS[4]	20,000	293	2.02
Present work	10,000	293	0.45

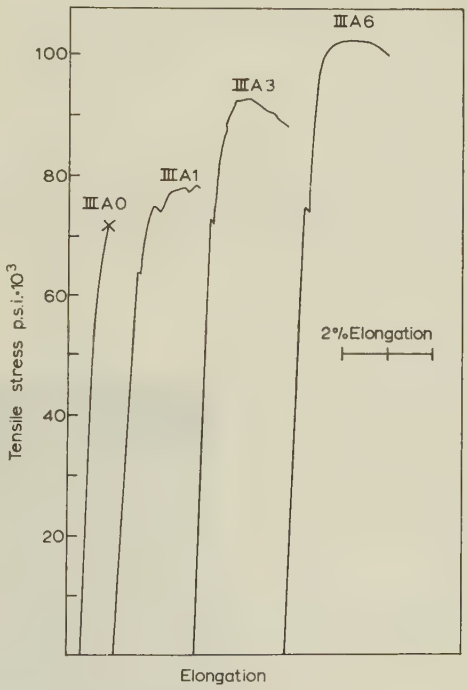


Fig. 3. Stress–strain curves for niobium with varying oxygen content (mean grain diameter 0.012 cm) tested at 77°K.

Tests at 77°K

This series shows a change from twinning to apparent yielding with increasing oxygen content. Seven samples out of ten of the two lowest oxygen contents (series Ao and A1) showed metallographic evidence of twinning. Samples IV A1, V A1, and IV Ao showed no evidence of twinning. Two samples, III Ao and I A1, fractured and twinning was observed throughout the specimens. Fig. 6 shows the fracture in sample III Ao and the associated twinning. Audible clicking was heard at the onset of twinning with samples II Ao, II A1 and III A1. All samples of series A3 and A6 were

examined metallographically for twinning and none was observed. The samples of series A3 and A6 showed a very small apparent yield point which was of an approximately constant value and this is possibly due to the formation of a single Lüders band followed by rapid work hardening. There is a progressive increase in the maximum tensile stress with increase in oxygen content.

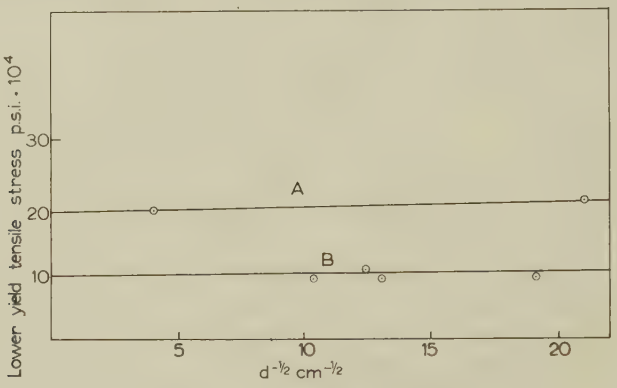


Fig. 4. Lower yield stress as a function of $d^{-\frac{1}{2}}$ for niobium tested at 293°K: A, SMALLMAN (strain rate $2.02 \cdot 10^{-4}$ sec^{-1}); B, present work (strain rate $4.5 \cdot 10^{-5}$ sec^{-1}).

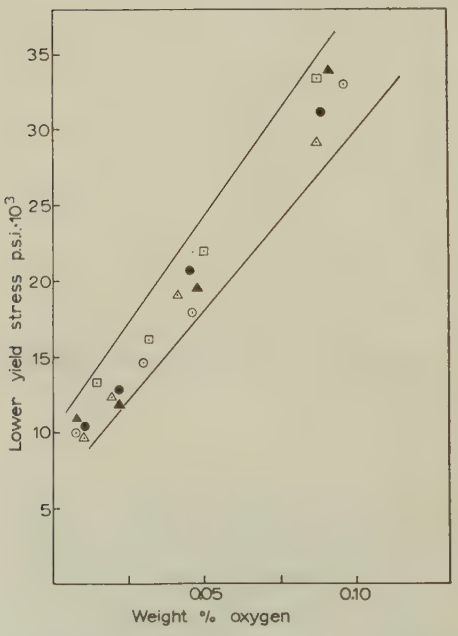


Fig. 5. Lower yield stress as a function of oxygen content for all grain sizes at 293°K: □, grain size I; △, grain size II; ▲, grain size III; ●, grain size IV; ⊙, grain size V.



Fig. 6. Twinning associated with the fracture of a niobium specimen containing 0.008 wt.% oxygen (mean grain diameter 0.013 cm) tested at 77°K. (× 100)

A plot of apparent yield stress against oxygen content is shown in Fig. 7. In the case of samples which fractured the fracture stress is plotted, and for samples which twinned the stress is that at the onset of plastic strain. The tensile values for the A3 and A6 series were taken at the apparent yield stress. There is again much scatter, but the apparent tensile stress for yielding increases at first, and then remains at an approximate constant value. However, the maximum stress continues to increase.

Samples with a high oxygen content have a higher yield stress than low oxygen samples and thus might be expected to twin more readily. However, it appears that the purer the sample, the more readily twinning occurs.

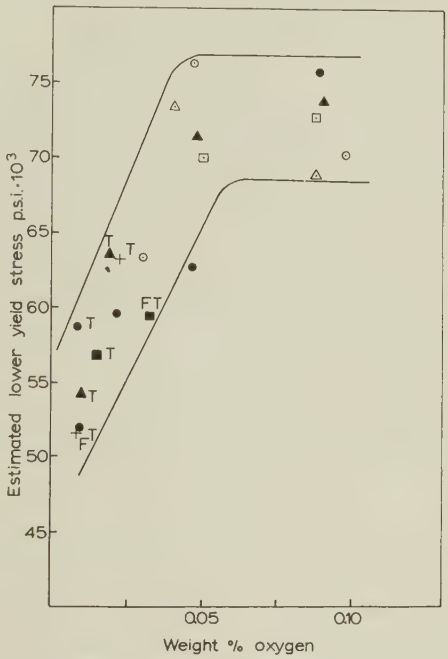


Fig. 7. Lower yield stress as a function of oxygen content for all grain sizes at 77°K. (F indicates fracture, T indicates twinning): □, grain size I; +, △, grain size II; ▲, grain size III; ●, grain size IV; ⊙, grain size V.

ACKNOWLEDGEMENTS

The authors would like to thank the United Kingdom Atomic Energy Authority for financial assistance, Murex Limited for the gift of some high purity niobium, the Swinden Laboratories of the United Steel Companies for assistance with the carbon analysis, and Prof. A. G. Quarrell for his encouragement.

REFERENCES

1 A. H. Cottrell, *Trans. A.I.M.E.*, 212 (1958) 192.
2 J. Codd and N. J. Petch, *Acta Met.*, 3 (1955) 186.
3 A. Cracknell and N. J. Petch, *Acta Met.*, 3 (1955) 186.
4 M. A. Adams, A. C. Roberts and R. E. Smallman, Yield and fracture in polycrystalline niobium, *U.K.A.E.A. Rept. A.E.R.E. M/R 2530* (1959).

[5] C. R. TOTTLE, *J. Inst. Metals*, 85 (1956–57) 375.
[6] A. T. CHURCHMAN, *J. Inst. Metals*, (1960) 221.
[7] E. T. WESSEL AND D. D. LAWTHERS, *The Ductile-to-Brittle Transition in Niobium*, Symposium on Columbium, Electrochemical and Metallurgy Div. of the Electrochemical Society, Washington, D.C., May, 1958.
[8] B. F. DYSON, R. B. JONES AND W. I. MCG. TEGART, *J. Inst. Metals*, 87 (1958–59) 340.
[9] A. A. JOHNSON, *J. Less-Common Metals*, 2 (1960) 241.
[10] A. CALVERLEY, M. DAVIS AND R. F. LEVER, *J. Sci. Instr.*, 34 (1957) 142.
[11] A. V. SEYBOLT, *Trans. A.I.M.E.*, 200 (1954) 774.
[12] R. P. ELLIOTT, *Am. Soc. Metals Preprint No. 143* (1959).
[13] L. YOUNG, *Trans. Faraday Soc.*, 52 (1956) 502.
[14] H. A. JOHANSEN, G. B. ADAMS AND P. VAN RYSSELBERGHE, *J. Electrochem. Soc.*, 104 (1957) 339.
[15] R. D. MISCH AND W. E. RUTHER, *J. Electrochem. Soc.*, 100 (1953) 531.
[16] J. N. GREGORY AND D. MAPPER, *Analyst*, 78 (1953) 414.
[17] J. N. GREGORY AND D. MAPPER, *Analyst*, 80 (1955) 225 and 230.
[18] E. BOOTH, F. J. BRYANT AND A. PARKER, *Analyst*, 82 (1957) 50.
[19] D. F. WOOD AND D. A. WILLIAMS, *I.C.I. Report*, MD/RR/160/57.
[20] Springfield Laboratories, U.K.A.E.A., Private communication.
[21] B. A. WILCOX AND R. A. HUGGINS, *J. Less-Common Metals*, 2 (1960) 297.
[22] E. S. TONKIN AND R. MADDIN, *Univ. Penn. Tech. Rept. No. 2, No. NR 511 (19)*, School of Metallurgical Engineering, University of Pennsylvania, Philadelphia 4, July 16, 1956.

ÜBER DAS VANADIN(III)-OXYDCHLORID VOCl

HARALD SCHÄFER UND FRIEDEL WARTENPFUHL

Anorganisch-Chemisches Institut der Universität Münster (Deutschland)

(Received October 24th, 1960)

ZUSAMMENFASSUNG

Für Vanadin(III)-oxydchlorid VOCl wurde in der Umsetzung von V_2O_3 mit VCl_3 im Temperaturgefälle eine Darstellungsweise gefunden, die wohlausgebildete Kristalle liefert.
Angaben über das chemische, thermische und magnetische Verhalten des VOCl und über seine Struktur werden mitgeteilt.
VOCl ist mit der Reaktion $VOCl + 2\ VCl_4(g) = VOCl_3(g) + 2\ VCl_3(g)$ im Temperaturgefälle transportierbar.
Für thermodynamische Rechnungen werden die Werte $\Delta H(VOCl) = -149$ kcal und $S(VOCl) = 19$ cal empfohlen.

SUMMARY

VOCl can be prepared in well-shaped crystals in a temperature gradient. Some information is given about the chemical, thermal and magnetic behaviour of VOCl and its structure.
VOCl can be transported in a temperature gradient by means of the reaction $VOCl + 2\ VCl_4(g) = VOCl_3(g) + 2\ VCl_3(g)$.
For thermodynamic calculations the values $\Delta H(VOCl) = -149$ kcal and $S(VOCl) = 19$ cal are recommended.

Die Entstehung des Vanadin(III)-oxydchlorids VOCl ist schon mehrfach beobachtet worden. Im Rahmen einer eindrucksvollen Studie über Vanadinverbindungen erhielt ROSCOE[1] die Verbindung VOCl beim Erhitzen eines $VOCl_3$-H_2-Stromes

$$VOCl_3(g) + H_2 = VOCl(f) + 2\ HCl \qquad (1)$$

als leichtes, flockiges, braunes Pulver. Später gewannen RUFF UND LICKFETT[2] VOCl als braunen kristallinen Rückstand, als sie VCl_3 4 Stunden im trockenen CO_2-Strom auf etwa 700°C erhitzten,

$$3\ VCl_3(f) + CO_2 = VOCl + 2\ VCl_4(g) + CO \qquad (2)$$

WEDEKIND UND HORST[3] stellten VOCl auf gleichem Wege her und ermittelten die Dichte zu 2.824 g/cm³ bei 16°C. Schliesslich beobachteten EHRLICH UND SEIFERT[4], dass beim Erhitzen vom VCl_3 im Sauerstoff-haltigen Stickstoffstrom oberhalb 300° (neben anderen Produkten) VOCl entsteht, vermutlich nach Gl. (3)

$$3\ VCl_3 + 1/2\ O_2 = VOCl + 2\ VCl_4(g) \qquad (3)$$

und dass $VOCl_2$ im reinen N_2-Strom bei 300°C nach Gl. (4) disproportioniert

$$2\ VOCl_2 = VOCl + VOCl_3(g) \qquad (4)$$

Die Autoren ermittelten die Gitterkonstante der Verbindung und als pyknometrische Dichte 3.22 g/cm³.

Die *eigenen Untersuchungen* stehen im Zusammenhang mit Studien über Oxydchloride der Übergangsmetalle[5,6,7]. Sie betreffen vor allem die Gewinnung wohlausgebildeter VOCl-*Kristalle* durch *Transport im Temperaturgefälle*[8] und die thermodynamischen Grössen der Verbindung.

DARSTELLUNG VON VOCl

Als Ausgangssubstanzen dienen VCl_3, dargestellt[9] durch Umsetzung von V_2O_5 mit S_2Cl_2, und V_2O_3, das durch Reduktion von V_2O_5 mit H_2 gewonnen wird[9]. Beide Stoffe werden nach Gl. (5) miteinander umgesetzt,

$$V_2O_3 + VCl_3 = 3\ VOCl \qquad (5)$$

Ein Quarzrohr mit etwa 180 mm Länge und 15 mm Durchmesser wird unter Ausschluss von Luftfeuchtigkeit mit 2 g VCl_3 und 1 g V_2O_3 beschickt, hochevakuiert und abgeschmolzen. Das Rohr wird 1 bis 2 Tage so in ein Temperaturgefälle gelegt, dass sich die Ausgangssubstanz bei 720°, die leere Rohrhälfte aber bei 620°C befindet. Nimmt man nach dieser Zeit das Rohr aus dem Ofen, so sieht man in der Mitte des Rohres ein dichtes Haufwerk rotbrauner, bis zu 5 mm langer VOCl-Kristalle. Feinkristallisiertes VOCl liegt ausserdem als dichte, braune Masse in der 720°-Hälfte. An verschiedenen Stellen des Rohres befinden sich ferner pfirsichblütenfarbige Kristallblättchen von VCl_3, sowie in geringer Menge gelbe Tropfen von $VOCl_3$, rotbraune Tropfen von VCl_4 und grüne Kristalle von VCl_2.

Zur Isolierung des VOCl wird das Rohr unter trockenem Stickstoff geöffnet und evakuiert, wobei sich $VOCl_3$ und VCl_4 verflüchtigen. Dann wird der Inhalt des Reaktionsrohres zur Auflösung von VCl_2 und VCl_3 mehrfach mit Dimethylformamid aufgeschwemmt und dekantiert. Die ungelöst bleibenden VOCl-Kristalle werden mit Alkohol und Äther gewaschen und im Vakuum getrocknet.

Analyse. V massanalytisch mit $FeSO_4$ gegen N-Methyldiphenylaminsulfosäure, nach Voroxydation mit $KMnO_4$. Cl argentometrisch gegen N-Methyldiphenylaminrot.

gefunden : 49.6% V; 34.8% Cl
berechnet für VOCl: 49.75% V; 34.62% Cl

STRUKTUR UND MAGNETISCHES VERHALTEN

Das Debye-Scherrer-Diagramm des VOCl entspricht weitgehend demjenigen des TiOCl[6]; die Verbindungen sind isotyp, wie schon EHRLICH UND SEIFERT feststellten. VOCl kristallisiert demnach rhombisch in der Raumgruppe D_{2h}^{13}. Die Bestimmung der Gitterkonstanten ergab

$$a = 3.78\ Å;\ b = 3.30\ Å;\ c = 7.91\ Å;\ z = 2;\ \text{Röntgendichte} = 3.45\ g/cm^3$$

Die Gitterkonstanten wurden an einer mit CaF_2 geeichten Aufnahme bestimmt. Sie

stimmen innerhalb der Messgenauigkeit mit den Angaben von EHRLICH UND SEIFERT überein. Die pyknometrische Dichte ermittelten wir zu D = 3.44 g/cm³ bei 25°C. Sie entspricht der Röntgendichte und liegt wesentlich höher, als die mit 2.82 und 3.22 g/cm³ von früheren Autoren pyknometrisch bestimmte Dichte. Es hängt dies damit zusammen, dass die früheren Präparate relativ feinteilig waren, während unser im Temperaturgefälle transportiertes VOCl in gut ausgebildeten Kristallen vorliegt (Abb. 1).



Abb. 1. Vanadin oxydchlorid VOCl. Länge der Kristalle bis 5 mm.

VOCl ist paramagnetisch mit einem zwischen 90 und 295°K wenig von der Temperatur abhängigen Wert[10] von x(Mol) $= 255 \cdot 10^{-6}$. Das Curie'sche Gesetz ist also nicht erfüllt und der für isolierte V^{3+}-Ionen erwartete Wert wird bei weitem nicht erreicht. Ähnlich verhält sich V_2O_3[11]. Auch bei den entsprechenden Titanverbindungen TiOCl und Ti_2O_3 liegt Antiferromagnetismus vor[6].

WEDEKIND UND HORST fanden für x(Mol, VOCl) einen rund elf-fach grösseren Wert, der vermutlich auf den stark gestörten Gitterbau und auf Unreinheit des Präparates zurückzuführen ist. Dessen schon erwähnte, sehr niedrige Dichte gibt einen weiteren Hinweis hierfür.

CHEMISCHES UND THERMISCHES VERHALTEN

Über das Verhalten von VOCl-Kristallen bei Reagenzglasversuchen orientiert die folgende Tabelle. Die Dauer der Reagenzeinwirkung betrug bis zu 24 Stunden.

Beim *Erhitzen von VOCl im Hochvakuum* findet Zersetzung statt: 0.1 g VOCl wurden im Quarzrohr an der Diffusionspumpe ($< 10^{-5}$ Torr) bei stetig ansteigender Temperatur erhitzt. Die Temperatur stieg in 3 Stunden von 540 auf 650°C. Bei 620° trat ein plötzlicher Druckanstieg ein; es entstand VCl_3, das sich am kälteren Rohrende niederschlug, und es verblieb ein oxydischer Rückstand. Eine Sublimation von VOCl trat nicht ein.

TABELLE I

CHEMISCHES VERHALTEN VON VOCl

Reagenz	*Verhalten bei 20°C*	*Verhalten beim Kochen*
H_2O	keine sichtbare Reaktion	keine sichtbare Reaktion
HCl konz.	keine sichtbare Reaktion	keine sichtbare Reaktion
HNO_3 konz.	langsam gelöst; grüne Lösung	schnell gelöst[a]; gelbe Lösung
H_2SO_4 konz.	keine sichtbare Reaktion	schnell gelöst
Königswasser	schnell gelöst	sehr schnell gelöst
HF 40%	keine sichtbare Reaktion	sehr langsam gelöst; grüne Lösung
HF + HNO_3 (1 + 1)	sehr schnell gelöst	
HF + Fe^{3+} + H_2SO_4	keine sichtbare Reaktion	
H_2SO_4 + H_2O_2 (1 + 1, je 10%ig)	sehr heftige Reaktion; tief gelbe Lösung	
$KMnO_4$ in verd. H_2SO_4	wird gelöst	schnell gelöst
$K_2Cr_2O_7$ in verd. H_2SO_4	sehr langsam gelöst	langsam gelöst
$Ce(SO_4)_2$ in verd. H_2SO_4	sehr langsam gelöst	langsam gelöst
NH_3-Lsg. konz.	keine sichtbare Reaktion	keine sichtbare Reaktion
NaOH, 2 *n*	keine sichtbare Reaktion	keine sichtbare Reaktion

[a] wird auch von ROSCOE[1] angegeben.

Wird VOCl (0.1 g) in ein hochevakuiertes Quarzrohr (Vol. 10 cm^3) *eingeschmolzen* und das Rohr im Temperaturgefälle 800/700°C erhitzt, so liegt nach 15 Stunden ein Teil des VOCl unverändert am Ausgangsort in der 800°-Zone. Ein anderer Teil ist in die 700°-Zone gewandert und hat sich dort in Kristallen abgeschieden. Schliesslich ist auch ein Anteil des VOCl zerfallen, denn nach dem Abkühlen des Rohres findet man VCl_3-Kristalle und braune Flüssigkeitstropfen ($VOCl_3$, VCl_4).

Diese Beobachtungen finden zwanglos ihre Erklärung dadurch, dass VOCl bei den verwendeten Temperaturen noch keinen merklichen Sättigungsdruck besitzt, dass es jedoch durch reversible Einstellung der Reaktion

$$VOCl + 2\ VCl_4(g) = VOCl_3(g) + 2\ VCl_3(g) \qquad (6)$$

im Temperaturgefälle transportiert werden kann. Die für den Transport notwendigen gasförmigen Chloride entstehen als Folge des zunächst eintretenden, teilweisen VOCl-Zerfalls.

THERMOCHEMIE DES VOCl

Man kann sowohl die Bildungsenthalpie als auch die Normalentropie des VOCl mit brauchbarer Genauigkeit abschätzen: Wir betrachten die formale Reaktionsgleichung

$$\alpha\text{-}Fe_2O_3 + 2\ VOCl = V_2O_3 + 2\ FeOCl \qquad (7)$$

Wird der Born–Haber'sche Kreisprozess zur Berechnung der Bildungsenthalpien der Verbindungen angewendet, so ergibt sich die Reaktionsenthalpie als Differenz der Gitterenergien. Diese werden auf beiden Seiten der Reaktionsgleichung jedoch ungefähr übereinstimmen, da die Oxyde Fe_2O_3 und V_2O_3 einerseits, und die Oxydchloride VOCl und FeOCl andererseits, im gleichen Gittertyp mit nahe übereinstimmenden

Abmessungen kristallisieren. Man setzt daher ΔH(Reakt.) = Null[12] und erhält mit $\Delta H(Fe_2O_3) = -196.5$ kcal[13], $\Delta H(V_2O_3) = -296.1$ kcal[14] und ΔH(FeOCl) = —99.0 kcal[5], schliesslich ΔH(VOCl) = —149 kcal*.

Dieser Wert gibt gemeinsam mit der geschätzten Normalentropie S(VOCl) = 19 ± 2 cal alle beobachteten Bildungs- und Reaktionsweisen des VOCl richtig wieder. Dies gilt insbesondere auch für seine Entstehung aus V_2O_3 und VCl_3 (*f*) für den thermischen Zerfall in V_2O_3 und VCl_3 (*g*) sowie für den VOCl-Transport im Temperaturgefälle. Bis Messwerte vorliegen, darf die Verwendung der genannten Werte für VOCl daher empfohlen werden.

LITERATUR

1 H. E. Roscoe, *Ann. Chemie Pharm.*, Suppl. 6 (1868) 77, 113.
2 O. Ruff und H. Lickfett, *Ber.* 44 (1911) 506, 518.
3 E. Wedekind und C. Horst, *Ber.* 45 (1912) 262.
4 P. Ehrlich und H. J. Seifert, *Z. anorg. allgem. Chem.*, 301 (1959) 282.
5 H. Schäfer, F. E. Wittig und M. Jori, *Z. anorg. allgem. Chem.*, 287 (1956) 61. (FeOCl)
6 H. Schäfer, E. Weise und F. Wartenpfuhl, *Angew. Chem.*, 69 (1957) 479; *Z. anorg. allgem. Chem.*, 295 (1958) 268. (TiOCl)
7 H. Schäfer und F. Wartenpfuhl, *Z. anorg. allgem. Chem.*, im Druck. (CrOCl)
8 Hierüber wurde in Vorträgen (z.B. in Graz und Wien, November 1958) bereits berichtet.
9 G. Brauer, *Handbuch der Präparativen Anorganischen Chemie*, Enke, Stuttgart, 1954.
10 Die Korrektur für die diamagnetischen Anteile ist mit x(Mol) = $-50 \cdot 10^{-6}$ berücksichtigt. Die Abhängigkeit von der Feldstärke war nur sehr gering; es wurde auf H ∞ extrapoliert.
11 W. Klemm und E. Hoschek, *Z. anorg. allgem. Chem.*, 226 (1936) 359.
12 Weitere Beispiele für die Anwendbarkeit dieser Rechenweise vgl. Ref. 6 sowie H. Schäfer und F. Kahlenberg, *Z. anorg. allgem. Chem.*, 294 (1958) 242.
13 F. D. Rossini, D. D. Wagman und Mitarb., *Selected Values of Chemical Thermodynamic Properties*, Washington, 1952.
14 L. Brewer, *Chem. Rev.*, 52 (1953) 1.

* Die entsprechende Überlegung mit der formalen Reaktion

$$Ti_2O_3 + 2\ VOCl = V_2O_3 + 2\ TiOCl$$

führt zum gleichen Ergebnis.

THE CONSTITUTION OF THE CHROMIUM–NIOBIUM–SILICON SYSTEM

H. J. GOLDSCHMIDT AND J. A. BRAND

The B.S.A. Group Research Centre, Kitts Green, Birmingham (Great Britain)

(Received November 8th, 1960)

SUMMARY

The constitutional diagram of the alloy system Cr–Nb–Si has been investigated for a 1000°C section, as well as some of the properties of the alloys. X-ray diffraction analysis has been used upon argon arc melted alloys. Some modifications are proposed to the known Cr–Si binary system. (The Nb–Si side had already been dealt with in a previous paper, the Cr–Nb side in a concurrent one.) The ternary diagram presented is highly complex, involving, in addition to eleven phases of binary origin, five new ternary compounds; three of the latter possess considerable homogeneity ranges: one is a new Laves phase, another a βNb_5Si_3 isomorph, stabilised to lower temperatures through Cr addition.

Melting points and oxidation resistance of the alloys are given, and the latter property, though limited to a 1000°C, 1-h survey, indicates promising areas for further study.

INTRODUCTION

The present study forms part of a wider programme of constitutional investigations in this laboratory relating to high-temperature resisting alloys, the results of which have been previously reported. In particular, silicides became of interest, besides carbides and intermetallic compounds, as they were found as integral phases in certain alloys of this kind. The study of the Fe–Nb–Si system[1] partly had its origin in the need for identifying such phases and determining their equilibria[2–5]. The Cr–Nb–Si system may be regarded as an obvious companion to this, in view of the presence, generally, of chromium as major element in such alloys, quite apart from the fundamental metal physics interest of the phase relationships, and from the aspect of niobium- and of chromium-base alloys.

No previous work on this ternary system has, to our knowledge, been done, although the binaries Cr–Nb, Cr–Si and Nb–Si have been studied, as will be discussed below. The present work dealt with the 1000°C equilibrium of this system.*

EXPERIMENTAL

The alloys were prepared from spectroscopically standardised high-purity chromium, niobium and silicon supplied by Messrs. Johnson Matthey Ltd. Apart from about 0.2% Ta in the niobium, there were no significant impurities. Weighed lumps of the elements were melted together in a laboratory tungsten electrode arc furnace under

* A broader survey in regard to the subject matter of this paper has been presented recently[18].

an atmosphere of argon, purified by the prior melting of a titanium button. The ingots were remelted several times to secure homogeneity, and annealed in the arc furnace at a temperature below the solidus, to remove coring effects. It was found that ingots prepared in this way had generally lost less than $\frac{1}{2}\%$ in weight, so chemical analysis was not normally performed. However in cases where a greater weight loss occurred and in critical regions of the diagram, chemical analysis was used to confirm the compositions.

Small pieces (about 0.25 g) of the alloys were annealed in evacuated silica capsules at 1000°C for a period of two weeks. By using lumps rather than powders any chance of contamination by SiO vapour was greatly reduced, the centre of the small pieces being powdered and used for X-ray examination after the anneal. The alloys were examined by normal Debye–Scherrer techniques using a 9 cm powder camera and Co $K\alpha$ radiation ($\lambda = 1.78529$ kX), except in special cases when Cr or Cu radiation was substituted.

THE BINARY SYSTEMS

The chromium–silicon system

No completely satisfactory diagram of this binary system exists, although BORÉN[6], KURNAKOV[7], and KIEFFER, BENSOVSKY AND SCHROTH[8] have mapped out the main features, agreeing on the existence of three intermetallic compounds Cr_3Si, CrSi and $CrSi_2$. These authors do not however report any homogeneity range for these compounds, nor do they agree on the composition of a fourth compound between Cr_3Si and CrSi. HANSEN[9] deliberately omits this range from his diagram (based mainly on

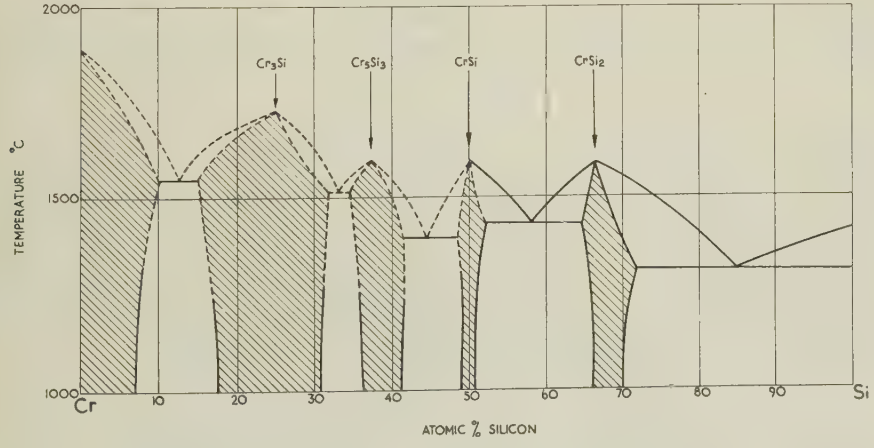


Fig. 1. Proposed chromium–silicon diagram incorporating modifications by present work.

the work of KURNAKOV AND KIEFFER *et al.*) and suggests the possibility that high and low temperature phases may exist. PARTHÉ and co-workers[10], using single crystal techniques, found a tetragonal unit cell for a compound they first considered to be Cr_3Si_2 but later decided was Cr_5Si_3, though pointing out that its composition range included Cr_3Si_2. Atomic positions were described similar to those found by ARONSSON[11]

for W_5Si_3; this structure type occurs frequently in transition metal silicides: Mo_5Si_3, V_5Si_3 and the high-temperature allotropes of Nb_5Si_3 and Ta_5Si_3 also have this structure.

In the present work these main features were confirmed; in addition, information regarding the solubilities of the phases for Cr and Si at 1000°C was obtained. Fig. 1 gives the new phase diagram obtained by modifying the previous ones in accordance with the present results.

About 7.5 at. %-silicon is dissolved substitutionally in the primary b.c.c. chromium lattice, causing a decrease in lattice constant from 2.8790 to 2.8768 kX. With increasing silicon content a phase with the β-tungsten (A15) type of structure appears, which has a homogeneity range from about 18 to 31% Si*; this evidently corresponds to the Cr_3Si phase. The lattice dimensions decrease from 4.567 kX to 4.554 kX with increasing silicon content.

The next phase extends from 36 to 41% Si and thus encompasses both compositions Cr_5Si_3 and Cr_3Si_2; the structure was confirmed to be that of W_5Si_3. A small contraction in lattice dimensions occurs with increasing silicon content. Additional photographs after anneals at 1400°C (1 h) and 800°C (6 weeks) and of the unannealed ingot all showed the same pattern, and it was concluded that this phase is stable throughout, up to its melting point.

The next phase occurs at the composition CrSi, and here no solubility range could be observed. The structure was confirmed to be that of FeSi (B20) and the lattice constant was 4.620 kX.

$CrSi_2$ was confirmed to have the hexagonal C40 type structure, also possessed for example by $NbSi_2$; the lattice dimensions ranging from $a = 4.427$, $c = 6.356$ to $a = 4.419$, $c = 6.350$ kX with increasing Si content indicate a range of compositions of a few percent.

No change in spacing of the silicon phase when in equilibrium with $CrSi_2$ was observed, and it was concluded that chromium has negligible solubility in silicon.

The niobium–silicon system

This system was discussed in the earlier report[1] on the Fe–Nb–Si ternary system, from which Fig. 2 is taken (KNAPTON's[12] diagram, with which the authors substantially agree). Briefly, the compounds occurring are: $NbSi_2$ with the C40 structure, Nb_5Si_3, existing in two allotropic forms, α and β, with the change point at around 2000°C, and Nb_4Si. The latter does not appear to be stable much below its melting point, but is liable to be retained metastably even after a prolonged heat-treatment at 1000°C. (A fuller discussion on Nb_4Si stability is contained in ref. 1.)

Silicon possesses a solubility of 2 to 3% in pure niobium at 1000°C.

The chromium–niobium system

This binary system was redetermined by the authors and is being reported concurrently as part of their work on the Cr–Nb–Mo system[13] which may be referred to for details, including the diagram. A phase "Cr_2Nb" exists, with the cubic Laves structure of Cu_2Mg type and a homogeneity range of about 5% at 1000°C. The mutual primary solubilities of chromium and niobium are restricted, as shown, increasing

* All compositions in this paper will be given as atomic %, unless otherwise stated.

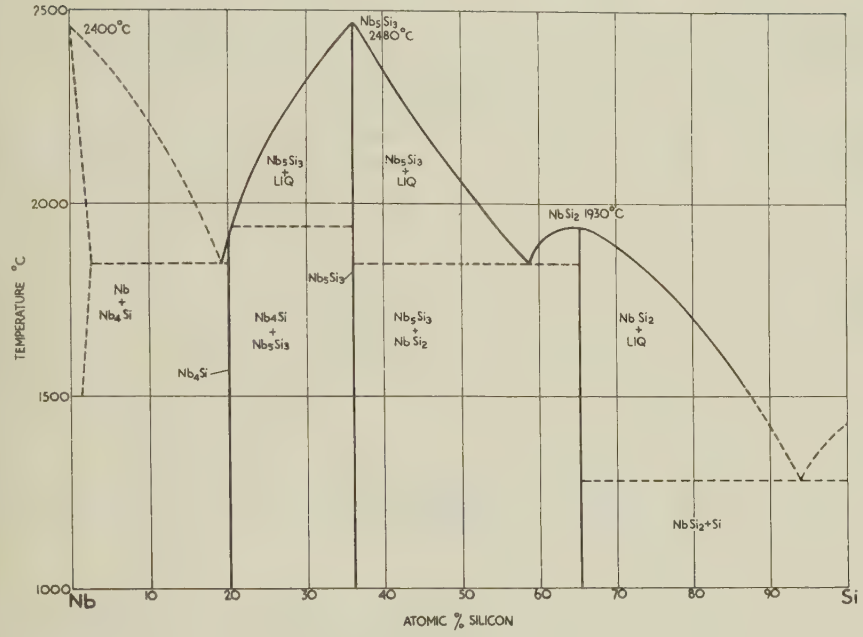


Fig. 2. The niobium–silicon diagram according to KNAPTON.

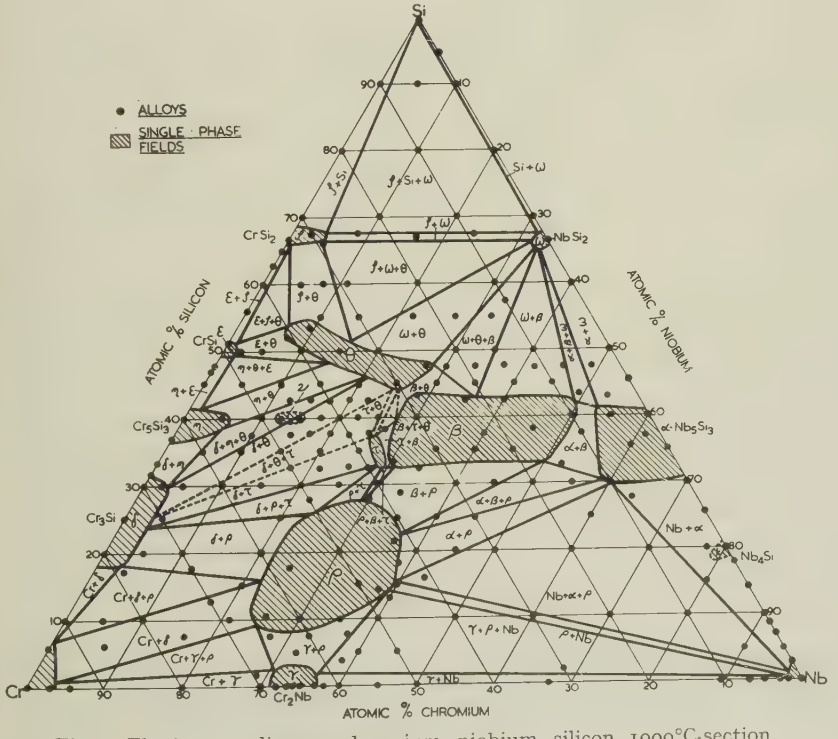


Fig. 3. The ternary diagram chromium–niobium–silicon, 1000°C, section.

with temperature; the capacity for precipitation hardening is thus given, both out of Cr and Nb.

THE TERNARY FIELD

In view of the number of intermediate compounds occurring in the binary systems, a highly complex ternary field is only to be expected. The full diagram derived is shown in Fig. 3. In addition to the eleven binary phases (including the metastable Nb_4Si), five ternary phases appear which are believed not to have been previously reported. Their positions may be seen in Fig. 3. Two of these compounds have well known structures, namely "ϱ" the hexagonal Laves type, and "β" the W_5Si_3 ($=\beta Nb_5Si_3$) type; the structures of the remaining three ternary compounds (θ, τ and ν) are believed to be new. Interplanar spacings of these phases are given in the Appendix.

Special points of interest in the system were the pseudo-binary sections $CrSi_2 \rightleftharpoons NbSi_2$ and $Cr_5Si_3 \rightleftharpoons Nb_5Si_3$. $CrSi_2$ and $NbSi_2$ are both isomorphous to the C40 structure type, and a complete series of solid solutions was in principle possible. It was found however that the two phases were in equilibrium with each other, and only a limited intersolubility existed. This result had been predicted by KIEFFER AND BENESOVSKY[14] by comparison with the $TaSi_2$–$CrSi_2$ system and is a result of the size disparity between Cr and Nb atoms.

In the $Cr_5Si_3 \rightleftharpoons Nb_5Si_3$ pseudo-binary system a rather more complicated situation occurs. As mentioned, Nb_5Si_3 exists in two allotropic forms[12,15]: α at temperatures up to about 2000°C, and β stable at higher temperatures. Cr_5Si_3 has the same structure as βNb_5Si_3. A further "Nb_5Si_3" phase ($D8_8$ structure) also exists, but is only stabilised by impurities such as carbon. At 1000°C αNb_5Si_3 has a considerable solubility for Cr, Nb and Si, but with increased Cr the ternary phase "β" with the βNb_5Si_3 structure appears at about 20–25% Cr_5Si_3. Thus Cr has the effect of stabilising the β form of Nb_5Si_3 down to at least 1000°C to give a ternary single-phase field of considerable extent. Representative β compositions are: $Cr_2Nb_3Si_3$ and $CrNb_2Si_2$. Between β and Cr_5Si_3 two further new intermetallic compounds occur. One of these (τ) has the approximate composition $Cr_{37}Nb_{27}Si_{36}$. It has a b.c.c. lattice with a spacing of 8.11 kX. The second phase (ν) has the approximate composition $Cr_{45}Nb_{15}Si_{40}$. ν does not fit into the general pattern of phase equilibria, but appears to be metastably retained in a haphazard fashion over a certain composition region (resulting in some uncertainty in the phase diagram in this part, see Fig. 3). At the composition quoted, the ν phase appeared pure and is stable up to its melting point. Since it gave only a poor powder photograph, indexing was impossible.

A further new ternary phase (θ) occurs at about 50% Si, with a range of compositions of from 6 to 28% Nb (representative empirical formula: $Cr_7Nb_3Si_{10}$). Single crystal photographs were used to derive an orthorhombic unit cell with $a = 15.82$, $b = 4.90$, $c = 7.51$ kX. The space group is either Ibam or Iba2. A structural investigation is in progress, but already the projection perpendicular to the b axis shows that the phase can be regarded as having a stoichiometric composition $Cr_3Nb_2Si_6$, lying outside the single θ phase region, at any rate for 1000°C equilibrium.

The remaining ternary compound ϱ is the hexagonal Laves phase of Zn_2Mg type which is isomorphous with the ϱ-phase Fe_2Nb found in the iron–niobium system[1]. This ternary compound starts replacing the cubic Laves phase Cr_2Nb at a silicon content of 2.5%, and has a considerable solubility for all three of the primary ele-

ments. It is interesting to note that the area covered by the two Laves phases in the present system corresponds fairly closely to that covered by the Laves phase in the Fe-Nb-Si system[1]. Since the Cr and Fe atoms are of approximately equal size, this suggests that the size-factor is the governing one in deciding Laves phase occurrence and extent, but electron concentration will influence which type of Laves phase

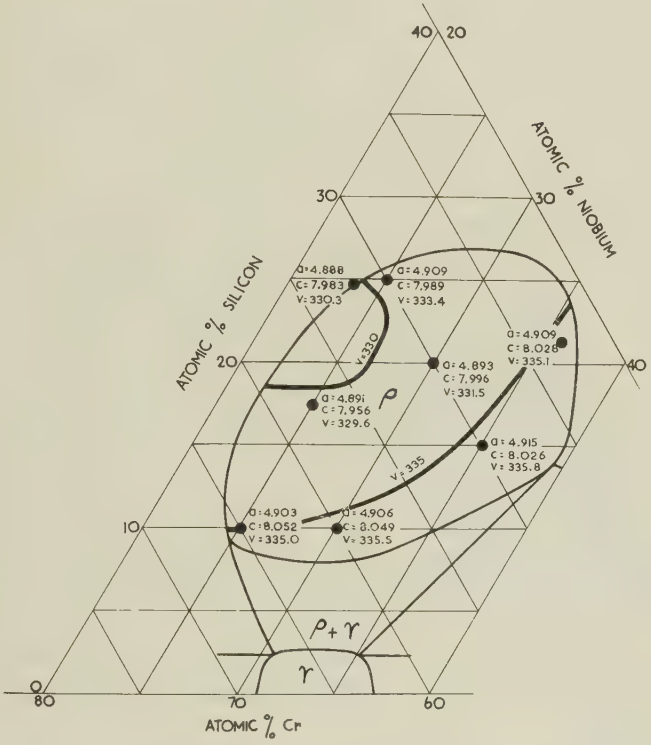


Fig. 4. Lattice parameter variations within the ternary Laves phase (ϱ) region: a and c in kX units; atomic volume V in kX^3.

stacking occurs. Silicon clearly stabilises the hexagonal $MgZn_2$ type, whether by transformation, as for Cr, or *ab initio*, as for Fe.

In Fig. 4 variations in the lattice parameters a and c, as well as in $V(=\sqrt{3}a^2c)$, the volume of the unit cell, are shown. An interesting feature is that the part of the single-phase boundary facing pure niobium lies on a line of constant unit cell volume.

SOME PHYSICAL PROPERTIES OF THE ALLOYS

Melting points

Melting temperatures were determined by measurement with an optical pyrometer on partly molten specimens in the arc furnace. A high accuracy is not claimed, and the values given in Fig. 5 should be regarded as only approximate. In a multi-phase

system as complicated as this it is not surprising that the melting points appear to vary widely in a somewhat haphazard fashion. The values concerned are close to the liquidus temperatures.

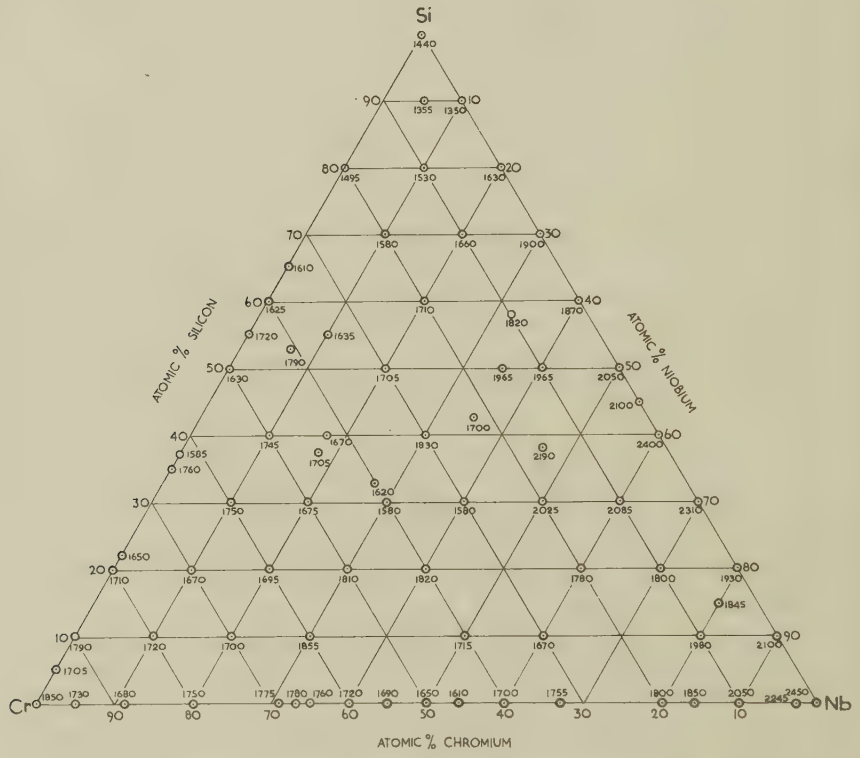


Fig. 5. Chromium–niobium–silicon system; melting temperatures (°C).

Oxidation-resistance

Oxidation rates in still air at 1000°C were obtained on small spheres of the alloys. After oxidation the scale was removed, and the resultant loss in weight per unit area used as a measure. The results are shown in Fig. 6. As might be expected, the largest values were obtained among the niobium-rich alloys; in Fig. 6 the shaded portion indicates the region in which a loss in weight greater than 0.1 mg/mm² was observed. It is noteworthy that the addition of 3% silicon to pure niobium causes an initial deterioration from 0.89 to 2.4 mg/mm², thereafter a recovery, whilst the improvement with Cr, say along the 10% Si level, is marked.

Over a wide region of the diagram the oxidation was either very small, or too low to be measured (indicated by [o] in Fig. 6), and alloys of these compositions may have useful applications in heat-resisting materials (see below).

CONCLUSIONS

The overall picture of the Cr–Nb–Si system shows a high degree of complexity. In addition to the 11 binary phases, there are 5 new ternary compounds of typical

compositions: $\varrho = Cr_{50}Nb_{30}Si_{20}$; $\beta = Cr_{20}Nb_{40}Si_{40}$; $\tau = Cr_{37}Nb_{27}Si_{36}$; $\nu = Cr_{45}Nb_{15}Si_{40}$; $\theta = Cr_{35}Nb_{15}Si_{50}$.

Of these, 3 have a very considerable homogeneity range; the two and three phase-assemblages are as shown in Fig. 3. Points of special interest are the appearance of

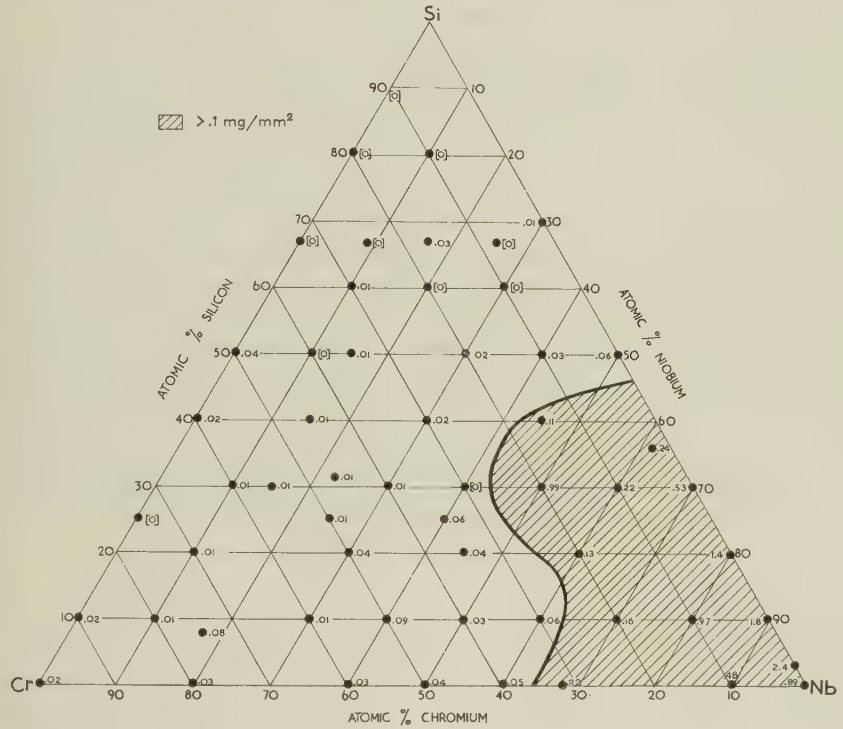


Fig. 6. Chromium–niobium–silicon system: oxidation rates in still air at 1000°C (mg/mm²). Test 1 h.

the ternary hexagonal Laves phase, stabilised from the binary cubic one, Cr_2Nb, by silicon addition, and of the ternary compound (β) which is an isomorph to the binary βNb_5Si_3 (high-temperature form), but is stabilised by chromium-addition to lower temperatures; a similar, but not as pronounced trend was already indicated by iron addition in the Fe–Nb–Si system.

From the practical aspect, there appear many alloys of good or fair oxidation-resistance at high-temperatures, but except for those containing a high proportion of primary niobium solid solutions, they were invariably brittle; it would therefore appear unlikely that attractive mechanically strong heat-resisting alloys based directly on the Cr–Nb–Si system will be developed. However, in applications where brittleness can be permitted, or where it can be mitigated by combination with a more ductile base material (for example in sprayed coatings or diffusion layers, or, using powder-metallurgical methods, bonding the present compounds with a tougher matrix), some of these alloys might prove of considerable interest in utilizing their oxidation-resistance and hardness. Also, in as far as chromium-base alloys are now

rightly attracting attention for use in high-temperature service, the same should apply to the Cr-corner, where the Cr_2Nb, the ϱ and the Cr_3Si phases are potential precipitation hardeners to the Cr primary solid solution.

The workable alloys in the niobium corner of the diagram, which can be hardened by either of the two Laves phases, by Nb_4Si or by Nb_5Si_3, are unfortunately not very oxidation-resistant; this is due to the formation of a non-protective Nb_2O_5 layer. There are two ways, however, in which such Nb-rich alloys might still be used as a base under oxidising conditions. Firstly, the composition might be changed through certain fourth-element additions, with the object of either structurally modifying the β and α Nb_2O_5 oxides[16], or of forming new oxide structures, such as those of rutile or niobite type; for this a considerable range of alloy additions amongst the transition and other metals can serve (a separate investigation on this aspect has appeared[17]). Secondly, a protective coating can be used on niobium-base Nb–Cr–Si alloys, on lines already being followed on molybdenum-base and similar alloys; recent metal–ceramic developments offer here a number of possible choices, for deposits amongst silicides (*e.g.* $MoSi_2$ or $NbSi_2$), oxides (*e.g.* of Al_2O_3/Cr base), carbides (*e.g.* of NbC or TiC base), pure metals and alloys (*e.g.* Cr, heat-resistant steel or Nimonic type), or indeed the Cr-richer compounds found in the present Cr–Nb–Si system itself.

APPENDIX

Interplanar spacings of three new Cr–Nb–Si ternary compounds

(vw = very weak, w = weak, m = medium, s = strong, D = diffuse; d = interplanar spacing, I = line intensity)

θ Phase

d	I	hkl
3.95	vw	400
3.63	vw	211
3.38	vw	202
3.10	m	501,112
2.83	w	411
2.59	vw	312
2.43	m	020
2.257	s	303
2.208	s	611
2.161	s	512,602
1.841	s	213
1.824	s	321
1.800	vw	420
1.759	m	022
1.607	vw	004,521
1.566	w,D	422,204
1.530	w	620?
1.458	w	404
1.300	w	
1.278	vw	
1.240	vw	
1.216	vw	
1.170	m	
1.157	w	
1.141	w	
1.115	m,D	
1.077	vw	
1.065	vw	

τ Phase

d	I	hkl
3.30	w	211
2.86	w	220
2.343	vs	222
2.168	s	321
2.033	m	400
1.908	mw	411
1.855	mw	330
1.816	w	420
1.587	w	510,431
1.435	m	440
1.225	m	622
1.173	w	444

ν Phase

d	I
2.95	w
2.47	w
2.39	m
2.29	w
2.13	s
2.09	w
2.02	m
1.70	vw
1.44	vw
1.40	vw
1.25	vw

ACKNOWLEDGEMENTS

The authors wish to express their sincere thanks to Mr. D. A. OLIVER, C.B.E., Director of Research, The B.S.A. Group Research Centre, for his encouragement and interest, and to Mr. M. J. GREGORY and Mr. M. D. ECCLESTON for their valued assistance in the experimental work.

REFERENCES

1 H. J. GOLDSCHMIDT, *J. Iron Steel Inst. (London)*, 194 (1960) 169.
2 D. A. OLIVER AND G. T. HARRIS, *J. West. Scot. Iron Steel Inst.*, (1946–47) 97; *Trans. Inst. Marine Engrs.*, 59 (1947) 78.
3 H. J. GOLDSCHMIDT, *Metallurgia*, 43 (1951) 1.
4 H. J. BEATTIE AND F. L. VER SNYDER, *Nature*, 179 (1956) 208.
5 H. J. BEATTIE AND W. C. HAGEL, *J. Metals*, (1957) 911.
6 B. BORÉN, *Arkiv Kemi, Mineral. Geol.*, 11 (1933) 28 pp.
7 N. N. KURNAKOV, *Compt. rend. acad. sci. U.R.S.S.*, 26 (1940) 362; 34 (1942) 118; *Izvest. Sektora Fiz. Khim. Anal.*, 16 (1948) 77.
8 R. KIEFFER, F. BENESOVSKY AND H. SCHROTH, *Z. Metallk.*, 33 (1953) 437.
9 M. HANSEN, *Constitution of Binary Alloys*, McGraw-Hill, New York, 1958.
10 E. PARTHÉ, H. NOWOTNY AND H. SCHMID, *Monatsh.*, 86 (1955) 385.
11 B. ARONSSON, *Acta Chem. Scand.*, 9 (1955) 1107.
12 A. G. KNAPTON, *Nature*, 175 (1955) 730.
13 H. J. GOLDSCHMIDT AND J. A. BRAND, *J. Less-Common Metals*, 3 (1960) 44.
14 R. KIEFFER AND F. BENESOVSKY, *Iron and Steel Inst. Special Rept. No. 58*, (1954) p. 292.
15 R. KIEFFER, F. BENESOVSKY AND H. SCHMID, *Z. Metallkunde*, 46 (1956) 247.
16 H. J. GOLDSCHMIDT, *J. Inst. Metals*, 87 (1959) 235.
17 H. J. GOLDSCHMIDT, *Metallurgia*, 62 (1960) 211, 241.
18 H. J. GOLDSCHMIDT, *J. Less-Common Metals*, 2 (1960) 138.

THE CONSTITUTION OF THE CHROMIUM–NIOBIUM–MOLYBDENUM SYSTEM

H. J. GOLDSCHMIDT AND J. A. BRAND

The B.S.A. Group Research Centre, Kitts Green, Birmingham (Great Britain)

(Received November 8th, 1960)

SUMMARY

The ternary system Cr–Nb–Mo has been studied from the aspect of phase constitution, as well as of some of the alloy properties; the wider implications are pointed out, both fundamentally and from the viewpoint of possible application in high temperature and age-hardening materials. Argon arc-melted alloys were examined for a 1000°C equilibrium by X-ray powder-photography. The diagram derived is characterised by an extensive miscibility bay within the primary single-phase (α) field, based on molybdenum. Lattice segregation effects are involved, the high temperature α matrix dividing into two isomorphs of different lattice dimensions: this entails various intermediate stages, with lattice strains and age-hardening effects developing; the Laves phase Cr_2Nb enters as a further precipitant. Spacing contours and tie-lines are given. The Cr–Nb binary system has been determined for various temperatures, and the new diagram proposed modifies previous data in certain respects.

Melting points, some mechanical properties and oxidation rates are given, and interesting composition areas of improved oxidation resistance are indicated; oxide constitution studied on the alloys is considered in this light.

INTRODUCTION

The Cr–Nb–Mo system is of interest, firstly because it contains alloys liable to offer attractive high-temperature resistant materials, and secondly (more fundamentally) because it represents a type of system in which we have three elements A, B, C of the same structure and of atomic size and electron valency such that A–C and B–C are completely intersoluble, but A–B are not soluble, or only slightly so. Under these conditions a ternary miscibility bay opens out, implying a tendency for the primary single-phase solid solution to segregate with decreasing temperature, into two isomorphs of different composition. This creates precipitation hardening conditions of a special type, and alloys may thus arise which, on suitable heat-treatment, possess valuable ageing properties. The application of this principle has been rather neglected in alloy constitutional work, but it is well known, for instance, in permanent magnet alloy systems of the "Alnico" and "Alcomax" types based on Fe–Ni–Al, and in the Fe–Ni–Cu diagram.

In the present system A = Cr (atomic radius $r = 1.25$ kX), B = Nb ($r = 1.5$ kX) and C = Mo ($r = 1.4$ kX). Whilst Mo forms a complete series of solutions with both Cr and Nb, Cr and Nb are mutually almost insoluble, forming an intermetallic compound Cr_2Nb of the cubic Laves phase type. Ternary Cr–Nb–Mo alloys are thus

likely to show additional precipitation effects through nucleation of this compound, besides that of the secondary b.c.c. phase. Other niobium-bearing systems of miscibility bay type are Nb–Ti–W, Nb–V–Zr, Nb–Mo–Zr and Nb–W–Zr. Quaternary additions, such as Ti and W to Nb–Mo–Cr, might be used to vary and control ageing effects in order to attain desired properties, by altering the miscibility bay boundary and its temperature gradient.

Previous work on Cr–Nb–Mo includes studies of the three binary systems, which will be dealt with under their separate sections; the ternary diagram has, to our knowledge, not yet been investigated.

X-ray analysis was used to survey the system, supplemented by determinations of melting temperatures, hardness, and oxidation resistance. The temperature section examined was that at 1000°C, but higher temperatures were occasionally used to clarify points of special interest.*

EXPERIMENTAL

The alloys were prepared from spectroscopic quality chromium, niobium, and molybdenum, supplied by Johnson Matthey Ltd., the only significant impurity being about 0.2 wt. % Ta in the niobium. Small buttons were melted in a laboratory argon arc-furnace as previously described in work on the Fe–Nb–Si system[1], re-melted several times and further homogenised in the arc-furnace by annealing at a temperature just below the melting point.

Melting losses were usually less than 2%, and chemical analysis of the ingots was only carried out where the melting losses were excessive, and in critical parts of the diagram.

Samples were annealed as small lumps in evacuated silica capsules at 1000°C for 14 days, then water quenched. The X-ray technique used was that of normal powder photography, using Co $K\alpha$ radiation ($a = 1.78529$ kX), the photographs being examined for constitution and lattice dimensions. The latter were important, in order to derive spacing contours within the body-centred single phase field and tie-lines within the two-phase fields.

Melting points were determined in the arc furnace on all the alloys by an optical pyrometer, giving the approximate liquidus temperature. Because of the small sample size, work on mechanical properties was for the present limited to hardness measurement and some hot-deformation tests on selected alloys.

Major interest attached to oxidation resistance, which was determined by measuring the loss in weight per unit surface area of specially melted small spheres of the alloys, exposed to still air at 1000°C for 1 h. For possible correlation of oxidation resistance with oxide constitution, the scales formed on selected alloys were also examined by X-rays.

THE BINARY SYSTEMS

The chromium-molybdenum system

Much previous work has been done on the Cr–Mo system, and the continuous series of solid solutions is well established. Previous investigations include the work of KESSLER AND HANSEN[2], KUBASCHEWSKI AND SCHNEIDER[3], BAEN AND DUWEZ[4], BLOOM AND GRANT[5], and TRZEBIATOWSKI *et al.*[6] whilst the system was also covered

* A broader survey in regard to the subject matter of this paper has been presented recently[20].

in a previous study on the Fe–Cr–Mo system[7]. The existence of the continuous solid solution was here again confirmed; Fig. 1 shows the consensus of known lattice spacing measurements, as published by PEARSON[8], which is accepted as basic in the present work.

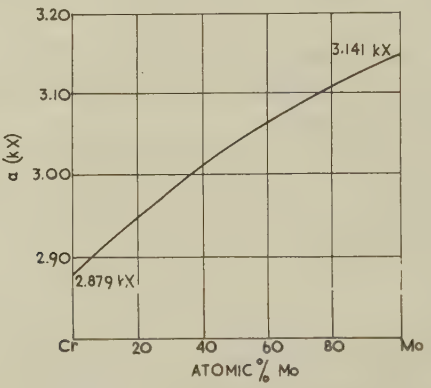


Fig. 1. Lattice spacings of Cr–Mo alloys (consensus of previous work).

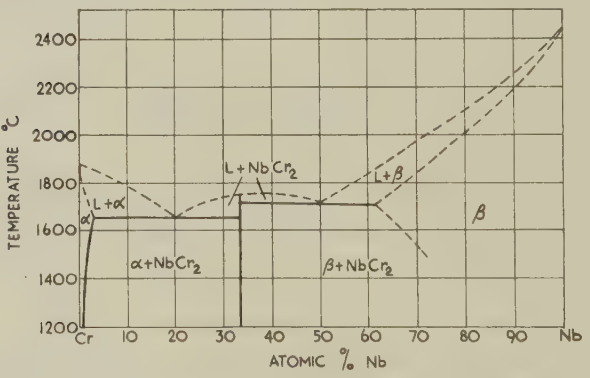


Fig. 2. Cr–Nb diagram, according to EREMENKO *et al.*

The chromium–niobium system

KUBASCHEWSKI AND SCHNEIDER[9] give details on this system for alloys with up to 36% Nb* (50 wt. %). They found an intermetallic compound with a wide homogeneity range, to which they tentatively ascribed the formula Cr_3Nb_2. The solubility of Nb in Cr is stated to amount to several percent, with the second phase appearing in their X-ray photographs at about 5% Nb. The annealing temperatures are said to be about 500°C below the observed melting point, which would be around 1300°C. DUWEZ AND MARTENS[10] indexed the powder pattern of the intermetallic compound, finding it cubic with $a = 6.976$ kX, and showed that its structure was the same as that of the Laves phase $MgCu_2$. Unlike $TaCr_2$ it is stable up to its melting point. ELIUTIN AND FUNKE[11] found the cubic Laves phase Cr_2Nb, and also a hexagonal compound Cr_3Nb_2 which was detected over an appreciable composition range. This

* All compositions will in this paper be given in *atomic* percent, unless otherwise stated.

latter result has not been confirmed by other workers, nor in the present investigation. EREMENKO, ZUDILOVA AND GALASKAYA[12] published a diagram shown in Fig. 2, in which the Cr_2Nb phase was represented by a vertical line at this composition. They agreed that it was in fact a Laves phase of the $MgCu_2$ type. The solid solubility of Nb in Cr was stated to be approximately $1\frac{1}{2}\%$ at 1350°C. No attempt was made to determine the solubility of Cr in Nb, but ELIUTIN AND FUNKE[11] report it as 20% at 1600°C, 12–13% at 1500°C, no doubt less at lower temperatures.

In the present investigation most attention was directed at the equilibrium at 1000°C, supplemented by melting point data, and by some annealing treatments at higher temperatures. Annealing at temperatures above 1000°C was done in an electrically heated molybdenum or tantalum wire helix of dimensions about 1/4 in. × 1 in. surrounded by radiation shields, and enclosed in the evacuated glass dome of an evaporating unit. A small lump of the specimen was placed on the rim of a molybdenum cylinder at the centre of the helix and could be rapidly withdrawn for quenching. Temperatures were measured by an optical pyrometer. Using this simple but effective technique, temperatures in excess of 2200°C were obtainable, and well controlled quenching experiments could be done from successive lower temperatures.

The diagram obtained is shown in Fig. 3. At the Cr end, we find a solubility for Nb

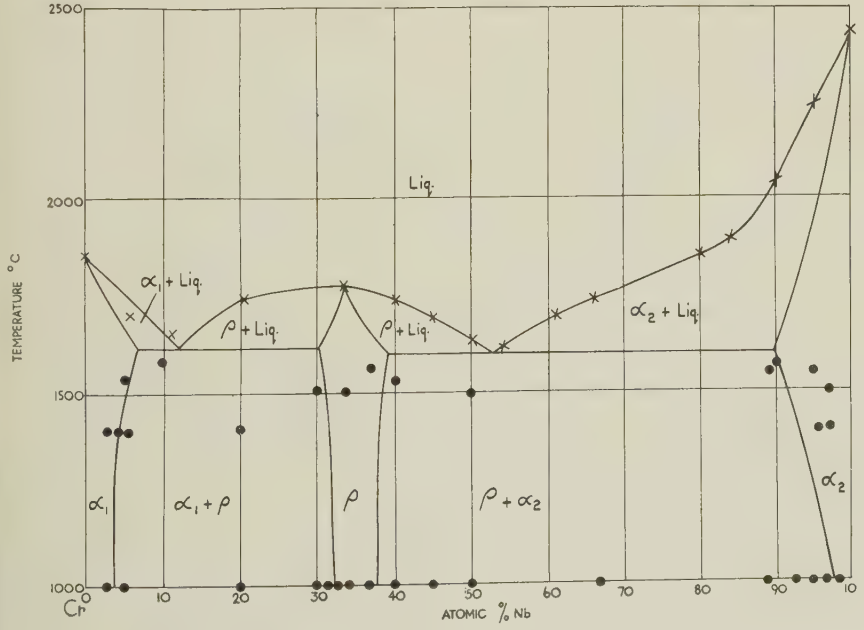


Fig. 3. Cr–Nb binary system (present results): ×, observed melting point; •, alloys.

of about 4% at 1000°C, which increases slowly with increasing temperatures. Niobium causes an expansion of the lattice from 2.880 kX for pure Cr up to 2.885 kX in an alloy saturated with Nb at 1400°C.

The intermetallic compound ϱ is confirmed to have the $MgCu_2$ type structure, with a homogeneity range extending from about 30 to 36% Nb. This variation of composition is reflected by variation of the lattice constant from $a = 6.967$ kX when ϱ is in equilibrium with chromium, rising to $a = 6.987$ kX when in equilibrium with niobium at 1000°C.

At the Nb end of the diagram about $2\frac{1}{2}$% Cr can be dissolved at 1000°C (microscopy was used to confirm the X-ray results on this point) rising to about 10% Cr near the eutectic temperature. The lattice spacing of Nb saturated with Cr at 1550°C is 3.248 kX compared with 3.2995 kX for pure Nb. Comparison with EREMENKO's diagram shows this appreciable difference (*cf.* Figs. 2 and 3).

The niobium–molybdenum system

Relatively little previous work has been done on the Nb–Mo system. BÜCKLE[13] and EREMENKO[14] have measured the lattice spacings of a number of alloys and agree that the two elements form a continuous series of solid solutions. This was confirmed in the present work; the lattice dimensions are shown in Fig. 4 and are in fair agree-

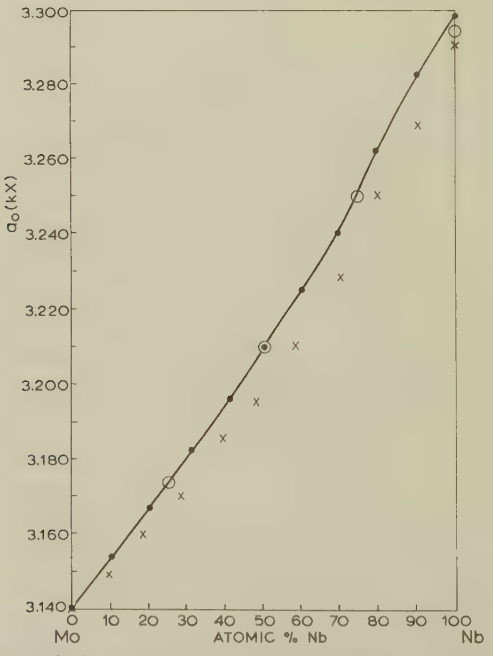


Fig. 4. Lattice spacings of Mo–Nb alloys: ●, present result; ○, BÜCKLE; ×, EREMENKO.

ment with the earlier results. An almost linear curve with a very small negative deviation from Vegard's law is apparent. No phase other than the b.c.c. solution was found, either in the annealed specimens, or in two specimens (30 and 70% Nb), examined in the raw ingot state; nor was there any superlattice, a possibility that had to be considered.

THE TERNARY FIELD

The ternary diagram derived is shown in Fig. 5. An extensive single-phase field of b.c.c. (α) solid solutions exists in the high molybdenum region, from which, on chromium and niobium addition, a miscibility bay opens out. The latter widens with descending temperature. Two branches of this α solid solution which will here be denoted "α_1" and "α_2" adjoin the Mo–Cr and Mo–Nb binary sides respectively. α_1 has the smaller, α_2 the larger lattice constants. The miscibility bay is sub-divided into a duplex $\alpha_1 + \alpha_2$ region, a comparatively large three-phase triangle $\alpha_1 + \alpha_2 + \varrho$, and the regions $\alpha_1 + \varrho$ and $\alpha_2 + \varrho$. Pure ϱ-phase is able to dissolve about 10% Mo at 1000°C. No ternary compound was found.

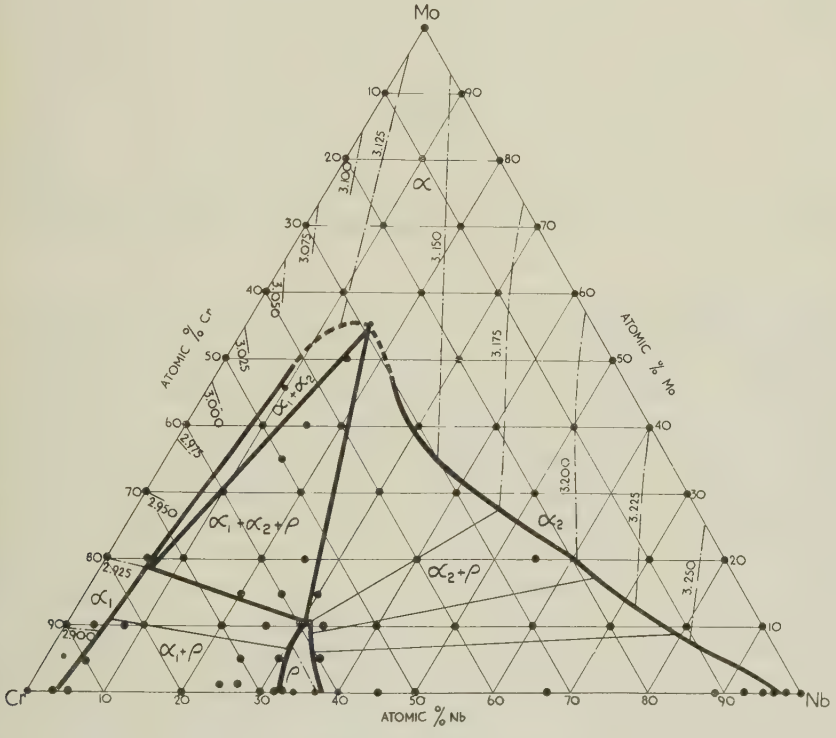


Fig. 5. The ternary diagram Cr–Nb–Mo, 1000°C section: — - - -, phase boundaries; ———, tie lines; — - — -, spacing contours (kX units); ●, alloys investigated.

The lattice constants of the α and ϱ phases were measured wherever the phase was present in sufficient quantity to make this possible. In Fig. 5 the values are plotted as contour lines within the α single-phase field; they were also used to locate the tie-lines in the two-phase fields and in delineating the phase-boundaries. Fig. 6 shows theoretical lines of constant lattice dimensions of the α phase, assuming the known atomic radii of Cr, Nb and Mo, and a linear change with composition. The general trend of contour lines is in good agreement over a large part of the solution

field, except adjoining the Cr–Mo side where a major swing of contour lines occurs. It will be seen from Fig. 1 that there is a positive deviation from Vegard's Law in the Cr–Mo system; this deviation becomes reduced on adding Nb.

The lattice spacing of the Laves phase ϱ, when saturated with molybdenum, is 6.981 kX.

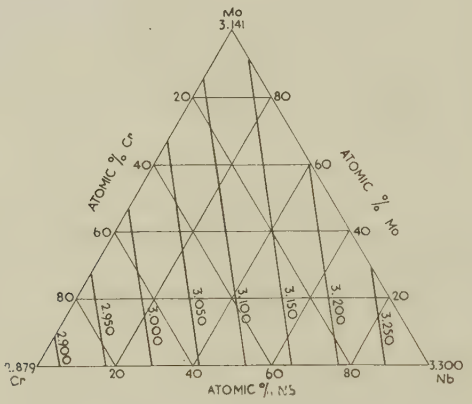


Fig. 6. Theoretical lattice spacing contours (kX), based on known atomic sizes.

Variation of miscibility bay with temperature

The contraction of the miscibility bay with increasing temperature was demonstrated in the first place by X-ray study of the alloys as melted, *i.e.* effectively as quenched out of the single-phase α region. These alloys proved to be single-phase, as against 2- or 3-phase after the 1000°C anneal, the lattice spacing of parent α being intermediate to those of the α_1 and α_2 phases derived. More explicitly this can be shown by annealing fragments of a given alloy, in this case $Cr_{50}Nb_{15}Mo_{35}$, so as first to attain 1000°C equilibrium, and then quenching after further heat-treatments at a sequence of increasing temperatures. At 1000°C, $\alpha + \alpha_2 + \varrho$ were present; at 1100°C, ϱ had disappeared, and with further increasing temperature the composition of the two α phases became closer, finally merging at 1400°C.

Table I shows the approach in lattice dimensions during this process. It implies that on tempering an alloy quenched from the single-phase α region, strain-hardening effects would occur, through incipient precipitation of the second b.c.c. phase. This may occur either homogeneously or heterogeneously, as demonstrated by the manner of X-ray line-broadening; depending on position within the bay and thermal history, an alloy may contain, besides the parent α-phase, a second constituent shown as either a band of compositions corresponding to those along the miscibility bay ceiling traversed during precipitation, or a distinct α-phase of definite composition approaching that of the final precipitant. Various intermediate (non-equilibrium) stages characterised by different line-configurations, can be obtained by heat-treating for different times at constant temperatures.

The maximum difference in spacing between coexisting α constituents is approximately 7–8%. This occurs, for example, for an alloy $Cr_{40}Nb_{14}Mo_{46}$, whilst the difference descends to zero at $Cr_{40}Nb_9Mo_{51}$. This applies to 1000°C equilibrium, but

TABLE I

RESULTS OF VARIOUS HEAT TREATMENTS OF AN ALLOY CONTAINING 50% Cr, 15% Nb, 35% Mo, ILLUSTRATING THE CLOSURE OF THE MISCIBILITY GAP

Heat treatment				
First	*Second (30 min at each temperature before quenching)*	*Constitution*	*Lattice constant (kX)*	*% Difference in α spacing*
2 weeks 1000°C	—	$\alpha_1 + \alpha_2 + \varrho$	$\alpha_1 \approx 2.92$ (order of) $\alpha_2 = 3.148$	7.8
2 weeks 1000°C	1100°C	$\alpha_1 + \alpha_2$	$\alpha_1 = 2.931$ $\alpha_2 = 3.138$	6.8
2 weeks 1000°C	1200°C	$\alpha_1 + \alpha_2$ (α_2/α_1 proportion increasing)	$\alpha_1 = 2.965$ $\alpha_2 = 3.126$	5.4
2 weeks 1000°C	1300°C	$\alpha_1 + \alpha_2$	$\alpha_1 \approx 3.04$ (order of*) $\alpha_2 = 3.074$	≈ 1
2 weeks 1000°C	1400°C	α	$\alpha = 3.071$	0

* α_1 phase too weak to measure accurately.

it is important to note that at lower temperatures the equilibrium spacing difference of course increases, which would enter significantly on very slow cooling or tempering for extended periods; wide variations in intermediate lattice strain and precipitant hardening can be produced, not only in degree, but also in type. An example of hardness variations thus caused will be given in the next section.

At compositions near the apex of the miscibility bay, final equilibrium is extremely sluggish in attainment. Thus the $\alpha/(\alpha_1 + \alpha_2)$ boundary in Fig. 5 is shown only dotted in this portion, and altogether the precise delineation of the miscibility bay must be subject to a slight uncertainty in this respect.

Micrographic examination provides here, however, a helpful supplement. Thus an alloy $Cr_{30}Nb_{10}Mo_{60}$ shows a fine subgrain structure (see Fig. 7), representing a lamellar precipitate along lattice planes, coherent with the parent lattice. This alloy is situated close to the apex, and from X-ray evidence alone, is single-phase; this very thin lamellar precipitate nevertheless exists, subdividing the matrix into a regular cell array, differently oriented from grain to grain. The lamellae are, in this instance, about 0.5 to 1 μ thick, the mean cell width of the matrix being 5 to 6 μ. Using our ternary diagram, the segregate corresponds to Cr-enriched areas within the Mo-richer base. Precipitates of a more massive character, including ϱ, are shown in Fig. 8, while Fig. 9 illustrates an α_2 base alloy with crystal boundary precipitates of ϱ.

It is of interest to enquire whether during the $\alpha \rightarrow (\alpha_1 + \alpha_2)$ disintegration an intermediate stage of tetragonal distortion occurs, such as is observed in Fe–Cu–Ni alloys[15] and in Fe–Ni–Al base type permanent magnet alloys[16-18]. However, this could not be detected; the possibility of tetragonal line-splits is nevertheless not excluded, but would be entirely masked by line-broadening owing to heterogeneity in composition and lattice strain. Intermediate stages are marked by formation of "islands" within

the b.c.c. parent α lattice of which they still form an integral part, but representing lattice concentrates of Cr atoms within the Mo-richer base. This tendency toward segregation does not exist in Cr–Mo alloys, but is shown in the presence of Nb atoms. These islands would initially not be large enough to break away from the parent lattice but do so upon further growth.

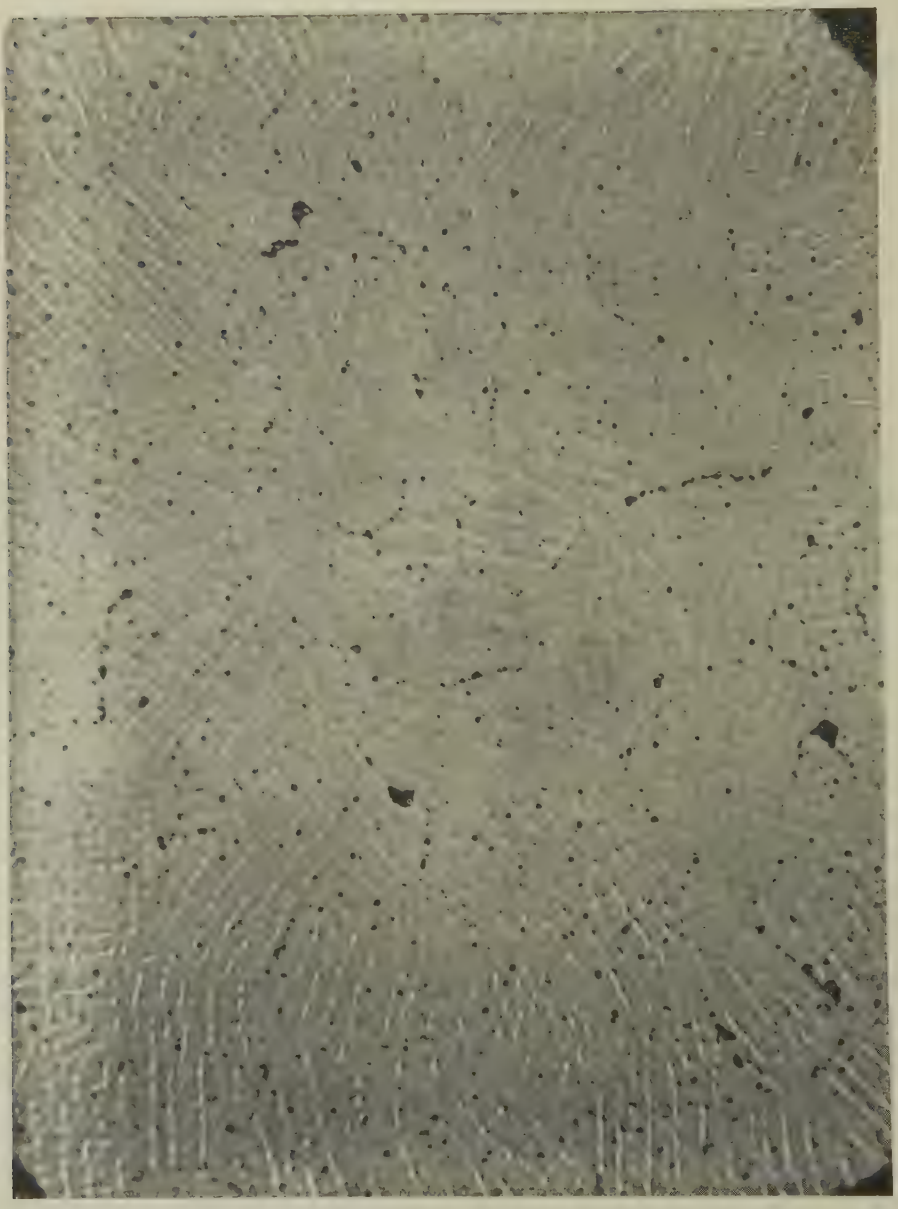


Fig. 7. Alloy 30% Cr, 10% Nb, 60% Mo (atomic), annealed 1000°C, 14 days. (×600) Initial state: as-quenched from α field.

In order to test whether the 1000 C anneal for 14 days has produced equilibrium, selected ternary alloys were further annealed for 3 months at this temperature. The X-ray result showed virtually no change in constitution, except for a very minor quantitative difference in 2 alloys.

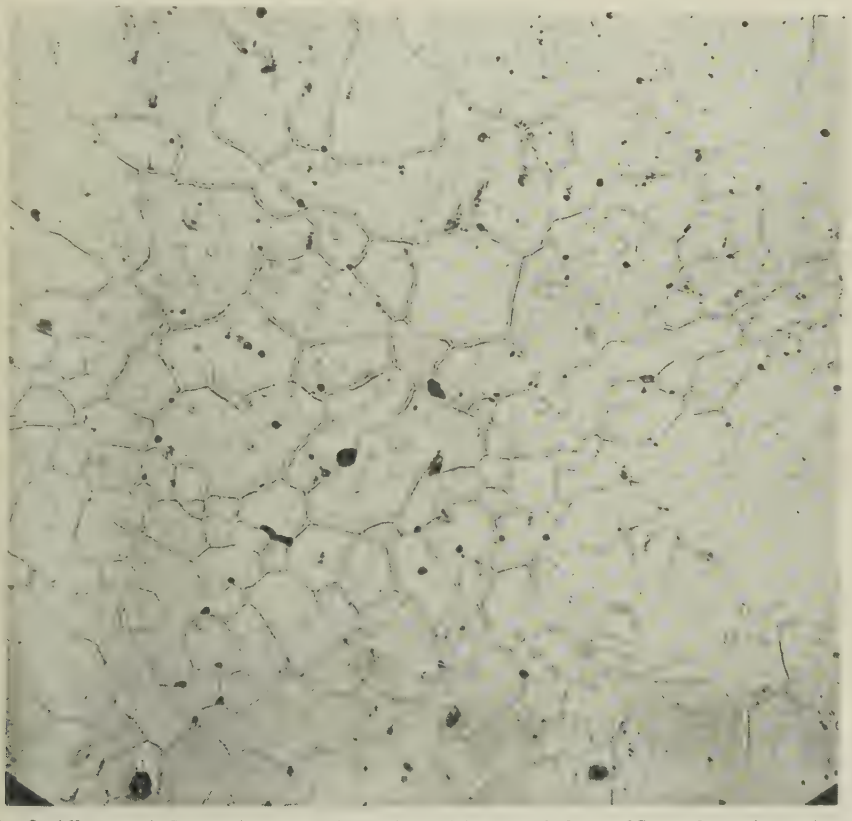


Fig. 8. Alloy 30% Cr, 30% Nb, 40% Mo (atomic), annealed 1000°C, 14 days. (×250)

MECHANICAL PROPERTIES

The alloy samples (arc-melted buttons) were not sufficient in size to allow a major study of mechanical properties, but a survey of hardnesses was carried out over the ternary system, and cold reduction tests were made on a number of alloys in order to estimate their ductility.

Hardness

The V.P.N. hardnesses determined on the as-melted ingots are shown in Table II.

It may be seen that a consistent picture emerges, in so far as alloys which are primary χ solid solutions show the relatively lower hardness values, whilst the presence of the intermetallic compound (ϱ) shows itself by high values, with a gradation as its amount decreases. The maxima on the two binary Cr-Mo and Nb-Mo solid solution sides should be noted.

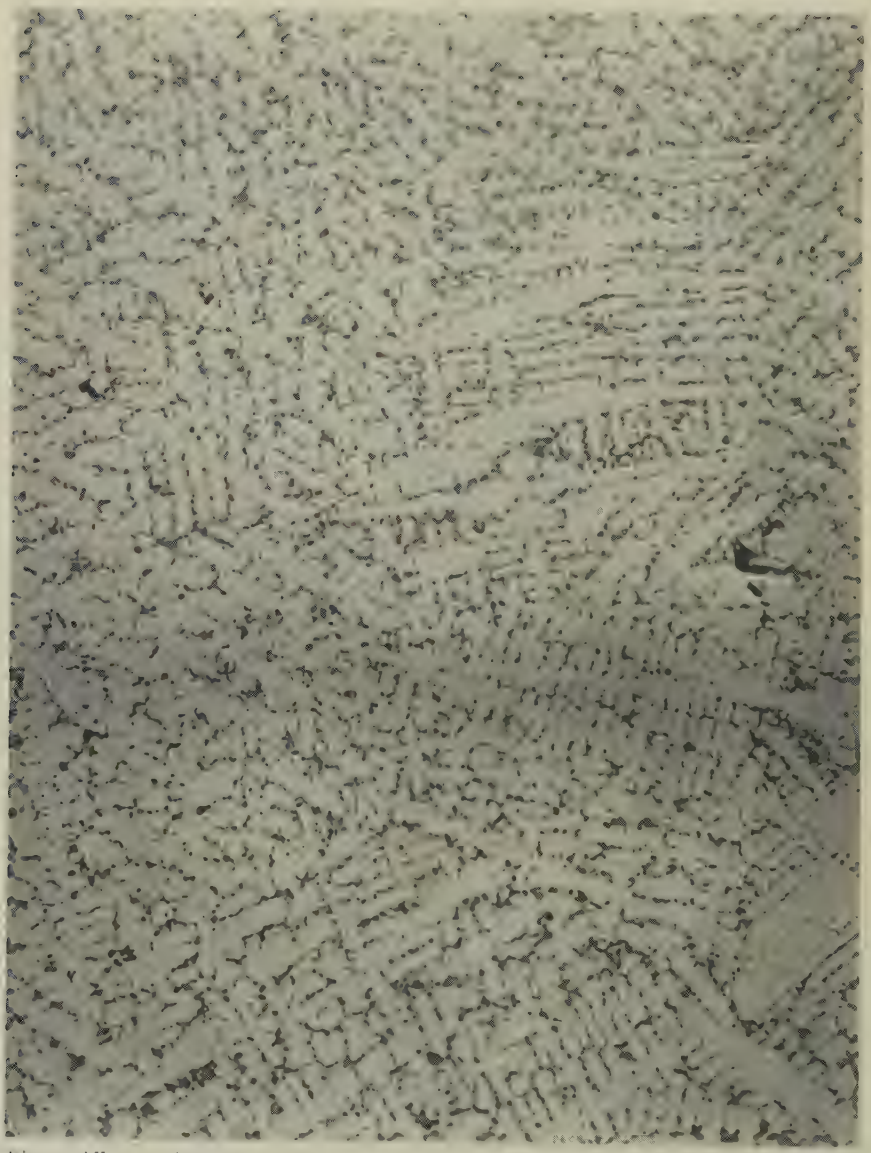


Fig. 9. Alloy 50% Cr, 20% Nb, 30% Mo, (atomic) annealed 1000°C, 14 days. (×250)

TABLE II

HARDNESS VALUES OF Cr–Nb–Mo ALLOYS (AS-MELTED INGOTS)

Composition Cr–Nb–Mo	*Hardness*[a] *(V.P.N.)*	
100– 0– 0	164	
0–100– 0	96	
0– 0–100	184	
65– 30– 5	892	(essentially pure ϱ phase)
70– 20– 10	686	
40– 50– 10	724	
10– 80– 10	313	
70– 10– 20	709	
55– 25– 20	850	
40– 40– 20	735	
25– 55– 20	550	
10– 70– 20	321	
70– 0– 30	550	
50– 20– 30	611	
0– 70– 30	391	
50– 10– 40	711	
40– 20– 40	762	
30– 30– 40	606	
10– 50– 40	475	
30– 10– 60	640	(hardness as-annealed 1000°C, 14 days: 683)
10– 30– 60	442	(hardness as-annealed 1000°C, 14 days: 382)
30– 0– 70	544	
0– 30– 70	368	
10– 10– 80	317	

[a] Mean of several readings.

Ductility

Regarding ductility of the alloys, it should be recalled that of the three component metals, only niobium is ductile, chromium and molybdenum being brittle (although they can be rendered ductile by special additions and treatments).

In the Cr–Nb–Mo system, it was noted that during powder preparation for X-ray specimens, alloys could be filed over a considerable composition area although more readily fragmented by crushing, and it is considered that such alloys indicate a conditional ductility, possibly enhanced by higher-temperature or other special treatments.

The present compression test was carried out on cubic samples of about 1 cm side under a maximum pressure of 10 tons. In most cases cracking occurred after zero or little cold reduction, whilst in other cases appreciable reductions before cracking were possible. Typical results are given in Table III*.

These tests, which can only be regarded as exploratory, will of course merely serve as a first pointer, and zero reduction does not necessarily imply rejection, because in this system different heat-treatments can make a vital difference to mechanical properties; furthermore, hot reduction tests at various high temperatures would be

* Thanks are expressed to Dr. R. SMITH of this laboratory for these as well as some of the hardness tests.

important and liable to show very different performances; lastly, small quaternary additions, such as of titanium or other elements, used for example to improve the ductility of pure molybdenum, should be investigated for further enhancement. This programme must be left to further work.

TABLE III

COLD-REDUCTION OF ALLOYS

Composition (Cr–Nb–Mo)	*Result*
100– 0– 0	Extensive cracks appeared after 12% reduction
0–100– 0	No cracks appeared after 28% reduction
0– 0–100	Edge cracks appeared after 6% reduction
10– 80– 10	Cracks appeared after 15% reduction
10– 70– 20	Cracks appeared after 5% reduction
20– 60– 20	Cracks appeared after 30% reduction
20– 50– 30	Cracks appeared after 5% reduction
0– 10– 90	Cracks appeared after 40% reduction
25– 55– 20	No reduction possible without cracking
65– 30– 5	
55– 25– 20	
50– 20– 30	
70– 10– 20	

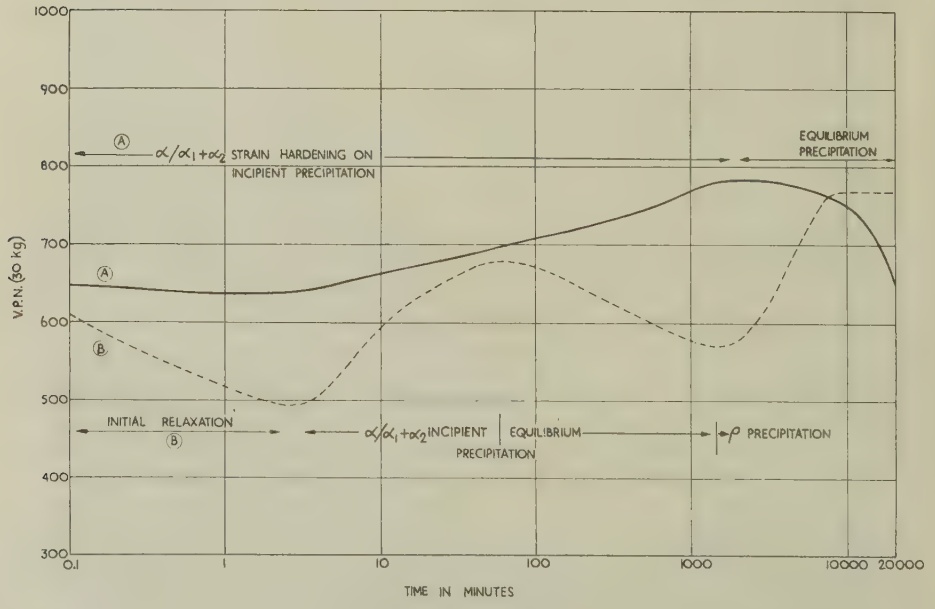


Fig. 10. Variation of hardness of two Cr–Nb–Mo alloys with time at 1000°C. Initial state: as-melted and quenched (α single phase). Alloy A: 44% Cr, 11% Nb, 45% Mo (atomic); $\alpha_1 + \alpha_2$. Alloy B: 38% Cr, 12% Nb, 50% Mo (atomic); $\alpha_1 + \alpha_2 + \varrho$.

Hardening effects during $\alpha \rightarrow (\alpha_1 + \alpha_2)$ segregation

A series of experiments were carried out to observe any possible hardening effects during precipitation within the miscibility bay, and using alloys initially in the as-

melted pure (single-phase) α condition. The alloys were annealed at 1000°C for predetermined times and the hardnesses determined. The resulting variations are shown in Fig. 10. Two alloys were examined, as shown, one (A) corresponding to $\alpha_1 + \alpha_2$ when in equilibrium, the other (B) to $\alpha_1 + \alpha_2 + \varrho$. For A, a pronounced hardening occurs during initial $\alpha \rightarrow (\alpha_1 + \alpha_2)$ precipitation, whilst on final attainment of $\alpha_1 + \alpha_2$ equilibrium, the alloy softens again. There is no doubt that this is due to transistory lattice strain effects in the sense discussed above. A parallel X-ray examination was carried out on these samples clearly showing a gradual transition from single-phase α through two composition-bands (high-strain) first adjoining in lattice spacing, then separating, gradually losing the parent α constituent, and finally approaching the equilibrium $\alpha_1 + \alpha_2$ state. Alloy B behaves in a rather more complex manner. After a brief initial softening, probably due to relaxation of cooling stresses from the melt, rapid hardening sets in due to incipient $\alpha/(\alpha_1 + \alpha_2)$ precipitation (and corresponding to increasing lattice-stress), followed by softening on approach to equilibrium and then a secondary, and greater, hardening through ϱ formation. The time-scale for primary $(\alpha_1 + \alpha_2)$ hardening is considerably shorter in alloy B than alloy A. Thus these alloys are certainly hardenable, and the degree, type and rate of hardening can be controlled in a given case as required, by varying compositions and annealing temperatures and times.

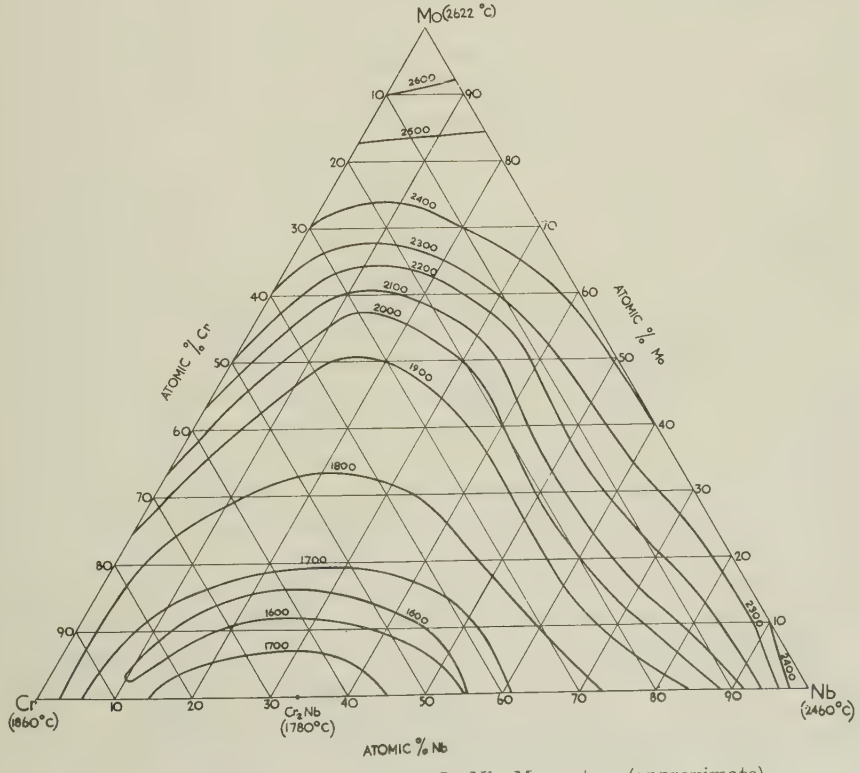


Fig. 11. Liquidus isothermals in the Cr–Nb–Mo system (approximate).

MELTING POINTS

The observed liquidus temperatures are shown as contour lines in Fig. 11; whilst high accuracy is not claimed, it is believed that the diagram is correct in its general features. Individual determination is correct within ± 25°C. A ternary eutectic minimum below 1600° is observed.

OXIDATION RESISTANCE

The oxidation resistance of many of the alloys was determined in tests at 1000°C for 1 h in air. The samples were small arc-melted spheres, and the figure determined was loss of weight per unit surface area.

Furthermore, an X-ray examination was carried out on some of the oxide scales formed on the test samples, with the view to correlating this with protective properties.

The binary sides Cr–Mo and Nb–Mo give the oxidation rate values shown in Fig. 12. In the Cr–Mo system the good oxidation behaviour of chromium is substantially maintained up to 40% Mo; then an abrupt and increasing deterioration occurs, up to 100% Mo. For Nb–Mo alloys the trend is in principle similar: though Nb itself has, of course, an inferior oxidation resistance to Cr, this becoming worse only slowly, until at about 40% Mo a sharp deterioration occurs. These abrupt breakdowns in both cases are probably connected with the formation of free MoO_3, whilst for molybdenum contents lower than 40% this element will have been able to enter the lattice of the non-volatile base oxide of Cr_2O_3 or Nb_2O_5 respectively. Constitutionally, the only phases present in the binary scales were pure Cr_2O_3 on the Cr–Mo alloys and βNb_2O_5 on Nb–Mo alloys. This persisted even at quite high Mo contents (*cf.* Fig. 13), and no new mixed or Mo-base oxide was observed.

The oxidation data for the ternary alloys are plotted on Fig. 13. It may be seen that good or fair oxidation resistance extends over a wide composition area, which even approaches closely to pure niobium; a well defined boundary between areas of "fair" and "poor" oxidation resistance runs across the diagram. Two contour lines, dividing the ternary field into areas of oxidation rates <1, 1 to 5, and >5 mg/mm^2/h are shown in Fig. 13. There are considerable local variations, and more stress should be laid on the order rather than the precise values of the figures; but it is noteworthy that an alloy containing 80% Nb, 10% Cr, 10% Mo already shows a very encouraging oxidation resistance. This alloy (*cf.* Fig. 5) is still single-phase α, and shows moderate ductility. Thus, the addition of only minor amounts of chromium to niobium-rich Nb–Mo alloys causes an abrupt and large improvement in oxidation resistance.

On the Cr–Nb binary side, the satisfactory oxidation resistance of pure chromium is substantially maintained up to quite high Nb content, *viz.* at least 60% Nb, the largest deterioration occurring from 90 to 100% Nb. The Laves phase Cr_2Nb is of inherently attractive oxidation resistance, although its brittleness would exclude such alloys for many applications. (It is suggested that brittleness does not in itself bar an alloy from practical application if other properties are attractive; it could be used *e.g.* in coatings and sinter-components or bonded with an additional metal, or the compound could be incorporated as a minor phase in a ductile matrix.)

Additions of minor amounts of molybdenum to the Cr_2Nb Laves phase causes some but no major deterioration in oxidation rates.

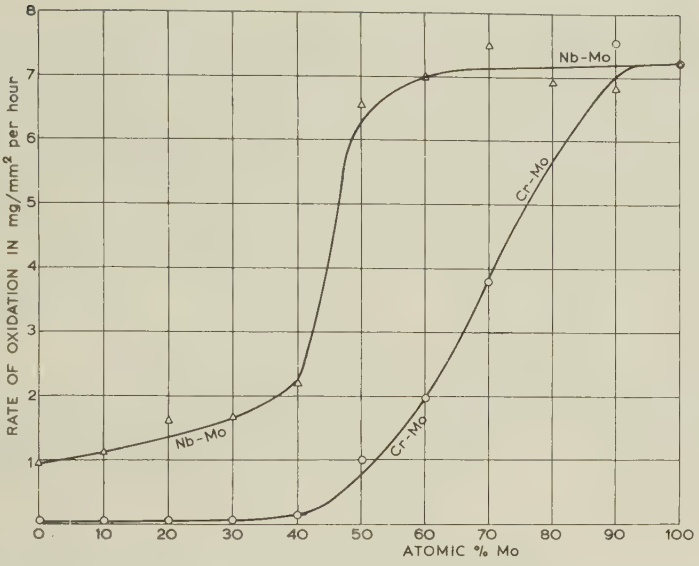


Fig. 12. Oxidation rates of binary alloys Cr–Mo and Nb–Mo at 1000°C in still air (mg/mm²); test 1 h.

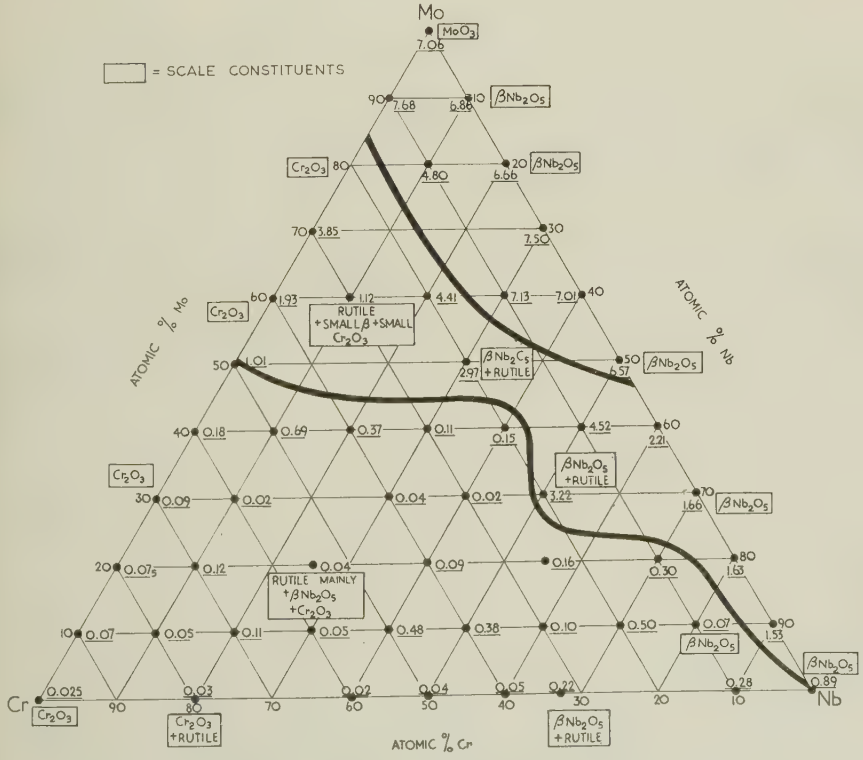


Fig. 13. Oxidation rates of ternary Cr–Nb–Mo alloys at 1000°C in still air (mg/mm²); test 1 h, including phase constitutions of oxide scales.

The constitutions of scales, as determined on selected ternary samples, are also shown in Fig. 13. Apart from the Cr_2O_3 (hexagonal, hematite type structure), and βNb_2O_5 already noted on two of the binary sides, the rutile type of structure enters prominently over wide composition areas. The stoichiometric composition for rutile would be of course $(Nb,Cr,Mo)O_2$, but a degree of non-stoichiometry in the direction of metal-deficiency is very probable; in a systematic survey of systems containing Nb_2O_5 + additional oxides, carried out in separate work[19], the rutile structure has has been shown to be one of the major phases occurring: as will be discussed in that investigation the sequence (1) $\beta Nb_2O_5 \rightarrow$ (2) Rutile $\rightarrow$ (3) Hematite type structure, is of much wider significance, but it is well illustrated in the Cr–Nb–Mo system. Formally the consistent decrease of oxygen content: $MeO_{2.5}$, MeO_2, $MeO_{1.5}$ is here reflected by three phases βNb_2O_5, $(Nb,Cr,Mo)O_2$, Cr_2O_3. Partial solid solutions of Mo and Cr in Nb_2O_5 and of Mo and Nb in Cr_2O_3 also occur.

It is not possible to ascribe an inherent "good" or "bad" oxidation resistance to any of the oxide phases observed, but clearly factors such as compatibility with the base, volume ratio, deviation from stoichiometry, phase transformations in the oxide with temperature, and internal structural distortions, determine whether the assembly is protective or not. Strongly adhesive and protective scales have been observed on alloys even for Nb_2O_5 solid solutions, whilst the presence of rutile may or may not be beneficial. Also the evolution of volatile MoO_3 is liable to crack or damage an otherwise adhesive phase aggregate.

CONCLUSIONS

The constitutional study of the Cr–Nb–Mo system shows that, as predicted, a miscibility bay occurs, narrowing with increasing temperature. Such a system yields alloys exhibiting lattice strain hardening effects (akin to those known in Fe–Ni–Al, Fe–Cu–Ni and other permanent magnet type alloys) due to incipient precipitation of a secondary phase isomorphous with the matrix, and, in this case, of an intermetallic compound; these effects have here been demonstrated. Thus an alloy which is single-phase α as quenched from high temperatures can be hardened by controlled nucleation of either the alternate b.c.c. phase of different lattice-dimensions (and this in a homogeneous or heterogeneous manner) or of the Laves phase (ϱ) or by both mechanisms jointly. These properties are capable of modification by suitable additions to the ternary system. For example, certain fourth metals might be added which are partly or wholly soluble in a given Cr–Nb–Mo alloy, in amounts up to the solubility limit, so as to produce variations in both position and declivity of the miscibility bay boundary. Such suggested added elements are firstly the surrounding transition metals Ti, V, W, Zr, Ta, Fe, Ni, Co, secondly Al, Si, C and B, each for specific reasons. These variations would of course modify atomic size ratios, valency and structural factors, and, through altering the critical phase-boundaries, would result in modified hardening and "tempering" conditions. In particular, additions that would promote sluggishness at a given temperature might be beneficial, in retarding α/α lattice-segregation and ageing, so that a given stage in nucleation could be maintained for more prolonged periods at higher operating temperatures. In alloy A, on which the age-hardening was demonstrated above, the effect proceeded relatively speedily, rising to a maximum in 33 h at 1000°C (Fig. 10), but this could certainly be enhanced by composition and temperature changes.

It is shown further that good or fair high-temperature oxidation resistance can be attained over a considerable region of the system, and that, in particular, small additions of chromium to Nb-rich Nb–Mo alloys cause a major improvement in oxidation resistance. Although an excess causes brittleness (through Laves phase formation), alloy areas adjoining the primary miscibility boundary are indicated, in which attractive mechanical and oxidation resistance properties might well be combined.

From the metal-physical aspect some of the present alloys, namely the precipitation hardening ones adjoining the boundaries of the miscibility bay, offer points of particular structural interest.

ACKNOWLEDGEMENTS

The authors wish to pay tribute to Mr. D. A. OLIVER, Director of Research, B.S.A. Group Research Centre, for his continued encouragement. Mr. M. D. ECCLESTON has given valued assistance with the experimental work.

REFERENCES

1 H. J. GOLDSCHMIDT, *J. Iron Steel Inst. (London)*, 194 (1960) 169.
2 H. D. KESSLER AND M. HANSEN, *Trans. Am. Soc. Metals*, 42 (1950) 1008.
3 O. KUBASCHEWSKI AND A. SCHNEIDER, *Z. Elektrochem.*, 48 (1942) 671.
4 S. R. BAEN AND P. DUWEZ, *Trans. Am. Inst. Mining Met. Engrs.*, 191 (1951) 331.
5 D. S. BLOOM AND N. J. GRANT, *Trans. Am. Inst. Mining Met. Engrs.*, 200 (1954) 261.
6 W. TRZEBIATOWSKI, H. PLOSZEK AND J. LOBZOWSKI, *Anal. Chem.*, 19 (1947) 93.
7 H. J. GOLDSCHMIDT, *Iron and Steel Inst., Special Rept. 43*, (1951) p. 249.
8 W. B. PEARSON, *A Handbook of Lattice Spacings and Structures of Metals and Alloys*, Pergamon Press, London, 1958.
9 C. KUBASCHEWSKI AND A. SCHNEIDER, *J. Inst. Metals*, 75 (1948/49) 403.
10 P. DUWEZ AND H. MARTENS, *Trans. Am. Inst. Mining Met. Engrs.*, 194 (1952) 72.
11 V. P. ELIUTIN AND V. F. FUNKE, *Izvest. Acad. Nauk S.S.S.R., Otdel Tekh. Nauk*, No. 3 (1956) 68.
12 V. N. EREMENKO, G. V. ZUDILOVA AND L. A. GALASKAYA, *Metalloved. i Obrabotka Metal.*, 1 (1958) 11.
13 H. BÜCKLE, *Metallforschung*, 1 (1946) 53.
14 V. N. EREMENKO, *Ukrain. Khem. Zhur.*, 20 (1954) 227.
15 A. J. BRADLEY, W. F. COX AND H. J. GOLDSCHMIDT, *J. Inst. Metals*, 67 (1951) 189.
16 A. J. BRADLEY AND A. TAYLOR, *Proc. Roy. Soc. (London)*, A 166 (1938) 353.
17 D. A. OLIVER AND H. J. GOLDSCHMIDT, *E.R.A. Report N/T41*, (1947).
18 A. J. BRADLEY, *J. Iron and Steel Inst. (London)*, 163 (1949) 19; 168 (1951) 233; 171 (1952) 41.
19 H. J. GOLDSCHMIDT, *Metallurgia*, 62 (1960) 211, 241.
20 H. J. GOLDSCHMIDT, *J. Less-Common Metals*, 2 (1960) 138.

THE EFFECT OF STRAIN RATE, AND HEAT TREATMENT, ON THE TENSILE PROPERTIES OF EXTRUDED BERYLLIUM RODS BETWEEN 25 AND 600°C

A. B. BROWN

Babcock & Wilcox, Renfrew (Scotland)

F. MORROW AND A. J. MARTIN

Atomic Weapons Research Establishment, Aldermaston, Berks. (England)

(Received December 15th, 1960)

SUMMARY

Extruded bars of beryllium ingot and sintered powder have been tensile-tested at temperatures between 25 and 600°C. The fracture mode has been found to depend on the temperature and the strain rate, and the incidence of repeated yield phenomena has been noted between 300°C and 500°C.

The ductility at 600°C of the more impure pebble ingot material has been found to be particularly affected by heat treatments, which, from their effect on the yield phenomena and on hot-hardness measurement, appear to promote precipitation of certain impurities from solution.

INTRODUCTION

A preliminary investigation of the tensile properties of extruded beryllium rods has been completed. A number of different conditions have been evaluated, varying both the source and fabrication route of the beryllium, as well as the more customary variables of strain rate and temperature of testing. During the final stages of the programme heat treatment has been introduced successfully as a further variable.

There are already numerous papers in the technical literature on the tensile testing of beryllium[1–13], but in view of the considerable effect of prior history on subsequent properties, it is very necessary to evaluate metal produced from different sources and fabrication routes. At the present time the available mechanical test data tend to emphasise the properties of thermally reduced beryllium fabricated by the powder metallurgy route favoured in America. In the current programme, the properties of the metal produced by certain alternative routes have been examined. Beryllium from two sources has been studied, namely electrolytic "flake" and thermally reduced "pebble metal". Two fabrication routes have been investigated: extrusion of cast ingot, and extrusion of pressureless sintered block.

As well as the interpretation of tensile data, consideration has been given to certain auxiliary features such as fractography and metallography, multiple yield point phenomena, chemical analysis, crystallographic texture, and the redistribution of impurities by heat treatment.

In compiling and comparing mechanical test data, emphasis has been placed on the ductility values. The sharp rise of ductility between room temperature and 300°C in extruded bar, and the subsequent fall from 400 to 600°C has been the subject of much discussion[2,4,7,9,12]. It is generally agreed that the improvement of ductility up to 300°C is the result of a decreasing resistance to prismatic (1010) slip in the hexagonal lattice. The subsequent drop in ductility, however, has required a more complex explanation, since intergranular failure and strain ageing occur together at temperatures above 300°C. A close study has been made, therefore, of the macrostructure of fractured surfaces from tensile specimens.

PROGRAMME OF TENSILE TESTS

Three batches of material were employed in the programme: Flake ingot (extruded at two temperatures, 1000°C and 1050°C), Pebble ingot, extruded at 1050°C, and pressureless sintered powder (produced from vacuum-cast electrolytic flake) extrudes at 1050°C. Some of the pebble ingot extrusion was used for heat treatment tests, and a further small batch of extruded flake ingot was also made available.

TABLE I

FABRICATION AND TESTING DETAILS OF BARS USED IN THE INVESTIGATION OF STRAIN RATE

Material	*Flake ingot extrusion*		*Pebble ingot extrusion*	*Flake pressureless sinter extrusion*
Analysis reference Table III	*Column 1*	*Column 2*	*Columns 3a, b, c,*	*Columns 4a, b.*
Extrusion temperature (°C)	1,000	1,050	1,050	1,050
Extrusion ratio	44 : 1		44 : 1	44 : 1
Number of tests	30	30	23	21
Testing temperatures (°C)	100, 200, 300 400, 500, 600		Room temp. 100, 200, 300, 400, 450, 500, 600.	Room temperature 100, 200, 300, 400, 500, 600.
Strain rates (%/min)	0.2, 0.7, 1.8, 7.0, 14.0.		0.2, 1.8, 7.0	0.2, 1.8, 7.0

Initially, testing involved five strain rates from 0.2%/min to 14%/min, but after the completion of the first series of experiments, the number of strain rates was reduced to three, 0.2%, 1.8% and 7%/min. Tensile testing was conducted at 100°C intervals between 100°C and 600°C, but on a number of occasions additional tests were required, for example at 25, 450 and 700°C.

A detailed summary of the individual tests is shown in Table I; in Table II tests involving heat treatment are detailed.

TABLE II

BARS USED IN THE INVESTIGATION OF HEAT TREATMENT VARIABLES

Material	*Pebble ingot extrusion*	*Flake ingot extrusion*
Analysis reference Table II	*Columns 3a, b, c*	*Column 5*
Heat treatments	(1) Anneal 400°C, 336 h (2) Anneal 500°C, 336 h (3) Anneal 780°C, 120 h slow cool 120 h	(1) As-received (2) Anneal 780°C 120 h, slow cool 120 h
Number of tests	(1) 2 (2) 1 (3) 5	(1) 6 (2) 5
Testing temperatures (°C)	(1) 400 (2) 500 (3) Room temp. 400, 500, 600, 700	(1) 100, 200, 300, 400, 500, 600. (2) 400, 500, 600
Strain rate	All tests at 1.8%/min	

PRODUCTION AND PREPARATION OF SPECIMENS

Prior to fabrication, both the electrolytic "Flake Metal" and the thermally reduced "Pebble Metal" were vacuum-induction-melted, and cast in an argon atmosphere, to 4 in. diameter ingots, either for direct extrusion or for powdering. For the manufacture of sintered compacts, the ingots were lathe-turned to swarf, and the swarf ball-milled to powder. The —200 mesh portion of this powder was pressureless-sintered in vacuum for 6 h at 1200°C, to 4 in. diameter blocks. Both the cast and sintered block were then sheathed in mild steel and hot-extruded to rod of $\frac{1}{2}$ in. diameter.

After de-sheathing, the extruded bars were machine-turned to No. 13 Hounsfield tensile specimens having a gauge length of 0.632-in. by 0.175-in. diameter. A standard machining procedure was adopted, removing the last 0.100-in. from the diameter along the gauge length by one cut of 0.050-in., one cut of 0.025-in., one of 0.01-in., two of 0.005-in., one of 0.002-in., and finally three cuts of 0.001-in. To remove surface-machining effects, 0.005-in. was removed from the diameter by etching and a further 0.005-in. by electro-polishing.

The only other pre-treatment given to specimens was annealing, which was applied to a small proportion of the total number. Heat treatment was carried out in vacuum in a stainless steel tube, the samples being supported in a beryllia crucible.

TENSILE APPARATUS

A Hounsfield tensile testing machine was modified as shown in Fig. 1, to suit the needs of the programme. Included in the apparatus was a resistance strain gauge dynamometer ring so that the load could be measured electrically and recorded autographically. The potential drop across the dynamometer was recorded on a Leeds and Northrup "Speedomax H" having a $\frac{1}{4}$-sec full scale deflection of 10 mV, and a chart speed of 30 in. per hour. A typical trace made during a tensile test at 400°C is reproduced in Fig. 2.

The temperature was controlled by a chromel–alumel thermocouple inserted into the furnace winding, while the specimen temperature was measured on a Doran potentiometer, employing a Platinum/Platinum–13% Rhodium thermocouple fixed loosely with asbestos tape to the test piece.

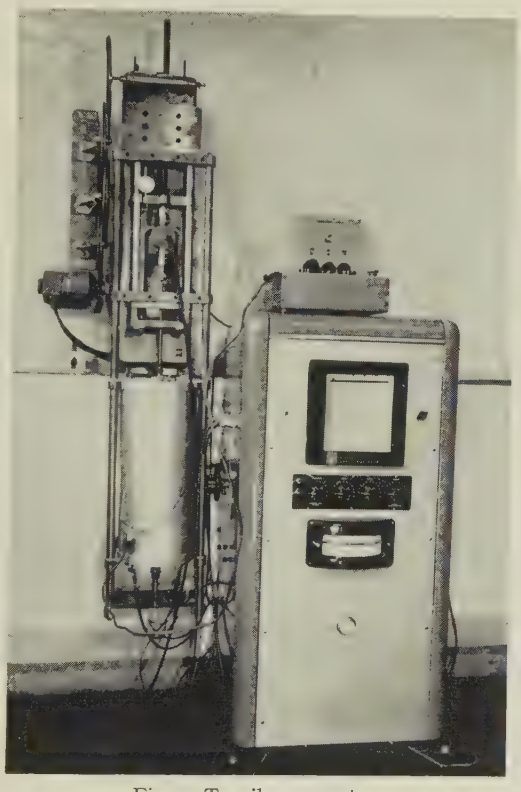


Fig. 1. Tensile apparatus.

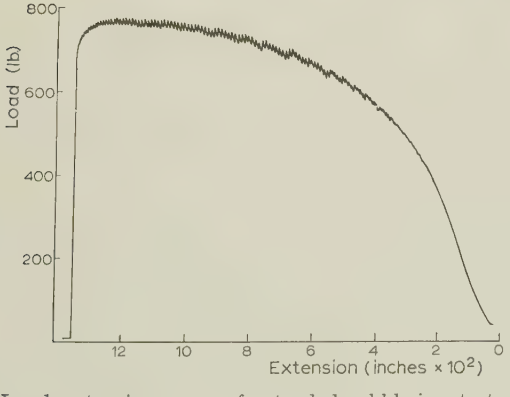


Fig. 2. Load–extension curve of extruded pebble ingot at 400°C.

The main advantage of the modified apparatus was its ability to detect and record multiple yield point phenomena. The rapid fluctuations of load caused by successive yielding could not be demonstrated satisfactorily on the piston and mercury column of the original Hounsfield machine.

TENSILE RESULTS

The tensile data obtained from the three materials, extruded flake ingot extruded pebble ingot and extruded flake sintered block, is shown in Figs. 3, 4 and 5 respectively.

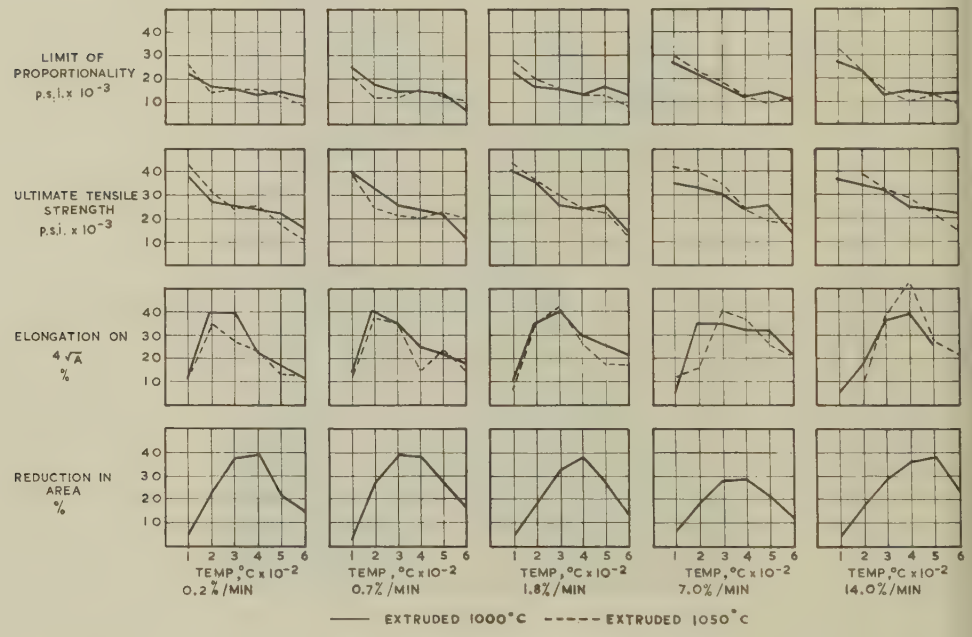


Fig. 3. Extruded flake ingot.

These figures provide comparisons of properties under four headings as follows:
(a) Extrusion temperature
(b) Purity
(c) Grain size
(d) Effect of strain rate.

(a) *Effect of extrusion temperature on the tensile properties of extruded flake ingot*

The extrusion temperature was employed as a variable in only one series of tests, the flake ingot extrusions. In Fig. 3, two sets of results are displayed, the dashed lines corresponding to bar extruded at 1050°C and the full lines at 1000°C.

In this temperature range of extrusion, it is evident that the properties of the two extrudes are very similar, and probably lie within the spread of experimental scatter.

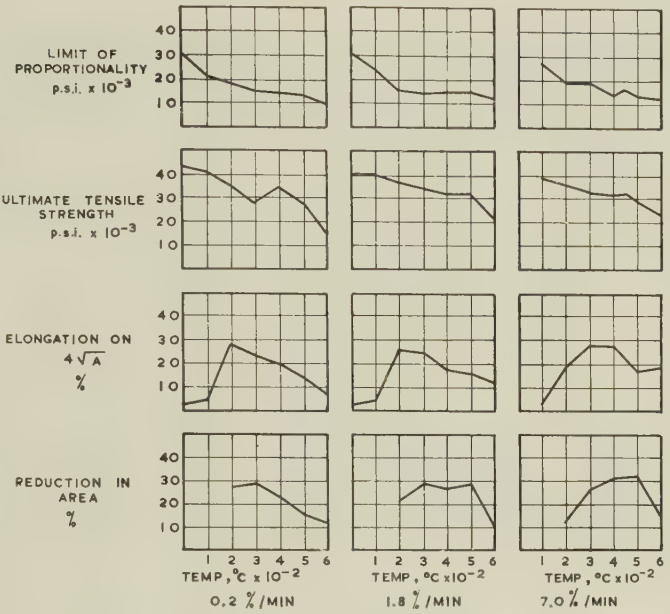


Fig. 4. Extruded pebble ingot.

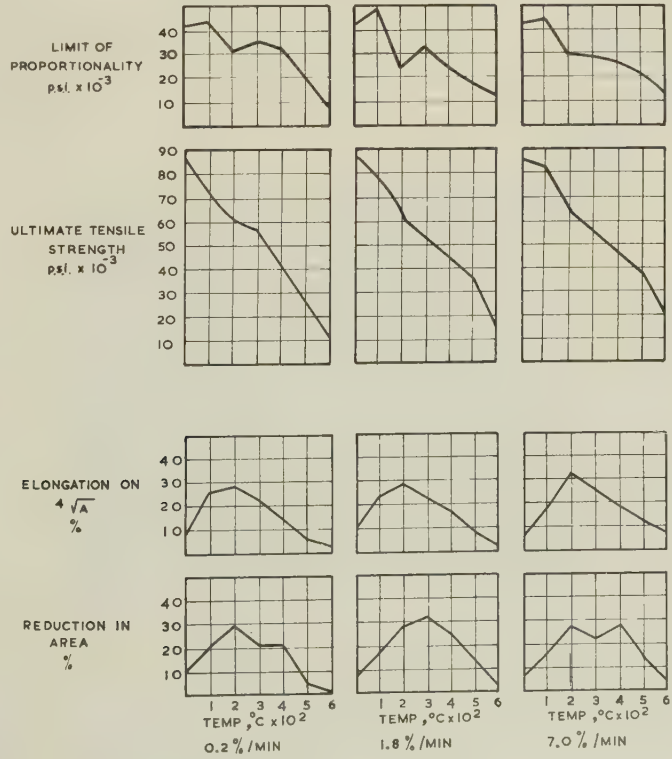


Fig. 5. Extruded flake pressureless sintered powder.

(b) *Effect of purity*

To compare the properties of two extruded bars on the basis of purity, the grain size must be similar: the comparison is restricted therefore to two materials, extruded flake ingot and extruded pebble ingot, the purities of which were significantly different, as can be seen from Table III.

TABLE III

ANALYSIS OF EXTRUDED BARS

Material	*Flake ingot extrusion*		*Pebble ingot extrusion*			*Flake powder extrusion*		*Flake ingot extrusion*
Reference number	*1*	*2*	*Triplicate analyses* *3a*	*3b*	*3c*	*Duplicate analysis* *4a*	*4b*	*5*
Iron	0.025	0.035	0.089	0.103	0.106	0.171	0.178	0.041
Aluminium	0.025	0.167	0.066	0.077	0.056	0.008	0.008	0.065
Silicon	0.030	0.033	0.058	0.076	0.119	0.109	0.094	0.061
Magnesium	0.0008	0.008	0.001	0.0006	0.001	0.003	0.002	0.002
Manganese	0.0009	0.012	0.006	0.011	0.004	0.004	0.004	0.0008
Copper	0.001	0.004			0.001			0.005
Nickel					0.022			0.018
Chromium					0.011			0.007
BeO					0.031 0.029			0.014
Combined carbon					0.03 0.05			0.005 0.002 0.006
Free carbon					0.009			0.011
Nitrogen	0.004	0.005						

The extrusions may be seen, from Figs. 3 and 4, to differ in two ways, which can be attributed to purity effects:

(i) The purer flake beryllium bar, exhibits greater ductility and lower strengths at all temperatures.

(ii) A plateau in the strength *versus* temperature curves, occurring at 300–500°C, is sustained at a higher level in the less pure pebble material.

This behaviour does not differ from that which is common to other metal systems, where the improved strength of solid solutions and dilute alloys generally is readily appreciated. The appearance of the plateau, item (ii), is, however, worth further comment.

In the temperature range 300–500°C, inflexions occur in plots of limit of proportionality and ultimate tensile strength against temperature. This temperature range is also associated with multiple yield point phenomena, indicative of strain ageing caused by the successive relocking of dislocations by mobile solute atoms. The juxtaposition of these two effects, multiple yielding and strain ageing, occurs in other systems, in steels, for example in the "blue brittle" range.

It might also be proposed that the plateau is caused by the precipitation of a second phase from a metastable solid solution at the testing temperature. This possibility was investigated by annealing specimens of the pebble bar for 336 h at 400°C and 500°C in vacuum, followed by testing at these temperatures. No alteration of properties was observed compared with the as-extruded bar. By annealing at a temperature of 780°C, however, it was possible to suppress the plateau completely and also to remove multiple yielding: consequently it is inferred that although precipitation may take place at higher temperatures, it does not occur in the temperature range associated with the plateau. A fuller discussion of this aspect of the programme will be reserved for a later section on the subject of heat treatment.

(c) *Effect of grain size*

The effect of grain boundaries is to hinder slip and hence increase the resistance to deformation; this is especially so in hexagonal metals, where, owing to the limited number of slip systems available, it is more difficult for accumulated stress on one side of a grain boundary to induce slip in the neighbouring grain. Fine-grained extrusions, therefore, give rise to higher rates of work hardening than coarse-grained structures.

A further influence of fine grain size is to retard the onset of failure by brittle cleavage; this is due probably to the more even distribution of stress concentrations by dislocations piled-up along the slip lines in a fine-grained structure. Also, in the case of beryllium, lack of uniformity of slip, as in a large-grained sample, has been said to give rise to bending stresses in neighbouring grains[6] and to crystal re-orientation during plastic deformation[7] both leading to easy cleavage of the longitudinally oriented basal planes.

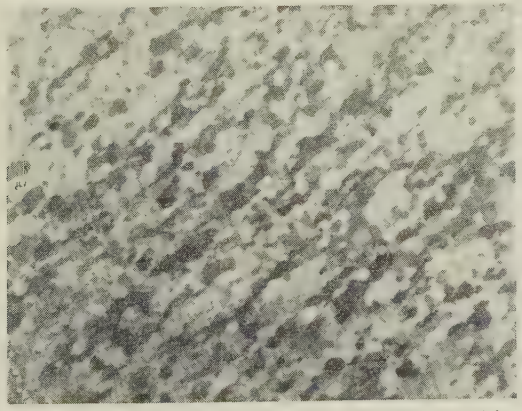


Fig. 6. Extruded flake sinter. (True magn. ×100; reduced in repr. 0.8).

The effect of grain size on the tensile properties of beryllium may be established from a comparison of Figs. 3 and 5, which show respectively flake metal extruded from ingot and powder bar. Fig. 6 and 7 illustrate typical microstructures of sinter and ingot extrusions.

Most noticeable in the graphs are the greatly superior properties of the fine-grained material in the lower temperature range, with respect to both strength and ductility. At room temperature the sinter route produces metal with an ultimate tensile strength of 85,000 p.s.i. and an elongation of 8–10%, whereas the equivalent data for the extruded ingot is 45,000 p.s.i. and 2–3%.

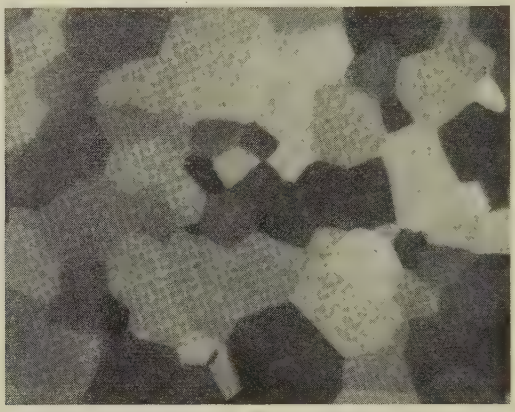


Fig. 7. Extruded pebble ingot. (True magn. × 100; reduced in repr. 0.8).

At higher temperatures, as the tensile strength falls, the relative properties of the two materials tend to reverse, within the range of grain sizes and strain rates employed in the series, owing to the influence of grain boundary failure. The deterioration of properties in the sintered beryllium is most marked in the elongation curves, reflecting the relative ease with which grain boundary failure occurs.

(d) *Effect of strain rate*

The influence of the rate of straining is revealed in three ways:

(i) at low rates of strain, in the temperature range 400–600°C, the proportion of the total extension contributed by grain boundary slip is increased, thus leading to early failure by cracking at triple points[14] and cavitation at grain boundary discontinuities[15];

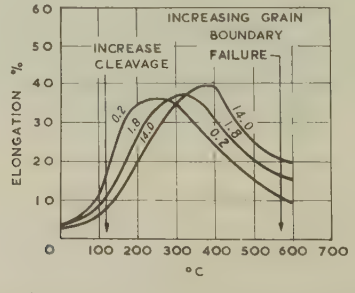


Fig. 8. Effects of strain rate and temperature on elongation characteristics of extruded ingot beryllium.

(ii) at low rates of strain, the time available for strain hardening by diffusion of impurities is longer, in the range 300–600°C, and the strength of the matrix relative to the grain boundaries at the higher temperatures becomes greater;

(iii) at high rates of strain, in the low temperature range from room temperature to 200°C, brittle cleavage fracture can be sustained at lower overall deformation.

Effects (i), (ii) and (iii) together control the shape of the elongation curves, as shown diagrammatically in Fig. 8. The strength curves, however, seem unaffected by strain rate, except in the high temperature range where low strain rates encourage intergranular failure and low fracture strengths.

TEXTURE OF EXTRUDED FLAKE INGOT

One of the extruded bars was submitted for X-ray reflection texture examination. Transverse specimens were cut at intervals from the bar and mounted for the measurement of prismatic reflections for $\phi = 0° - 60°$ in 10° intervals.

As is customary, a preferred crystal orientation was observed (Fig. 9) with C-axes orthogonal to the extrusion direction, and basal planes consequently parallel to the extrusion direction. No significant texture variation was noted along the bar.

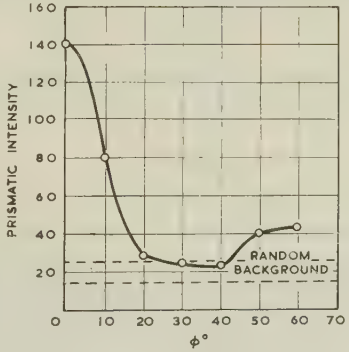


Fig. 9. X-ray texture curve of extruded flake ingot.

FRACTOGRAPHIC EXAMINATION

A comprehensive survey of the specimens fractured in the extruded pebble ingot series has been made. The microscope work was initiated mainly because of the lack of understanding of the general fracture modes, and, in particular, of the existence of certain "dark zones" on the fracture surface. The occurrence of these dark areas and the variation in the extent to which they occur as the testing temperatures increases from room temperature to 600°C, is shown for pebble ingot in Fig. 10. In this series the distinction between bright and dark areas is not as marked in the photograph as on visual examination, since the relatively coarse reflective grains made the fracture surfaces difficult to reproduce. At first it was thought, by reference to the literature[1,3], that the dark areas were caused by intergranular failure. Subsequent examination of test pieces with a low power stereoscopic microscope, X35, from all

test temperatures in the Pebble ingot series, revealed that grain boundary failure was distinctive only at 500°C and 600°C. At lower temperatures the dark area was associated with longitudinal splitting and elongation of grains, forming a jagged, needlelike fracture.

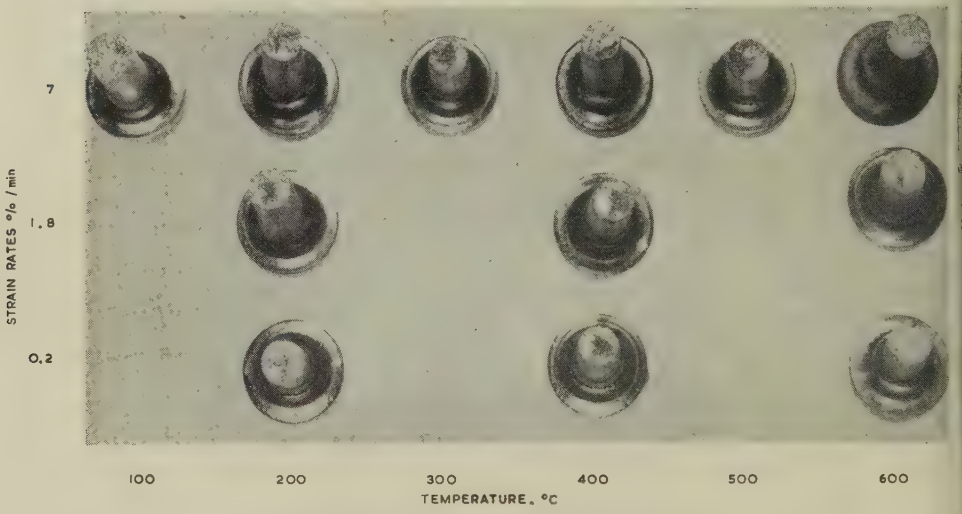


Fig. 10. Fractrographs of extruded pebble ingot.

Three fracture modes could be distinguished:

(a) Cleavage perpendicular to the direction of tension, producing highly reflective facets, observed at all temperatures, but particularly at 25 and 100°C and decreasing in quantity up to 600°C.

(b) A jagged mode of fracture, with elongation and intensive splitting of grains, observed at temperatures between 100 and 500°C.

(c) Intergranular failure, at 500 and 600°C.

EXAMINATION OF LONGITUDINAL SECTIONS OF FRACTURED EXTRUDED PEBBLE INGOT SPECIMENS

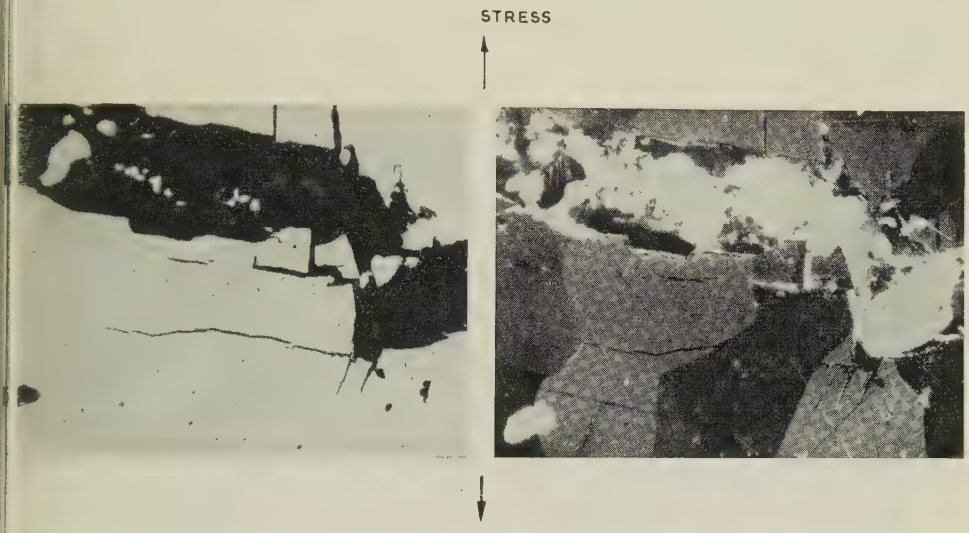
The microscopic survey of the pebble ingot series included specimens tested at all temperatures, and, where appropriate, at several strain rates. The display of photomicrographs, however, is restricted to typical sections selected to illustrate points of interest.

Dealing first with cleavage fracture, Figs. 11 and 12 show the bright cleaved region of a specimen tested at 200°C and at a strain rate of 1.8%/min. The fracture planes in the testing of single crystals have been determined by TUER AND KAUFMANN[7] and it may be presumed from a knowledge of the extrusion texture that the cleavage path in the above photographs follows $(11\bar{2}0)$ planes, interrupted by cleavage steps on (0001) planes parallel with the axis of the bar.

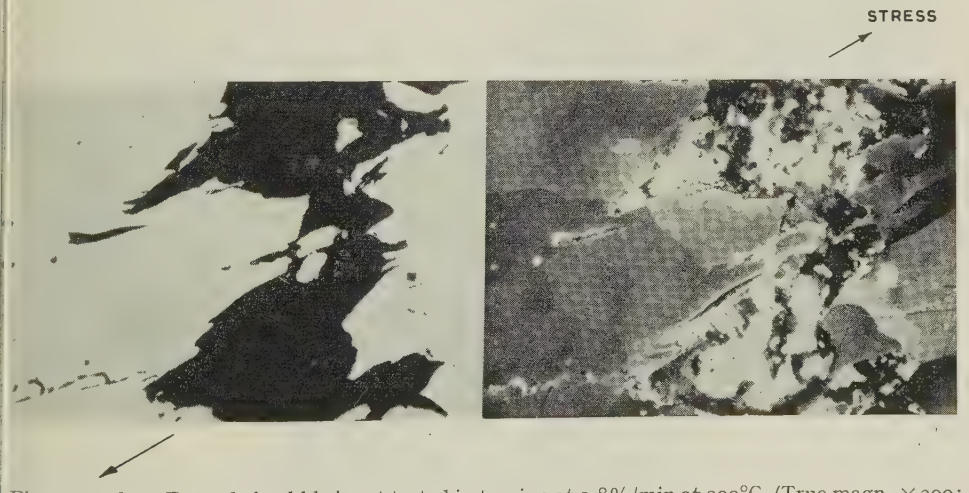
The dark area of fracture, also examined in the test piece at 200°C at 1.8%/min strain rate, is illustrated in Figs. 13 and 14. These photomicrographs are typical of

fracture in this zone up to 300°C. Indications of increased ductility are very slight, the darkness of the fracture being due to fragmentation of grains assisted by longitudinal splitting, rather than to the development of a fibrous structure.

Further understanding of the fracture mechanism was obtained by examining



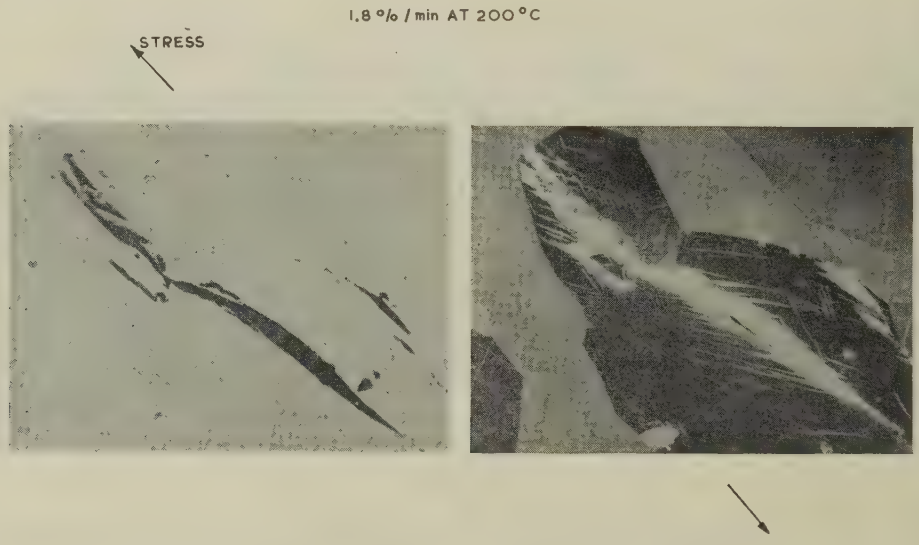
Figs. 11 and 12. Extruded pebble ingot tested in tension at 1.8%/min at 200°C. Bright area of fracture. (True magn. ×200; reduced in repr. 0.75)



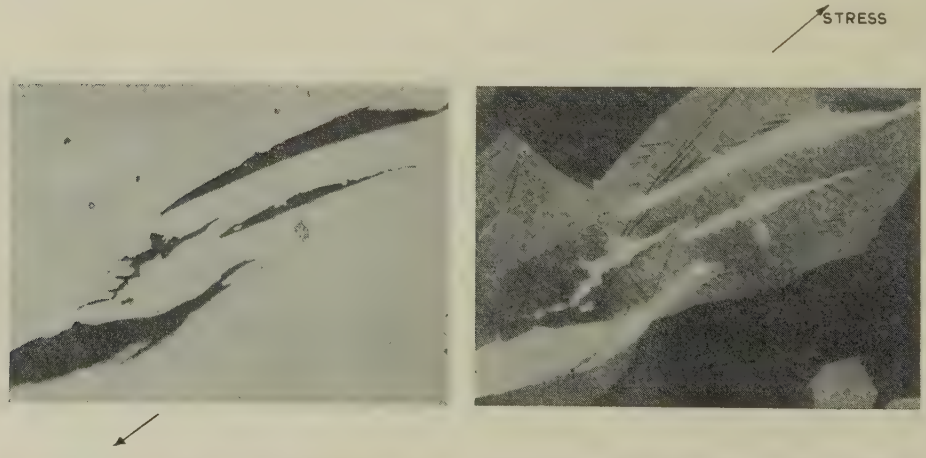
Figs. 13 and 14. Extruded pebble ingot tested in tension at 1.8%/min at 200°C. (True magn. ×300; reduced in repr. 0.75)

grains at some distance from the main fracture. Figs. 15 and 16, taken about 0.2 in. from the fracture, illustrate longitudinal splitting of grains, which are linked transversely in Figs. 17 and 18 to show a probable mode of fracture nucleation.

From the preferred orientation of the bar, and from the known behaviour of beryllium it is inferred that the longitudinal cracks are caused by the cleavage planes. An analysis of basal plane cracking has been made in terms of the formation of bend planes and kink bands[7], as shown in Fig. 19.

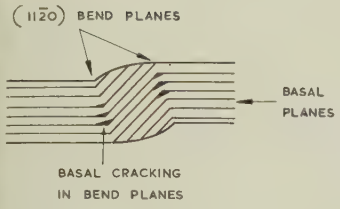


Figs. 15 and 16. Internal splitting of grains. (True magn. ×300; reduced in repr. 0.75)



Figs. 17 and 18. Linking of longitudinal cracks by transverse cleavage or shear to form dark area. (True magn. ×300; reduced in repr. 0.75)

In beryllium, the bend plane, or tilt boundary, is a $(11\bar{2}0)$ prism plane. The single crystal investigation of TUER AND KAUFMANN[7] demonstrated that bend planes form only by processes involving slip or bending of (0001) basal planes; or, in certain



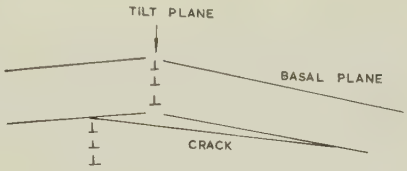


Fig. 20. Basal cracking by Stroh's mechanism.

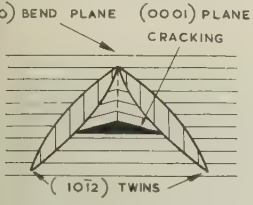


Fig. 19. Fracture of basal planes by kink band activity.

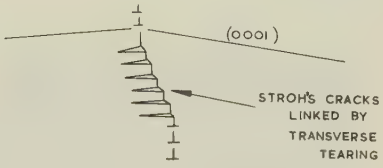
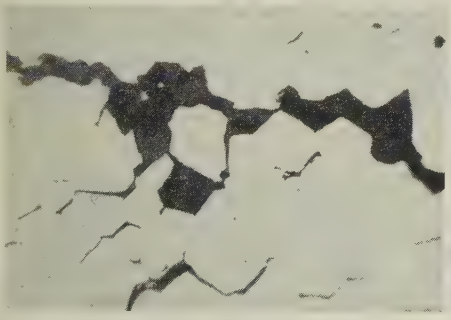
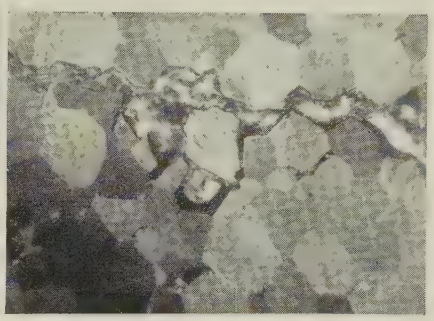


Fig. 21. Mode of (11$\bar{2}$0) fracture, due to BARNBY.





Figs. 22 and 23. Grain boundary failure at 600°C at a strain rate of 0.2%/min. (True magn. ×100; reduced in repr. 0.75)

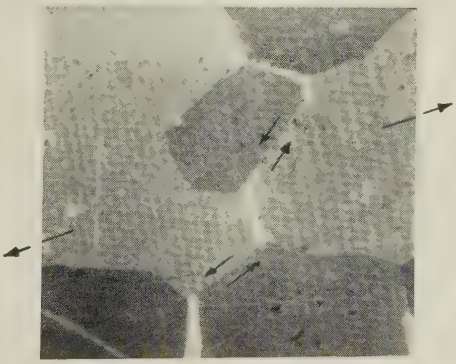


Fig. 24. Cracking initiated by grain boundary sliding at 600°C at a strain rate of 0.2%/min. (True magn. ×300; reduced in repr. 0.75)

orientations, when other modes of deformation are inhibited, by twinning. Invariably basal plane cracking occurs at the site of bend plane activity.

It is significant that the fracture strength of single crystals in compression can depend on the ability of the specimen to form kink bands. With orientations permitting slip on (0001) basal planes, failure occurs at 2500–3000 p.s.i. When the basal planes are perpendicular to the applied stress and are prevented from slipping, stresses of 15000–16000 p.s.i. can be reached, and at this point, twinning, with bend plane activity, leads to failure[16].

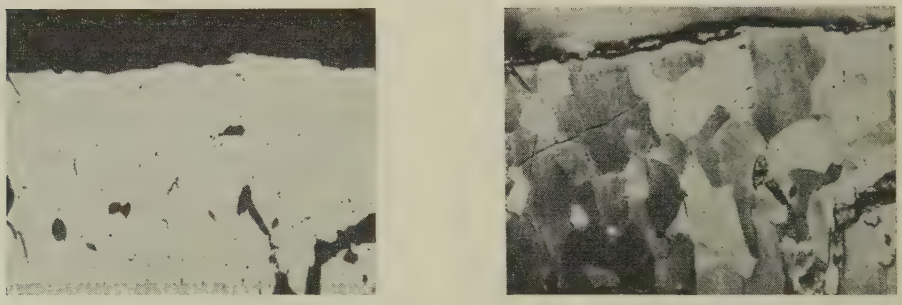


Fig. 25. Extruded pebble ingot; bright area of fracture at 400°C. (True magn. ×80; reduced in repr. 0.75)

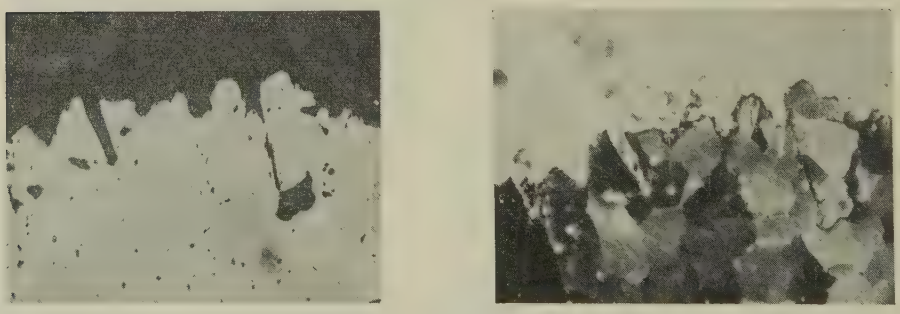
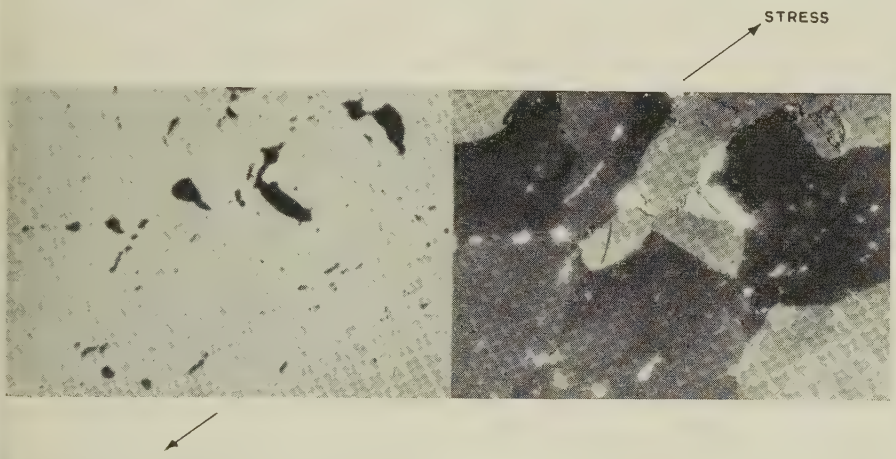


Fig. 26. Extruded pebble ingot; dark area of fracture at 400°C. (True magn. ×80; reduced in repr. 0.75)

The bend plane mode of fracture may be initiated by Stroh's mechanism illustrated in Fig. 20 whereby one part of the bend plane is anchored, and the remainder displaced by glide. BARNBY[17] has extended this principle to cleavage on $(11\bar{2}0)$ pyramidal planes (and also to the twin matrix interface) as shown in Fig. 21. Large numbers of small Stroh's cracks can be linked together by tearing of the intervening material to cause fracture. It is interesting to note that the above sequence appears to have taken place in Figs. 17 and 18, but, on a much larger scale than proposed by BARNBY; moreover, the multiple basal cracking is not associated with $(11\bar{2}0)$ cleavage, but with the dark fragmented region of fracture.

Deformation by twinning was seldom observed, with the exception of grains containing a longitudinal crack of the above type. Figs. 16 and 18 illustrate intense twinning on either side of the basal cleavage crack. There has been discussion as to whether such twins could be formed prior to fracture, or whether they might be caused by the fracture process itself. An analysis based on a mechanism whereby twins form successively in the distorted stress field at the tip of a moving (0001) crack has been made by BILBY AND BULLOCK[18], for which there is observational support in the hexagonal metal zinc[19]. Initiation of failure by twinning in the present investigation



Figs. 27 and 28. Extruded pebble ingot tested at 400°C and 0.2%/min. (True magn. × 300; reduced in repr. 0.75)

is not considered likely since the axial ratio of beryllium does not encourage twinning when the principal stress direction is parallel or nearly parallel to the basal plane.

At temperatures of 500 and 600°C fracture by intergranular cracking is easily recognised in the pebble metal. Figs. 22 and 23 illustrate grain boundary failure at 500°C at a strain rate of 0.2%/min. Fig. 24, taken at some distance from the zone of failure, shows cracking initiated by grain boundary sliding.

In the intermediate temperature range at 400°C, the path of fracture within the dark area was difficult to observe. Widespread basal splitting was not observed, neither was grain boundary breakdown. The specimen tested at 400°C and 0.2%/min strain rate is illustrated in Figs. 25 and 26 at low magnification, while Figs. 27 and 28 show, in greater detail, the region immediately behind the fracture. It is possible, as can be seen in the photomicrographs, that fracture under these conditions is being assisted by cavitation, but it would be imprudent to make conclusions on the appearance of only one specimen.

MULTIPLE YIELDING

Multiple yield point effects were observed during the tensile testing of beryllium in the temperature range 400–500°C. The appearance of a typical load–extension curve is shown in Fig. 2, reproduced from a test on extruded pebble ingot at 400°C and

1.8%/min strain rate. It was found to occur also in the flake ingot extrusions, and to a much lesser extent in the sintered powder bar. The phenomenon may signify three proposed deformation modes (a) twinning[20] (b) repeated strain ageing[12,22,23], (c) localised yielding, as with Luders bands[24].

(a) *Twinning*

Twinning during the deformation of single crystals of hexagonal metals may produce a load–extension curve consisting of a series of very irregular yields, as recorded for example by BOAS AND SCHMID[20].

It is unlikely, however, that twinning need be considered a major deformation mechanism in extruded beryllium in the temperature range 400–500°C where multiple yielding is encountered. The crystallographic orientation developed in beryllium after extrusion is one where the C-axes are orthogonal to the extrusion direction; in hexagonal metals, where the c/a ratio is less than $\sqrt{3}$, as in beryllium, twinning would not be expected with the C-axes perpendicular to the tension direction since the resulting re-orientation would be accompanied by a decrease of length in this direction[22,25].

The conditions for twinning in polycrystals are understandably more complicated, and grains otherwise unfavourably orientated might be constrained to twin, although KAUFMANN *et al.*[2] have reported that there is no twinning in longitudinal specimens of extruded ingot tested in tension above 300°C.

(b) *Repeated strain ageing*

Commonly, multiple yielding in polycrystalline materials is attributed to strain ageing during plastic deformation, within a limited temperature range where the mobility of impurity atoms and dislocations are related. The phenomenon may be enhanced in the freshly quenched condition[26] presumably because the maximum amount of impurity is then in solution (but also, it is said, because vacancies which assist diffusion can be retained)[21]. It also depends on the presence of certain specific impurity elements, for example, copper and magnesium in aluminium[27], or carbon and nitrogen in iron.

One of the difficulties of the theory of repeated dislocation locking is the relatively slow rates of diffusion of substitutionally dissolved copper and magnesium in aluminium. Analogous elements in beryllium also are probably substitutional. COTTRELL[21] has proposed that the mobility of the substitutional atoms can be increased by the formation of vacancies: for this reason, multiple yielding does not appear in aluminium, as also in beryllium, until there has been appreciable prior deformation. However, aluminium quenched from 520°C with retained vacancies displays multiple yielding immediately[26]. In iron, the mobility of interstitial carbon and nitrogen is relatively unaffected by vacancies.

During the series of tests on the extruded Pebble ingot, a record was kept of the incidence of multiple yielding, and the effect of temperature and strain rate noted. In addition to the standard tests at 100°C intervals, a further three specimens were fractured at a temperature of 450°C, which, as shown in Table IV, appears to lie in the centre of the limiting temperature range. Evidently the effect is reduced at lower temperatures and higher strain rate, or at higher temperatures and lower strain rates. At 450°C, the effect was independent of strain rate within the range employed.

These observations could be interpreted in terms of the relative mobilities of impurity atoms and dislocations. At low temperatures and high strain rates the dislocations break away and are not locked again, whereas at high temperatures and slow strain rates the impurities can diffuse with the dislocations. In either case there is no repeated yielding.

TABLE IV

NUMBER OF YIELDS DETERMINED IN TENSILE TESTS ON EXTRUDED PEBBLE BAR

Temp.	*Strain rate %/min*	*No. of yields*
300	0.2	0
	1.8	0
	7	0
400	0.2	118
	1.8	112
	7	40
450	0.2	120
	1.8	80 (premature fracture)
	7	120
500	0.2	0
	1.8	118
	7	130
600	0.2	0
	1.8	0
	7	0

The mechanism by which the impurity atom and the dislocation are re-united after yielding provides an interesting subject for discussion. The mechanism may depend on the nature of the testing machine.

In general, two types of tensile machine are available:

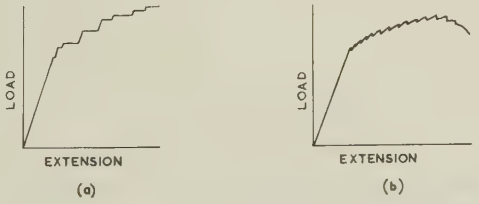


Fig. 29. Effect of tensile machine on multiple yielding.

(i) Constant rate of loading machine, operated by a deadweight: the load–extension curve recorded on such a machine under multiple yielding conditions is shown in Fig. 29a.

(ii) Constant strain rate machine: in this apparatus the load is applied by the elastic strain in a threaded tie bar. Such a machine may be "hard" or "soft" depending

on the amount of elastic strain in the tie bars at a given load. A typical load–extension curve during multiple yielding is shown in Fig. 29b.

In a deadweight machine, the stops in the plastic range of the curve consist of yielding, work hardening, and consequent arrest of plastic deformation, followed by a period during which the load increases until further yielding is permitted, the cycle repeating to fracture. It is evident that the arrest period may be the interval during which ageing occurs.

In a constant strain rate machine, the plastic range of the curve is composed of alternate yielding and elastic re-tightening of the machine, once again providing a time interval which might accommodate ageing.

It is reasonable to propose that the presence or absence of multiple yielding during a tensile test will be affected by the duration of the halt in plastic extension. This will depend, in case (i) on the rate of load application, and in (ii) on the rate of straining and on the softness of the machine (it is possible that a soft machine will sustain multiple yielding at higher strain rates than a hard one). In a constant strain rate machine, whether hard or soft, the load will fall after yielding to some value, at which the specimen is no longer required to yield. In a soft machine this drop in load causes a relatively greater elastic alteration in the remaining parts of the machine, which has to be "taken up" again before re-attaining the yield strength. With a hard machine, re-application of load should be more swift. For the same drop in load, the time available for ageing is longer in a soft machine than a hard one. Possibly justification for the Cottrell theory could be obtained by experiments of this type, in which a machine could be softened by introducing rings, or hardened by reducing the diameter of the specimen.

(c) *Luders bands*

A serrated load–extension curve may be observed due to the stepwise progression of Luders bands from one end to the other of a test piece. This mechanism has been observed[24] in the tensile testing of iron wires at 200°C. The load in such a test may not increase until yields have progressed throughout the specimen, when subsequent yielding occurs by a secondary set of Luders bands at increasing loads.

It may seem unlikely that Luders bands could form in beryllium, owing to the limited number of slip systems, but the preferred grain orientation developed by extrusion might assist the passage of slip bands across grain boundaries.

THE EFFECT OF HEAT TREATMENT ON THE MECHANICAL PROPERTIES OF EXTRUDED PEBBLE INGOT BERYLLIUM

A limited programme of heat treatment was carried out using extruded pebble metal. The purpose of the experiments was twofold:

(a) to separate the effects due to thermal precipitation, if any, from those due to strain rate. This was considered necessary since the time at temperature varied from 5 h for tests at the slow strain of 0.2%/min, to 1 h for tests at 7.0%/min.

(b) to cause maximum thermal precipitation, if any, by slowly cooling from a temperature below that at which grain growth could occur.

Under heading (a) one specimen was annealed for 336 at 400°C in vacuum, followed by tensile testing at 400°C employing strain rates of 1.8%/min. A further specimen was

given a similar treatment at 500°C. The treatments at 400°C and 500°C appeared to have very little effect, as shown in Fig. 30 and need no further discussion.

The possibility of precipitation during very slow cooling from a higher temperature, problem (b), was investigated by annealing several specimens for 120 h at 780°C in vacuum, followed by cooling to room temperature over a further 120 h. The temperature of 780°C was chosen as a temperature at which atomic migration might be

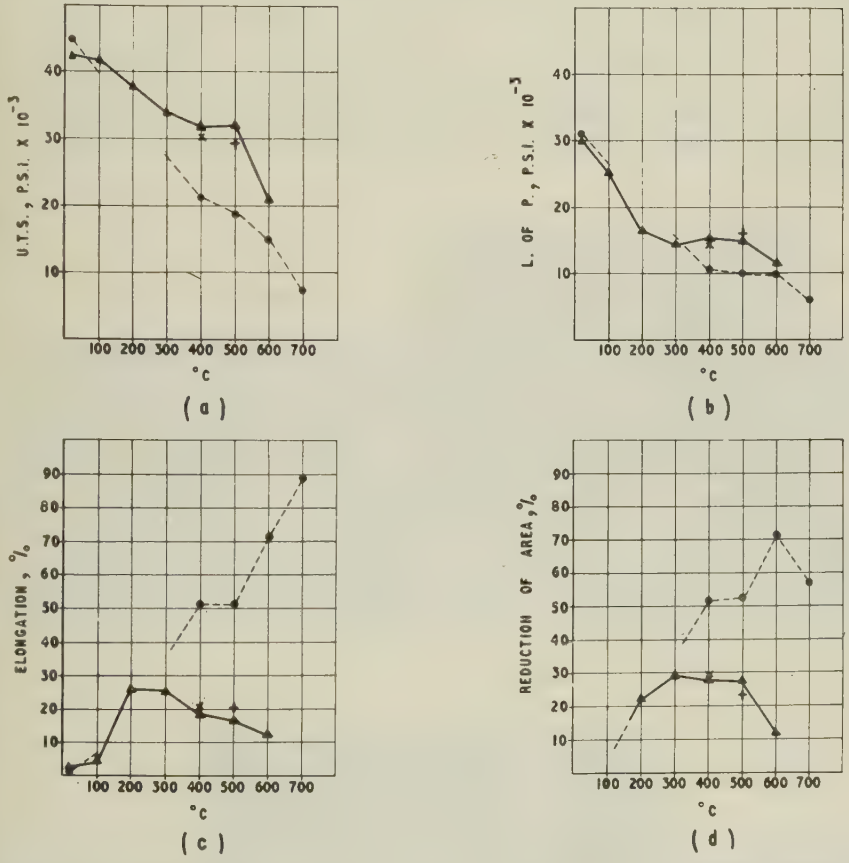


Fig. 30. Heat treatment of extruded pebble ingot; ▲, as-extruded; ●, annealed, 780°C, 120 h, slow cooled; ×, annealed, 400°C, 336 h, slow cooled; +, annealed, 500°C, 336 h, slow cooled.

rapid, without causing attendant grain growth. Five specimens were available for this experiment, and tensile tests at 1.8%/min strain rate were conducted at 25°, 400°, 500°, 600° and 700°C. The results obtained from the second treatment are also shown in Fig. 30 superimposed upon the properties of the as-received bar.

As can be seen, heat treatment at 780°C produced a marked effect on mechanical properties, very high elongations being obtained in the temperature range formerly connected with grain boundary failure. A detailed summary of the alterations brought about by annealing is listed below:

(a) greatly increased ductility was observed at temperatures from 400–700°C;

(b) concurrent with the increase of ductility, there was a reduction of strength so

that the plateau previously observed in the limit of proportionality and ultimate tensile strength curves disappeared;

(c) multiple yielding, observed in the "as-received" bar, was absent in the heat treated condition;

(d) room temperature properties were unaffected by heat treatment;

(e) there was a change in the fracture mode at high temperatures, intergranular failure being replaced by a fibrous ductile mode.

THE EFFECT OF HEAT TREATMENT ON THE FRACTURE MODE OF EXTRUDED PEBBLE INGOT

A photographic comparison of fracture modes in tests at 600°C, before and after heat treatment is shown in Figs. 31 and 32. Fig. 31 illustrates the ability of the annealed

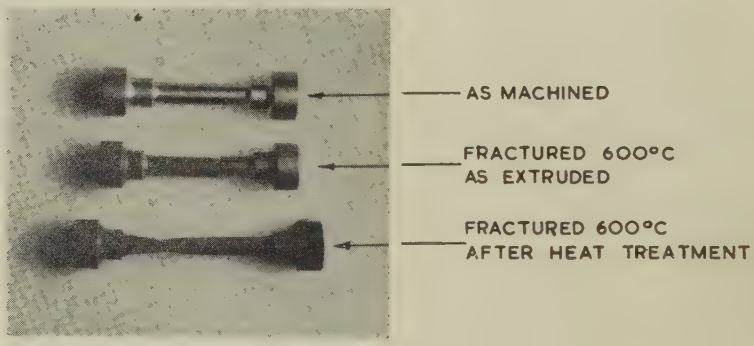


Fig. 31. Heat treatment of extruded pebble ingot. Actual size.

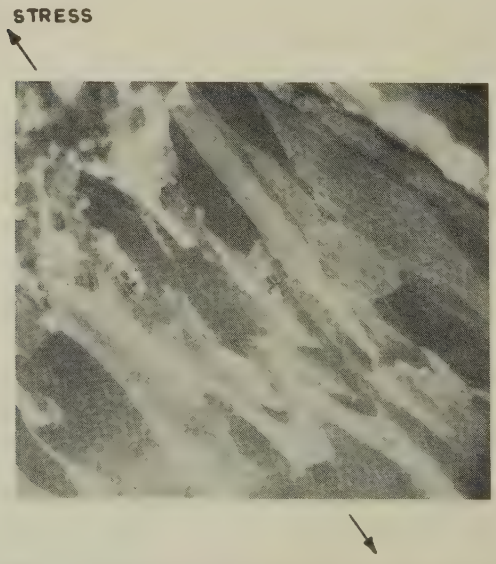
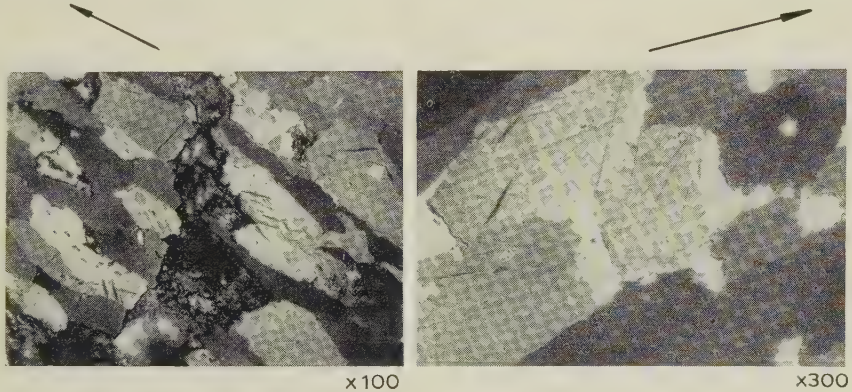


Fig. 32. Fracture at 600°C of extruded pebble ingot after heat treatment. (True magn. ×100; reduced in repr. 0.75)

specimen to neck, a feature which has been absent from all previous tests. In Figs. 23 and 24, from the as-received bar tested at 600°C, referred to previously in the section on fractography, attention is redrawn to the influence of grain boundary sliding at elevated temperatures. In contrast, the appearance of the heat-treated specimen fractured at 600°C, in Fig. 32, reveals no indication of intergranular failure, and displays a remarkable degree of grain elongation.

The graphs in Fig. 30 show a continuous improvement of elongation, after annealing, up to the maximum testing temperature of 700°C, but with deterioration of the Reduction of Area value from 600–700°C. Less necking was observed in the 700°C specimen, and the high ductility at this temperature was considered to be due, at least in part, to intergranular parting. Microsections from this test piece (Figs. 33 and 34) revealed less grain deformation, while intergranular holes were numerous.



Figs. 33 and 34. Heat treatment of extruded pebble ingot, tested at 700°C. (Reduced in repr. 0.75)

HEAT TREATMENT OF EXTRUDED FLAKE INGOT

In view of the known difference in purity between pebble and flake beryllium, a difference in the reaction of these two materials to heat treatment might be expected.

A new series of flake ingot specimens was tensile-tested in the as-received condition at 100°C intervals with a strain rate of 1.8%/min up to 600°C, while a further batch of five specimens was heat treated from 780°C as before. A comparison of the two sets of results is shown in Fig. 35.

The response of this batch of flake beryllium to heat treatment was not marked: in particular, no improvement of "necking" of fracture was obtained. In this series too, no multiple yielding effect was observed either before or after annealing.

THE INFLUENCE OF HEAT TREATMENT ON HARDNESS *versus* TEMPERATURE CURVES

Concurrent with the tensile programme at A.W.R.E., an investigation of the hot hardness and ageing characteristics of beryllium, from various routes was in pro-

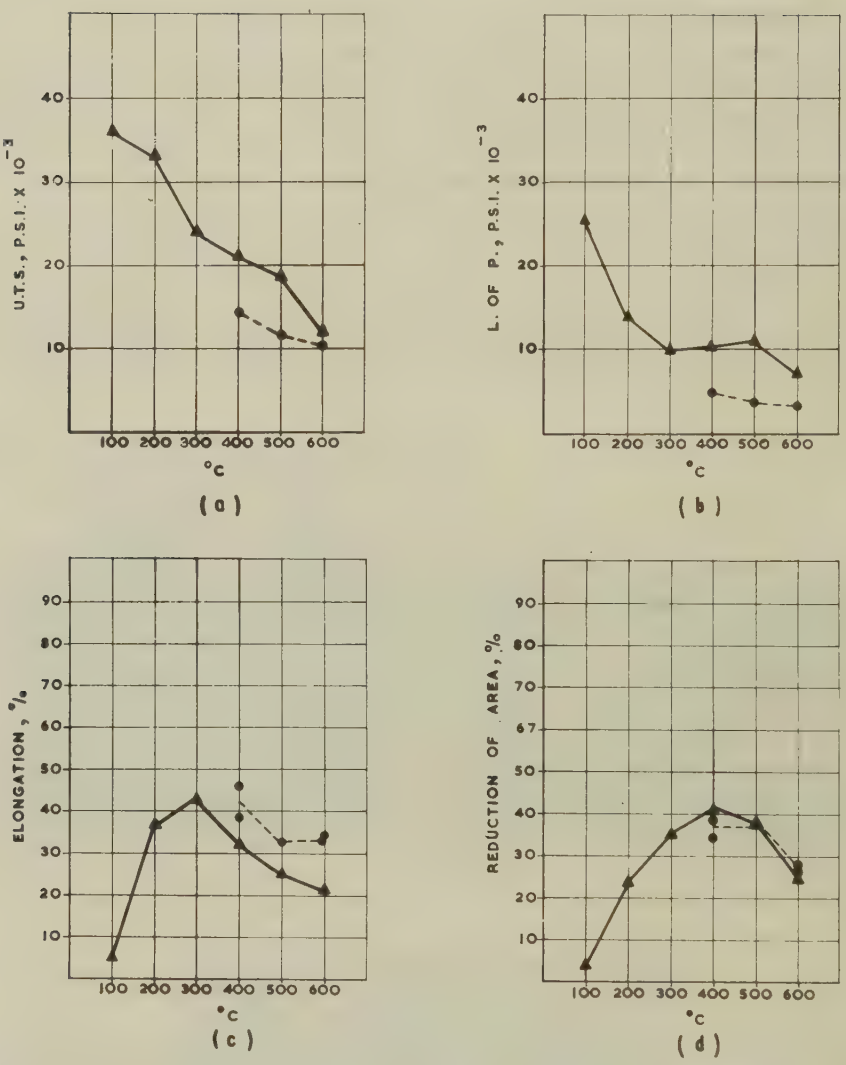


Fig. 35. Heat treatment of extruded Flake ingot; ▲, as-extruded; ●, annealed, 780°C, 120 h, slow cooled.

gress[28]. In Fig. 36 is shown a hardness plot of flake and pebble bar, in the as-extruded state, measured over the range room temperature to 600°C. Clearly, the extruded Pebble ingot is considerably harder in the temperature interval 300–500°C, which is the range previously associated with solution hardening effects.

After annealing from 780°C, the hardness curve of the pebble metal was lowered to to coincide with the flake metal curve, as in Fig. 37. It was found, however, that the original characteristics of the pebble metal curve could be recovered by quenching after a further solution treatment at 1000°C although the 1000°C treatment caused grain growth accompanied by a small degree of softening. The heat treatment, therefore, was proved to be completely reversible.

Further tests were conducted in which specimens of extruded pebble ingot were annealed at 600°C, 700°C and 800°C. The initial rate of softening was greatest at 800°C, but little significant difference between the 700°C and 800°C curves remained after 80 hours.

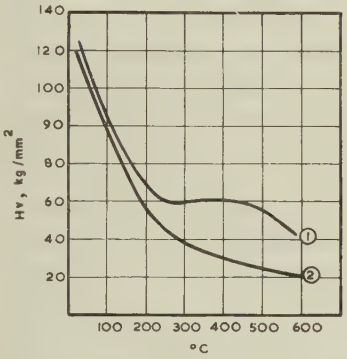


Fig. 36. Hardness curves for as-extruded ingot beryllium. Curve 1, extruded pebble ingot; curve 2, extruded flake ingot.

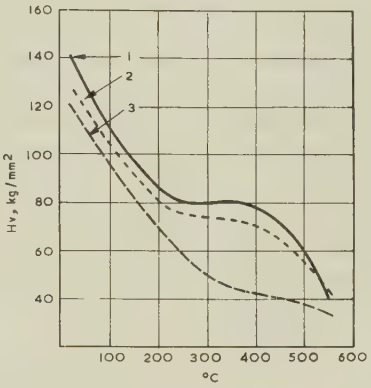


Fig. 37. Hardness curves for heat-treated extruded ingot pebble metal. Curve 1, as-extruded; curve 2, solution treated at 1000°C and quenched; curve 3, annealed at 780°C.

DISCUSSION OF HEAT TREATMENT EFFECTS

The variations in mechanical properties with heat treatment are most readily explained by a precipitation mechanism. The observations which lead to this conclusion are contained under the following headings:

(a) the disappearance of multiple yielding after annealing;

(b) the removal of the solution hardening plateau;

(c) the removal of the hardness "plateau" in extruded pebble metal on annealing, followed by rehardening after solution treatment and quenching from 1000°C.

Verification of the precipitation theory, however, requires the identification of the element(s) involved. With the analysis data at present available this is not simple, although it is possible to make tentative suggestions.

Considering the metallic elements (Table III), the impurities which are present in significant quantities are iron, silicon, aluminium and, to a lesser extent, nickel. Nickel in the quantity present is known to be completely soluble at room temperature[29], while silicon[29] is insoluble (although this latter system is not known accurately at the beryllium-rich end). The beryllium-iron system has been determined reliably by the long-term annealing of diffusion couples[30], and it would appear that iron, in the quantity present, even in pebble metal, is completely soluble in the binary system, at 780°C, although circumstances might be complicated by the formation of ternary phases. The beryllium–aluminium system[31] also indicates complete solution of aluminium, at 780°C in the quantities analysed.

As can be seen from columns 3c and 5 in Table III, the oxygen content of the pebble material, as determined by neutron irradiation, is greater than that of the flake by

a factor of two. The carbide content determined by a gas evolution method, is also greater in the thermally reduced product, by a factor of approximately ten. Recent developments have allowed the estimation of both free and combined carbon, and it should be of interest to discover whether the relative proportions are affected by heat treatment. Finally, with respect to nitrogen, there is, unfortunately, no comparative data available.

Confining the discussion now to the two extrusions used in the heat treatment investigation, the pebble ingot, column 3c, and the flake ingot, column 5, it would seem reasonable that the annealing process makes the grains of metal more deformable by removing a stiffening solute. It is surprising, therefore, that the properties of the flake material should be poorer with respect to elongation at fracture at 600°C, although the overall purity is superior to the pebble metal. Clearly, the strength of the matrix in both materials after heat treatment is similar, as evidenced by the comparable hardness measurements in Figs. 36 and 37. The difference in the ductility as fracture between the two extrusions, therefore, is probably due to grain boundary effects which exert their influence on the fracture mode under tension, but have little influence during the hardness test.

From these observations, it may be postulated that, at elevated temperatures, the higher ductilities are obtained in the annealed pebble ingot extrude because the grain boundary strength is greater, and that this superiority might be due to two factors:

(a) the presence of grain boundary precipitates in pebble bar, which may or may not be affected by heat treatment;

(b) the redistribution of an impurity element(s) to the grain boundary.

It is proposed, therefore, that there is an element(s), presumably distributed throughout the grain matrix, which is responsible for solution hardening and its allied effects, and which can be precipitated by annealing. Furthermore, an element(s) distributed in the region of the grain boundary, which may or may not be affected by heat treatment, is responsible for the improvement in intergranular strength. Whether this element(s) is the same in each case is not known.

CONCLUSIONS

The findings of the various sections of the programme can be dealt with chronologically.

1. The tensile properties of flake ingot bar, between room temperature and 600°C, are not affected markedly by variations in extrusion temperature between 1000° and 1050°C.

2. The increased purity of the as-extruded flake ingot beryllium, compared with the pebble product, results in higher ductility and lower strength values up to 600°C. In particular, there is a plateau in the strength *versus* temperature curves between 300°C and 500°C which is attributed to solution hardening, and is sustained at a higher level in the less pure pebble material.

3. The finer grain size and higher oxide content inherent in the extruded powder metal greatly improves the low temperature strength and ductility, but may give inferior properties at 600°C.

4. The rate of tensile straining affects properties at all temperatures, but particularly in the range 300-600°C where strain ageing and intergranular failure are operative.

5. Three modes of failure are encountered in the ingot extrusion between 25 and 600°C:

(a) transverse cleavage of prism planes,
(b) longitudinal splitting of basal planes,
(c) failure originating at grain boundaries.

Fracture modes (b) and (c) both produce non-reflective surfaces, and may be confused without a microscopic examination.

6. Multiple yielding has been observed in the range 400–500°C. The effect is dependent upon strain rate, purity, grain size and possibly on the geometry of the test piece. It is also sensitive to heat treatments involving long term annealing followed by slow cooling from 780°C. Multiple yielding is co-incident with the plateau in the strength *versus* temperature curves, and can implement, therefore, the understanding of strain ageing phenomena.

7. Beryllium responds to heat treatment in the range 600–800°C. The result of heat treatment is a reduction of strength in the temperature range above 300°C (formerly associated with solution hardening) and the removal of multiple yielding. An outstanding increase of ductility of the pebble ingot extrusion has been obtained by heat treatment, but this improvement does not occur in the purer beryllium.

8. The mechanism of fracture in the heat treated pebble ingot extrusion has altered, at 600°C, from a brittle intergranular mode to a mode which allows extensive ductile elongation of grains.

9. The alteration of properties after annealing has been ascribed to purification of the matrix by precipitation of impurities. Evidence of this has been supplied not only by tensile testing but also by hot hardness studies.

10. The differing responses of pebble and flake bars is attributed to a purity effect, and it is suggested that this is such as to make the grain boundaries of the pebble material stronger than the flake.

11. It has not been possible, so far, to identify either the impurity(ies) responsible for strain ageing, or those responsible for grain boundary strengthening. Possibly these two effects might be caused by a redistribution after heat treatment of the same element.

ACKNOWLEDGEMENTS

The authors would like to thank Mr. G. C. Ellis, Superintendent of Research, for his encouragement throughout the research.

REFERENCES

1 F. C. Hull, *A.E.C., Research Rept. SR-393*, 1948.
2 A. R. Kaufmann, P. Gordon and D. W. Lillie, *Trans. A.S.M.*, 42 (1950) 785–844.
3 W. W. Beaver and K. G. Wickle, *J. Metals*, 6 (1954) 559–573.
4 D. R. Mash, *Trans. A.I.M.E.*, 203 (1955) 1235–1240.
5 D. W. Lillie, *The Metal Beryllium*, American Society for Metals, Cleveland, 1955, p. 304.
6 J. L. Klein, V. Macres, D. Woodward and J. Greenspan, *The Metal Beryllium*, 1955, p. 425.
7 G. L. Tuer and A. R. Kaufmann, *The Metal Beryllium*, 1955, p. 372.
8 H. T. Lee and R. M. Brick, *Trans. Am. Soc. Metals*, 48 (1956) 1003–1037.
9 R. G. O'Rourke *et al.*, *U.S. Atomic Energy Comm.*, Publ. (COO-312) 1956.
10 J. Greenspan, *Nuclear Metal Inc., 1957, NMI, 1174.*
11 *Brush Beryllium Technical Bulletin*, 1958.

12 GABER *et al.*, *Fiz. Metal. i. Metalloved. Akad. Nauk S.S.S.R. Ural. Filial*, 1 (1955) 529 (see J. WILLIAMS, *Met. Revs.* 3 (9) (1958).
13 L. R. WILLIAMS, *Nuclear Eng.*, 4 (1959) 9–18.
14 C. ZENER, *Elasticity and Anelasticity of Metals*, University of Chicago Press, Chicago, 1948, p. 158.
15 C. W. CHEN AND E. S. MACHLIN, *Acta Met.*, 4 (1954) 655.
16 A. N. STROH, *Phil. Mag.*, 3 (1958) 597.
17 J. T. BARNBY, *Fulmer Research Inst. Rept. P.258/1/March*, 1959.
18 B. A. BILBY AND R. BULLOCH, *Phil. Mag.*, 45 (1954) 631.
19 A. DERUGTTERE AND G. B. GREENOUGH, *Phil. Mag.*, 45 (1954) 624.
20 W. BOAS AND E. SCHMID, *Z. Physik*, 54 (1929) 16.
21 A. H. COTTRELL, *Phil. Mag.*, 44 (1953) 829.
22 E. SCHMID AND G. WASSERMAN, *Z. Physik*, 48 (1928) 370.
23 V. A. PHILLIPS, A. J. SWAIN AND R. EBORALL, *J. Inst. Metals*, 81 (1952) 625.
24 E. O. HALL, *J. Iron Steel Inst. (London)*, 170 (1952) 331.
25 S. F. PUGH, *A.E.R.E. Harwell, M/R1290*, 1953.
26 LUBAHN, *Trans. A.I.M.E.*, 185 (1949) 702.
27 A. W. MCREYNOLDS, *Trans. A.I.M.E.*, 185 (1949) 32.
28 R. THOMPSON AND B. BEGLEY, Unpublished data.
29 A. R. KAUFMANN AND P. CORZINE, *The Metal Beryllium*, 1955, p. 555–569.
30 S. H. GELLES, R. E. OGILVIE AND A. R. KAUFMANN, *Nuclear Metals Inc. Report 1207*, 1958.
31 H. W. L. PHILLIPS, *Annotated Equilibrium Diagrams, No. 19*, Institute of Metals (London), 1946.

X-ray microscopy and X-ray microanalysis

7 x 10"
viii + 541 pages
436 illustrations
27 tables
1960

Edited by:

ARNE ENGSTRÖM, M.D.
Professor of Medical Physics, Karolinska Institute, Stockholm (Sweden)

V. E. COSSLETT
Lecturer in Physics, Cavendish Laboratory, Cambridge (England)

HOWARD H. PATTEE, Jr., Ph.D.
Department of Physics and Biophysics Laboratory, Stanford University, Stanford, Calif. (U.S.A.)

The second international symposium on X-Ray microscopy and X-Ray microanalysis, held in Stockholm in 1959, was organized to present and discuss the results of the recent rapid developments in the field of X-ray microanalytical methods. The rapid advances in X-ray microprobe techniques made it possible to arrange the programme of the symposium and also the proceedings in three major sections, namely:

1. X-ray microabsorption
2. X-ray microemission
3. X-ray microdiffraction

The X-ray microscopic procedures based on absorption have found still wider uses. The proceedings show how new research procedures, with the latest types of equipment, can be applied to the fields of mineralogy, metallurgy, biology and medicine.
The development of the microprobe methods has been rapid and, as the proceedings of this symposium indicate, instruments are now commercially available which permit the recordings of X-emission spectra from areas as small as one micron in diameter.
Micro X-ray diffraction procedures are finding an increased use in a variety of fields and a presentation is made of methods and results of X-ray diffraction studies on microscopic objects. The proceedings are of interest to all who are concerned with non-destructive, quantitative analysis of microscopic objects of living and dead materials.

TABLE OF CONTENTS:

Section I: X-ray microabsorption - Introduction by Howard H. Pattee, Jr. - 45 papers
Section II: X-ray microemission - Introduction by V. E. Cosslett - 15 papers
Section III: X-ray microdiffraction - Introduction by A. Engström - 14 papers
Author Index
Subject Index

ELSEVIER PUBLISHING COMPANY
SPUISTRAAT 110-112 AMSTERDAM

mass spectrometry

and its use in organic chemistry

by

J. H. BEYNON

Research Physicist, Imperial Chemical Industries, Manchester (England)

The author has in this book summarized his experiences in applying mass spectrometry in the chemical industry. The application of the techniques to the identification of unknown organic substances and to related chemical problems forms the central theme. Instrument design, experimental techniques, as well as applications of wider relevance are also discussed. An important section appended to the text consists of a long compilation of mass and abundance values for various atomic combinations, which will be of great value in identificational work.

7 x 10″ viii + 638 pages 185 illustrations 2213 refs. 1960

CONTENTS

Introduction. 1. Instruments. 2. The Measurement of Mass. 3. The Measurement of Ionic Abundance. 4. Sources of Positive Ions. 5. Sample Handling. 6. The Recording of Positive Ion Beams. 7. Types of Ions in Mass Spectra. 8. Qualitative Analysis by Mass Spectrometer. 9. Correlations of Molecular Structure and Mass Spectra. 10. Other Applications of Mass Spectrometry.

Appendix:

1. Masses and isotopic abundance ratios for various combinations of carbon, hydrogen, nitrogen and oxygen. 2. Nomograms for determination of the origin of metastable ions. 3. Table of the masses and abundances of the naturally-occurring isotopes. 4. International atomic weights (1955). 5. Possible peaks in the mass spectra of fluorocarbons and their composition. 6. The mass spectrum of Fluorolube residues (above mass 69). 7. Some common mass doublets.

ELSEVIER PUBLISHING COMPANY

AMSTERDAM

217 E

CONTENTS

Effect of alloying on the mechanical properties of niobium
by R. T. BEGLEY AND J. H. BECHTOLD (Pittsburgh, Pa.) 1

Preliminary measurements on the thermal and electrical conductivities of molybdenum, niobium, tantalum and tungsten
by R. P. TYE (Teddington, Middx.) 13

Effect of oxygen on the mechanical properties of zone-refined niobium
by M. J. LEADBETTER AND B. B. ARGENT (Sheffield) 19

Über das Vanadin(III)-oxydchlorid VOCl
von H. SCHÄFER UND F. WARTENPFUHL (Münster) 29

The constitution of the chromium–niobium–silicon system
by H. J. GOLDSCHMIDT AND J. A. BRAND (Birmingham) 34

The constitution of the chromium–niobium–molybdenum system
by H. J. GOLDSCHMIDT AND J. A. BRAND (Birmingham) 44

The effect of strain rate, and heat treatment, on the tensile properties of extruded beryllium rods between 25 and 600°C
by A. B. BROWN, F. MORROW AND A. J. MARTIN (Renfrew, Scotland and Aldermaston, England) 62

All rights reserved

ELSEVIER PUBLISHING COMPANY, AMSTERDAM

Printed in The Netherlands by

NEDERLANDSE BOEKDRUK INRICHTING N.V., 'S-HERTOGENBOSCH

ILED IN STACKS

For Students and Teachers alike:

Inorganic Chemistry

A GUIDE TO ADVANCED STUDY

by

R. B HESLOP, M.Sc., F.R.I.C.

and

P. L. ROBINSON, D.Sc., F.R.I.C.

- An outline of current inorganic chemistry, sufficient for basic reading up to honours degree standard, is provided in one small volume.
- The approach is general and reasonably fundamental, thus, some of the material is suitable for advanced level and scholarship pupils in schools and for non-specialist students in universities and technical colleges.
- Teachers will find this book very useful when planning instruction at all levels.

6 x 9" viii + 542 pages + index 294 illustrations 136 tables
1960 45s. Dfl. 24.00

Write for additional information to:

ELSEVIER PUBLISHING COMPANY

110-112 SPUISTRAAT AMSTERDAM HOLLAND